LEVEL II

12

RADC-TR-79-252
Final Technical Report
October 1979

DEVELOPMENT OF HIGH STRENGTH OPTICAL FIBER WAVEGUIDES USING RESIDUAL SURFACE COMPRESSION

Catholic University of America

Sponsored by
Defense Advanced Research Projects Agency (DoD)
ARPA Order No. 3282

The views and conclusions contained in this document are those of the authors and should not be interpreted as necessarily representing the official policies, either expressed or implied, of the Defense Advanced Research Projects Agency or the U.S. Government.

ROME AIR DEVELOPMENT CENTER
Air Force Systems Command
Griffiss Air Force Base, New York 13441

This report has been reviewed by the RADC Public Affairs Office (PA) and is releasable to the National Technical Information Service (NTIS). At NTIS it will be releasable to the general public, including foreign nations.

RADC-TR-79-252 has been reviewed and is approved for publication.

APPROVED:

BERNARD BENDOW
Project Engineer

If your address has changed or if you wish to be removed from the RADC mailing list, or if the addressee is no longer employed by your organization, please notify RADC (ESO), Hanscom AFB MA 01731. This will assist us in maintaining a current mailing list.

Do not return this copy. Retain or destroy.

(9) Technical Final Rept. Jan 77 - May 79,

(6) DEVELOPMENT OF HIGH STRENGTH OPTICAL FIBER WAVEGUIDES USING RESIDUAL SURFACE COMPRESSION.

(10) R. K. Mohr
O. H. El-Bayoumi
N. Lagakos
H. Hojaji
P. Klocek
R. Ingel
D. S. Ma
J. H. Simmons
P. B. Macedo

(11) Oct 79

(12) 117

(16) 3282

(15) Contractor: Catholic University of America
Contract Number: F19628-77-C-0084 (ARPA Order-3282)
Effective Date of Contract: 1 Jan 1977
Contract Expiration Date: 31 May 1979
Short Title of Work: Development of High Strength Optical Fiber Waveguides Using Residual Surface Compression
Program Code Number: 7D10
Period of Work Covered: Jan 77 - May 79

(17) AR

(18) RADC

(19) TR-79-252

Principal Investigator: Dr. Pedro B. Macedo
Phone: 202 635-5327
Project Engineer: Bernard Bendow
Phone: 617 861-2207

Approved for public release; distribution unlimited.

This research was supported by the Defense Advanced Research Projects Agency of the Department of Defense and was monitored by Bernard Bendow (ESO), Hanscom AFB MA 01731 under Contract F19628-77-C-0084.

404 951

UNCLASSIFIED

SECURITY CLASSIFICATION OF THIS PAGE (When Data Entered)

REPORT DOCUMENTATION PAGE

READ INSTRUCTIONS BEFORE COMPLETING FORM

1. REPORT NUMBER: RADC-TR-79-252
2. GOVT ACCESSION NO.
3. RECIPIENT'S CATALOG NUMBER

4. TITLE (and Subtitle): DEVELOPMENT OF HIGH STRENGTH OPTICAL FIBER WAVEGUIDES USING RESIDUAL SURFACE COMPRESSION

5. TYPE OF REPORT & PERIOD COVERED: Final Technical Report, 1 Jan 77 - 31 May 79

6. PERFORMING ORG. REPORT NUMBER: N/A

7. AUTHOR(s): R. K. Mohr, O. H. El-Bayoumi, N. Lagakos, H. Hojaji, P. Klocek, R. Ingel, D. S. Ma, J. H. Simmons, P. B. Macedo

8. CONTRACT OR GRANT NUMBER(s): F19628-77-C-0084

9. PERFORMING ORGANIZATION NAME AND ADDRESS: Catholic University of America, Vitreous State Lab, B2 Keane Hall, Washington DC 20064

10. PROGRAM ELEMENT, PROJECT, TASK AREA & WORK UNIT NUMBERS: 61101E, 3282AR20

11. CONTROLLING OFFICE NAME AND ADDRESS: Defense Advanced Research Projects Agency, 1400 Wilson Boulevard, Arlington VA 22209

12. REPORT DATE: October 1979

13. NUMBER OF PAGES: 118

14. MONITORING AGENCY NAME & ADDRESS(if different from Controlling Office): Deputy for Electronic Technology (RADC/ESO), Hanscom AFB MA 01731

15. SECURITY CLASS. (of this report): UNCLASSIFIED

15a. DECLASSIFICATION/DOWNGRADING SCHEDULE: N/A

16. DISTRIBUTION STATEMENT (of this Report): Approved for public release; distribution unlimited.

17. DISTRIBUTION STATEMENT (of the abstract entered in Block 20, if different from Report): Same

18. SUPPLEMENTARY NOTES: RADC Project Engineer: Bernard Bendow RADC/ESO

19. KEY WORDS (Continue on reverse side if necessary and identify by block number):
Optical fibers
Strong fibers
Glass surfaces
Surface compression

20. ABSTRACT (Continue on reverse side if necessary and identify by block number):
The primary objective of this project was to maximize the compressive strengthening obtained in low loss fibers made by the molecular stuffing process. The process being the doping of a porous high silica glass rod made by a phase separation and leaching process. The rod is subsequently sintered to form a solid glass preform from which fibers may be drawn. The ultimate goal being a fiber having greater than 100 ksi surface compression and loss less than 10 dB/km. As a major part of this effort we have characterized the strengthening effects of compression and demonstrated that even moderate compression (Cont'd)

DD FORM 1 JAN 73 1473

UNCLASSIFIED

SECURITY CLASSIFICATION OF THIS PAGE (When Data Entered)

Item 20 (Cont'd)

can be of value in many applications.

Optical losses less than 10 dB/km are obtainable using molecular stuffing and we were able to produce preforms having greater than 75 ksi compression. Preforms and fibers having very high compression are difficult to produce and thus may not provide a practical method of dramatically increasing fiber strength. Surface compression on the order of 30 ksi is relatively easy to obtain, however, and compression of this magnitude can have significant effects on fatigue failure in many applications.

We were able to demonstrate that fibers having surface compression showed no strength degradation when aged under load in air as long as the tensile load was less in magnitude than that of the compression. In fact, the strength of abraded samples was observed to improve with time. It was also shown that surface compression reduced the rate of static fatigue for loads larger than the compression.

We conclude from our work that optical fibers may be strengthened and made resistant to static fatigue by surface compression. In many telecommunication applications static loads less than 20 ksi are expected and thus compression levels easily obtained by Molecular Stuffing would eliminate static fatigue failure and strength degradation for fibers used in those applications.

TABLE OF CONTENTS

I. INTRODUCTION

The primary objective of this project was to maximize the compressive strengthening obtained in low loss fibers made by the molecular stuffing process. The ultimate goal being a fiber having greater than 100 ksi surface compression and loss less than 10 dB/km. As a major part of this effort we have characterized the strengthening effects of compression and demonstrated that even moderate compression can be of value in many applications.

Optical losses less than 10 dB/km are obtainable using molecular stuffing, however, we were unable to produce preforms or fibers having greater than 75 ksi compression. Because of the difficulties involved in achieving very high compression we conclude that the major application of compressive strengthening may be the prevention of static fatigue for loads less than 30 ksi.

In this final report we summarize the results of our experiments to characterize compressive strengthening, including the effects on static fatigue and on aging. We also discuss our development of measurements of stress optic coefficients and stress profile measurements in fibers. Finally we present a description of the best dopant combinations we found for obtaining high stress in molecular stuffed fibers.

II. GENERAL BACKGROUND

A. Compressive Strengthening

It is well known that strengthening of glass articles can be achieved by placing the surface of the article in compression.[1] Glass articles having no or only minor internal flaws will fail

from the surface when the net tensile stress at the surface exceeds the value necessary to initiate or propagate surface cracks. Strengthening is achieved by compression because any tensile load must first exceed that compression before the surface is in net tension.

Traditional methods of producing surface compression on glass articles include thermal tempering, ion exchange and lamination. The first two methods are not well suited to optical fiber manufacture. They cannot be applied to fiber optics preforms due to the loss of stress under thermal cycling during fiber drawing but must be applied to the fibers themselves. Thermal tempering is suited only for relatively thick articles and ion exchange in fibers appears impractical. Finally, these two techniques produce an undesirable radially decreasing stress profile. The lamination technique of producing a fiber with a low expansion and high T_g clad around a high expansion low T_g core avoids these difficulties. Such a fiber profile is illustrated in Figure 1. Molecular Stuffing is one process which is suitable for producing laminated preforms and fibers. Such fibers can have uniform surface compression across a clad thicker than 10 μm and having greater than 40 ksi compression. This compression is greater than the static loads expected in most telecommunication applications.

The idea behind this strengthening technique is to produce a residual stress profile with the surface under compression. A relatively simple way of achieving laminated preforms having surface compression is by creating a suitable dopant concentration,

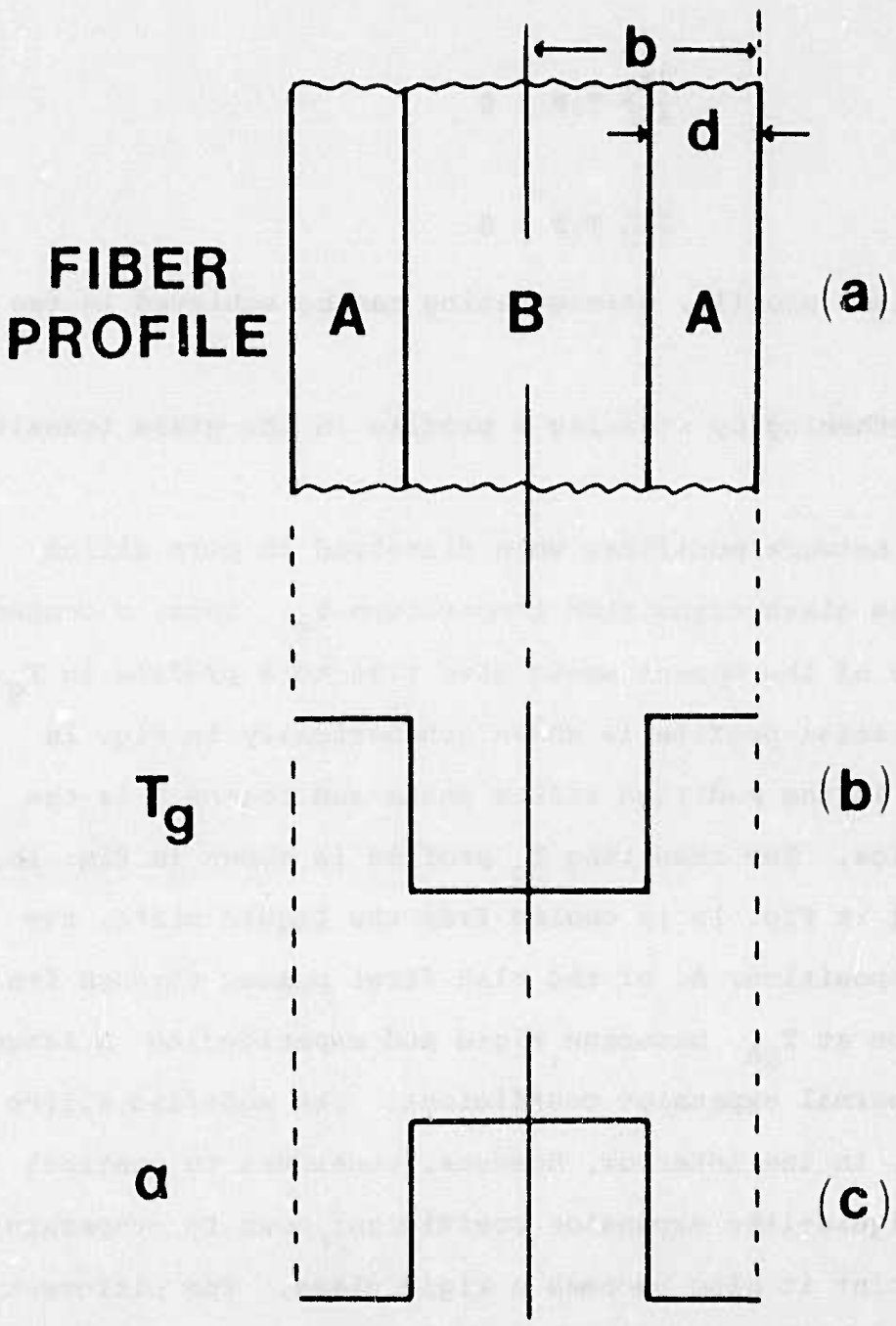

FIGURE 1 - Schematic of a compressively strengthened fiber cross section. a) composition profile, b) T_g profile c) expansion coefficient profile.

C, profile as shown in Fig. 1a, with two requirements on the dopants:

$$\frac{\partial T_g}{\partial C}\,T,P < 0 \qquad (1)$$

$$\frac{\partial \alpha}{\partial C}\,T,P > 0 \qquad (2)$$

From a composition profile, strengthening can be achieved in two ways:

a) Strengthening by creating a profile in the glass transition temperature T_g.

All known network modifiers when dissolved in pure silica act to lower the glass transition temperature T_g. Thus, a concentration profile of the dopant would give rise to a profile in T_g. Such a concentration profile is shown schematically in Fig. 1a where region B is the modified silica phase and region A is the unmodified silica. The resulting T_g profile is shown in Fig. 1b. As the material in Fig. 1a is cooled from the liquid state, the pure silica composition, A, of the clad first passes through its glass transition at T_{gA}, becoming rigid and experiencing a large reduction in thermal expansion coefficient. The modified silica composition, B, in the interior, however, continues to contract with a large liquid-like expansion coefficient down to temperature T_{gB} at which point it also becomes a rigid glass. The differential expansion between surface and interior in the temperature range T_{gA} to T_{gB} has the effect of placing the surface under a compressional stress. This compressional stress must be overcome before the surface can undergo fracture, so that the T_g profile of Fig. 1b

results in strengthening of the surface of the glass.

b) Strengthening by creating an expansion coefficient profile.

In this case we modify the glass in such a way that the resulting expansion coefficient profile is as shown in Fig. 1c. Thus, upon cooling the sample to room temperature, region B shrinks by a greater amount than region A, resulting in a compressive stress in A which increases the strength of the sample.

For a cylindrical fiber geometry it can be shown from the theory of thermal stresses,[2] that

(i) the residual axial compression σ_R is uniform throughout the clad and is given approximately by

$$\sigma_R = \frac{(\alpha_2 - \alpha_1^*)(T_{g2} - T_{g1})}{\frac{b^2 - a^2}{a^2}\frac{1}{3K_1^*} + \frac{(1 - 2\nu)}{E}} + \frac{(\alpha_2 - \alpha_1)(T_{g1} - T)}{\frac{b^2}{a^2}\frac{(1 - \nu)}{E}} \quad (3)$$

(ii) the residual tension, σ_{core} which is uniform throughout the core, is given by

$$\sigma_{core} = \sigma_R \left(\frac{b^2 - a^2}{a^2}\right) \quad (4)$$

where the subscripts 1 and 2 refer to properties of the core and clad respectively, the * refers to the property above the glass transition temperature, T_g, K_1^* is the bulk modulus, ν is Poisson's ratio, E is Young's modulus, b and a are the preform and core radii respectively and T is room temperature. A negative value of σ_R indicates compression.

It is interesting to notice certain important features of Eqs. (3) and (4) in relation to optical fibers:

1. The residual stress profile is "ideal" as shown in Fig. 2. Unlike the stress profiles in thermally tempered or chemically strengthened glass where the compression decreases rapidly with depth, the ideal profile has uniform compression across the clad. Protection against scratches or flaws is thus provided for the full clad thickness.

2. The residual compression in the clad and the residual tension in the core are sensitive functions of the parameter x, the clad thickness to radius ratio. The dependence of residual compression on x is shown in Fig. 3 for a high silica clad alkali borosilicate core system produced by a partial leaching process.[3] The residual compression increases rapidly with decreasing values of x.

For optical fibers where the clad acts both as the optical and strengthening member, one requires a clad thickness of at least one micron. If microbending losses are to be minimized, experience has shown that the optical clad must be increased to several microns. It is possible by Molecular Stuffing, however, using multiple dopants to obtain separate optical and mechanical clads satisfying requirements of a thin mechanical clad and a thick optical clad as shown schematically in Fig. 4. Using Griffith's equation from the theory of brittle fracture, it follows that for fibers of strength more than 100,000 psi all of the surface flaws and cracks are less than a micron deep. Thus, it seems that 1 μm will be an acceptable clad thickness for protection against static fatigue if practical difficulties

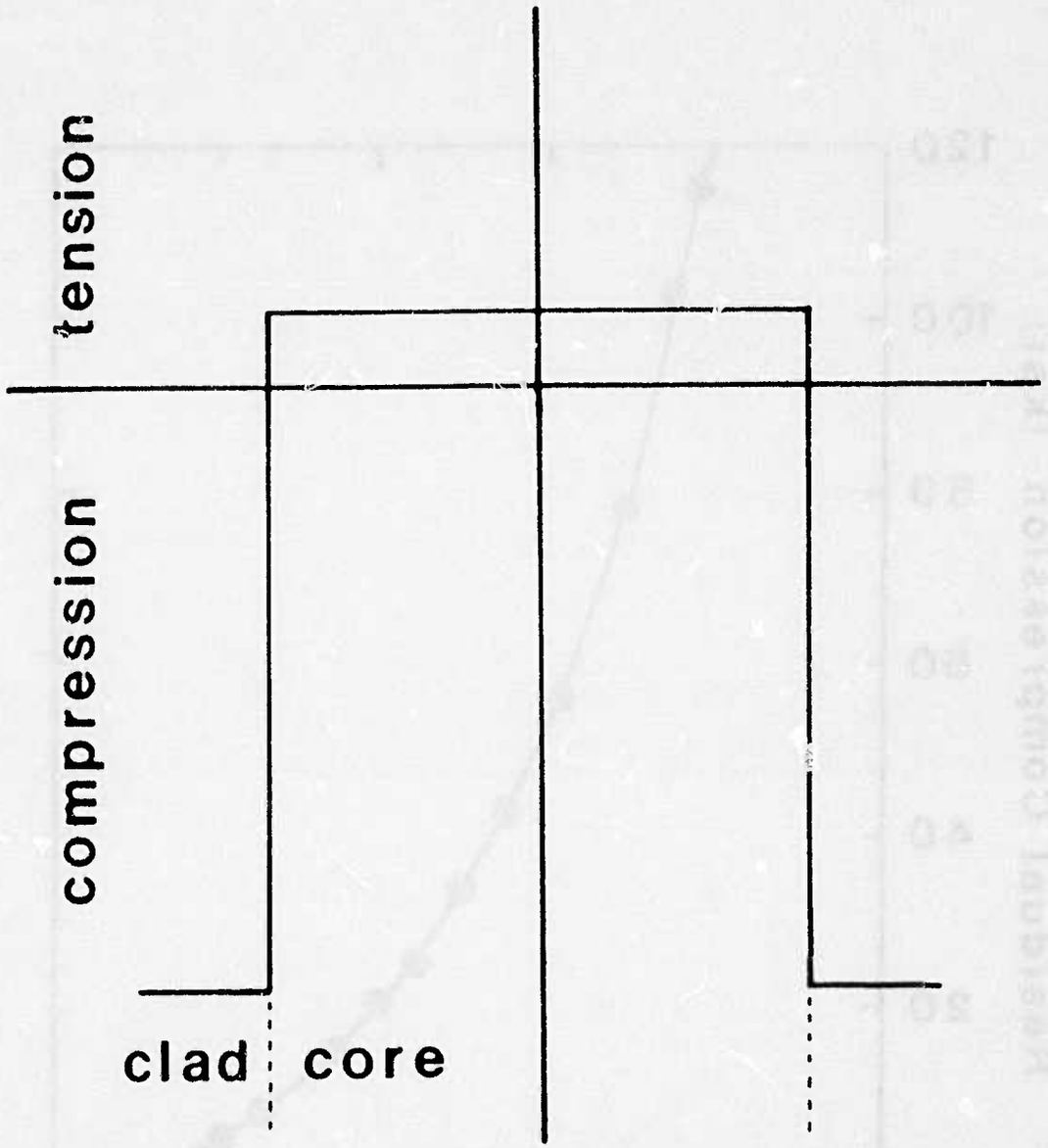

FIGURE 2 - Ideal Stress Profile.

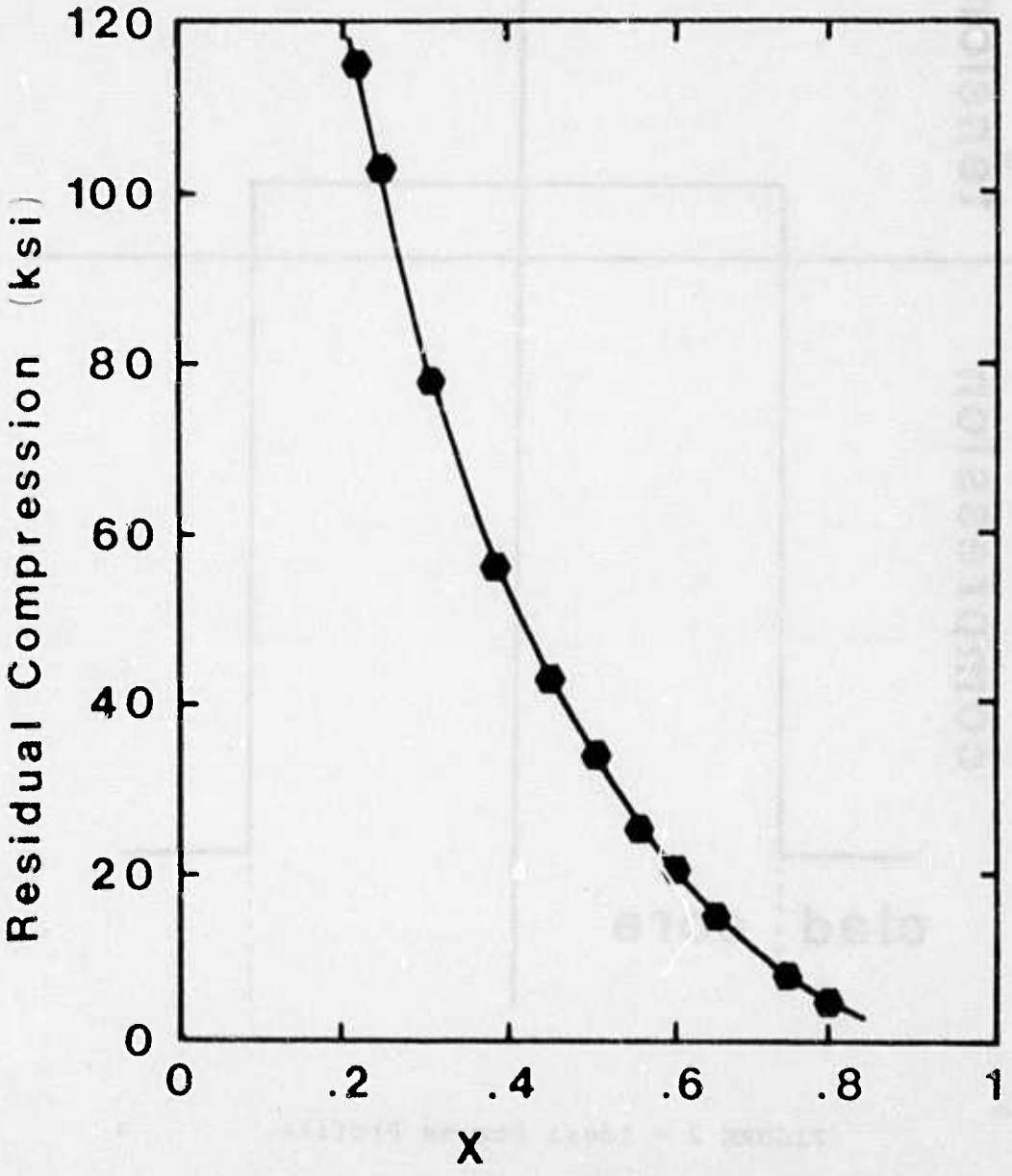

FIGURE 3 - Clad compression versus clad thickness to radius ratio, x, for partially leached rods.

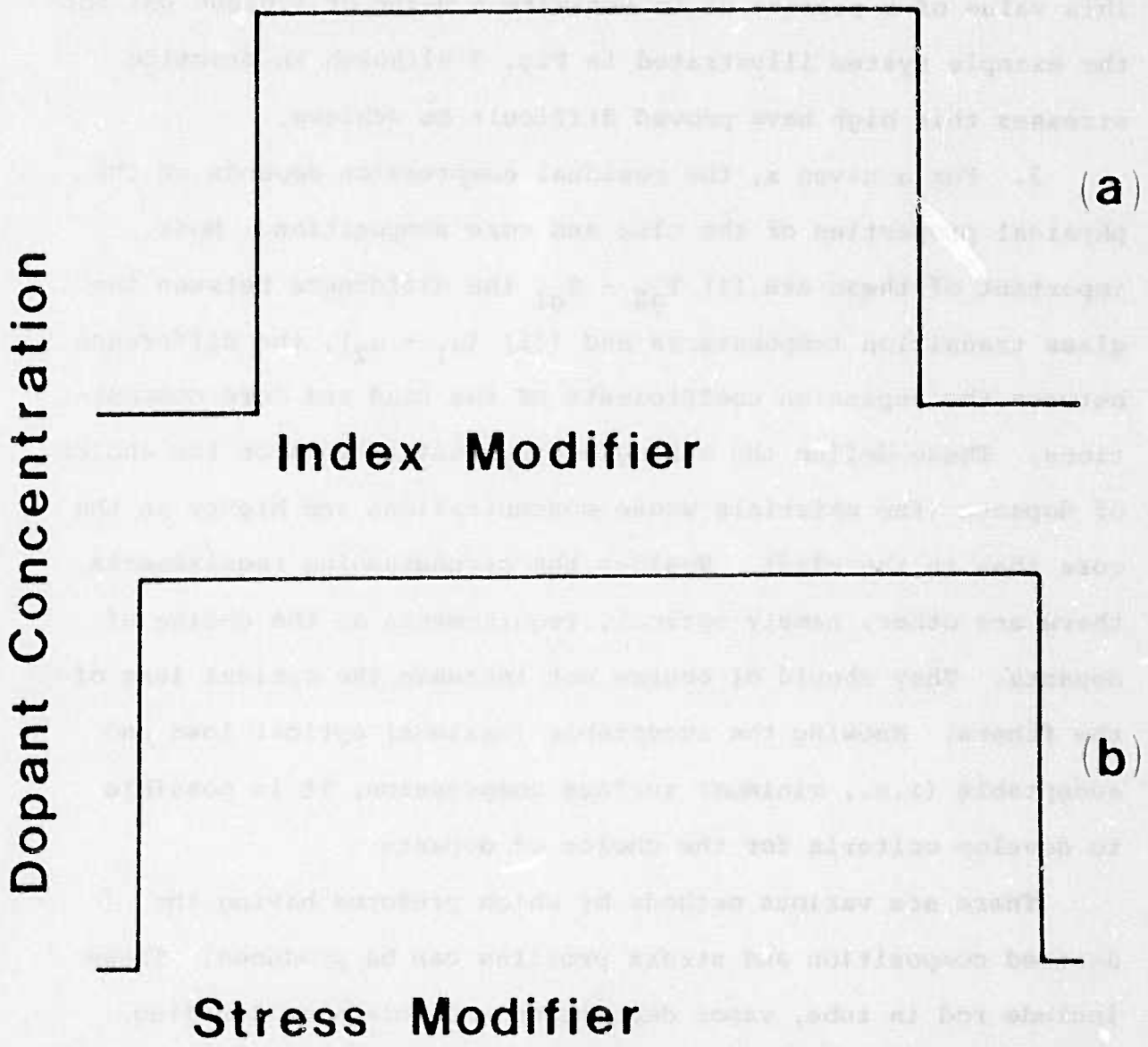

FIGURE 4 - Concentration profiles for index and stress modifier dopants in multiclad preforms.

of drawing fibers with such thin clads can be overcome. For a fiber of diameter 100 μm, a 1 μm clad thickness gives x = 1/50. This value of x permits us to estimate a value of 170,000 psi for the example system illustrated in Fig. 3 although in practice stresses this high have proved difficult to achieve.

3. For a given x, the residual compression depends on the physical properties of the clad and core composition. Most important of these are (i) $T_{g2} - T_{g1}$ the difference between the glass transition temperatures and (ii) $(\alpha_1 - \alpha_2)$, the difference between the expansion coefficients of the clad and core compositions. These define the strengthening restrictions on the choice of dopants (the materials whose concentrations are higher in the core than in the clad). Besides the strengthening requirements, there are other, namely optical, requirements on the choice of dopants. They should of course not increase the optical loss of the fibers. Knowing the acceptable (maximum) optical loss and acceptable (i.e., minimum) surface compression, it is possible to develop criteria for the choice of dopants.

There are various methods by which preforms having the desired composition and stress profiles can be produced. These include rod in tube, vapor deposition and Molecular Stuffing. The rod and tube method has serious interface problems and is thus undesirable. It is expected that manufacturing difficulties due to stresses and breakage during preform fabrication would make high stress vapor deposited preforms difficult to make though these difficulties can be overcome. In the Molecular Stuffing process, some residual compression is necessary for successful

processing and we have found that useful levels of compression have been relatively easy to achieve.

B. Molecular Stuffing Process

Molecular Stuffing is the name of a technique for making composition profiles in silicate glasses.[4] Step, graded, multi-step and a combination of graded and step composition profiles can be produced by Molecular Stuffing. We briefly describe here the basic procedure for producing a step composition profile suitable for strengthened fiber optics.

a. Brief Background on Molecular Stuffing

An inexpensive method of making glass with high silica content was first developed by Corning Glass Corporation and is called the Vycor Process. Vycor is principally used for its high temperature stability and high resistance to thermal shock. Even though a high silica glass is useful for fiber optics, Vycor (as supplied by Corning) is unsatisfactory because the optical loss is large, on the order to 2000 dB/km (at 1.0 μm).

In our research at the Vitreous State Laboratory we developed a phase separation and leaching technique for producing purified high silica glass which we call "Phasil" and which avoids the high optical loss associated with the Vycor process. In this process an alkali borosilicate glass is allowed to phase separate such that one obtains a microstructure consisting of two interconnected phases. The borate rich phase is ionic in nature and is found to be soluble in acids such as HCl. The other phase is mostly covalently bonded silica and is insoluble in these acids. The phase separated glass is then leached in HCl to remove the

borate rich phase. The skeleton of the silica-rich phase is then heat treated at a temperature where the pores collapse to give a homogeneous bubble-free glass of high silica content. It appears that Phasil can have optical losses comparable to that in fused silica and losses less than 5 dB/km have been observed.[4] This offers a new approach to the production of low loss and high strength waveguides.

To produce a radial composition profile, we take advantage of the fact that in production, Phasil is obtained in the form of a connected porous structure. In our technique, dopants are deposited in the pores to achieve the composition profile desired. A rod with such a profile can then be drawn into an optical fiber which will have a similar profile. We have named this method of producing profiled fibers starting from a porous structure "Molecular Stuffing."

b. Details of the Molecular Stuffing Process

Production of profiled glass fibers using the molecular stuffing technique involves several steps which are shown in the flow chart of Fig. 5 and are discussed below.

1. Glass Melting

A Na_2O-K_2O-B_2O_3-SiO_2 composition is selected such that a homogeneous glass is easily made at about 1400°C, i.e., the mixture has viscosity around 10^2 to 10^3 poise at 1400°C. Conventional glass melting procedures are used.

2. Heat Treatment

The glass is heat treated at a desirable temperature (550°C) for a suitable length of time such that it separates into two

MOLECULAR STUFFING

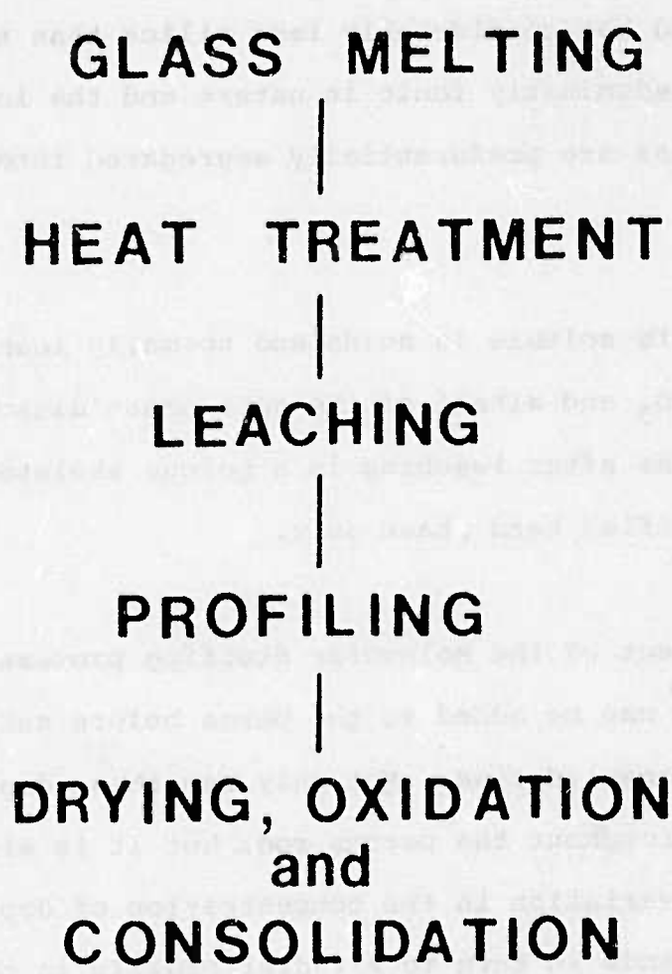

FIGURE 5 - Flow diagram of the Molecular Stuffing process.

phases having connected microstructure with an average size between 100-500 Å and a 50/50 volume fraction. One of the phases is mostly co-valently bonded SiO_2 referred to as the hard phase. The other phase contains most of the sodium and boric oxide of the original glass and has considerably less silica than the hard phase. It is predominatly ionic in nature and the ionic impurities in the glass are preferentially segregated into this phase.

3. Leaching

The ionic phase is soluble in acids and normally leaching is done with HCl; the B_2O_3 and alkali of the soft phase dissolve in the acid. What remains after leaching is a porous skeleton consisting of the purified hard phase only.

4. Profiling

An important aspect of the Molecular Stuffing process is that suitable dopants can be added to the pores before subjecting the porous glass to consolidation. Not only can these dopants be added uniformly throughout the porous rod, but it is also possible to create a variation in the concentration of dopants which concentration corresponds in turn to a radial profile in the refractive index, T_g or expansion coefficient depending on the nature of the dopants.

In practice the dopants can be introduced in many ways, but we have found that the deposition of dopants should be done by a precipitation process not involving evaporation of the solvent. The percentage of dopant incorporated may be controlled by varying the concentration of the solution. After uniform

precipitation of the dopant throughout the preform, a dopant-free cladding layer, having the composition of Phasil, is produced by redissolving the dopant to a desired depth, and washing it out with an unstuffing solution.

Dopants are deposited directly as salts which decompose to oxides. The compounds used for fiber optics include KNO_3, $CsNO_3$, $Bi(NO_3)_3$, $Rb(NO_3)$, $Pb(NO_3)$, H_3BO_3 and $Sr(NO_3)_2$.

5. Drying, Oxidation and Consolidation

After the dopants have been deposited in the porous skeleton, the structure must be dried, the dopants decomposed and converted to oxides and finally collapsed as a glass. These steps are accomplished by vacuum drying while gradually raising the temperature. Prior to collapse the porous preform may be subjected to an oxidizing or reducing atmosphere to obtain an optimum redox condition for any remaining impurities in the glass.

This process yields a preform which may then be drawn into a fiber by conventional means. Step and graded index preforms are presently being made commercially by this process having loss less than 10 dB/km.[4]

III. STRENGTH INCREASE OF FIBERS HAVING COMPRESSION

In order to determine to what ext nt fibers drawn from prestressed preforms retained the compression found in the preforms and to what extent this compression contributed to the fiber strength we undertook several experimental st ies, the first of which is discussed in this section. This section has three major objectives: the first is to demonstrate that

Molecular Stuffed preforms can be used to produce fibers with surface compression, the second is to show to what extent preform compression is transmitted to the fibers and the third is to show the manner in which surface compression contributes to fiber strength.

Fiber strength is statistical in nature and is determined primarily by the most severe flaw present in the region under test.[5,6] We have used Weibull Statistics incorporating a non-zero minimum strength in order to analyze the results of tensile tests of abraded prestressed fibers. An abrasion technique was developed which gave a sufficiently narrow distribution of initial flaws that compression effects could be clearly isolated allowing the comparison of the strengths of fibers with compression to those without compression. The observed strength improvement in the prestressed fibers was compared to the surface compression observed photoelastically and was found to agree within experimental error.

A. Theory

Fibers almost invariably fail because of a surface flaw. The depth, d, of a idealized Griffith flaw causing catastrophic failure at a fracture stress σ_f is given by[7]

$$d = \frac{2\ E}{\pi \sigma_f^2} \gamma \tag{5}$$

where γ is the fracture surface energy and E is Young's modulus. For 96% silica type glass[8] fracture stresses corresponding to flaw depths of 1 μm and 10 μm are 0.4 and 0.13 GPa respectively.

Weibull[9] derived a single mode probability distribution applicable to the strength of glass fibers. The cummulative failure probability for samples of equal length is

$$F = 1 - \exp\left[\frac{\sigma_f - \sigma_u}{\sigma_o}\right]^m \qquad (6)$$

where σ_u is the minimum fracture stress, normally taken as zero for glass, σ_o is a scale parameter and m is the Weibull parameter which describes the width of the probability distribution. Equation (6) can be rewritten as

$$\ln \ln\left(\frac{1}{1 - F}\right) = m \ln(\sigma_f - \sigma_u) + \text{constant} \qquad (7)$$

which is a form convenient for plotting the results of tensile tests.

One method of making a fiber with a non-zero value of σ_u is to give the fiber a compressive clad. Step index fibers having a similar step profile in composition are examples of laminated cylinders having a uniform residual stress, σ_R, given by Eq. 3.

The residual surface compression provides a minimum strength, assuming no failures due to internal flaws, equal in magnitude to $|\sigma_R|$ since any applied tensile stress $\leq |\sigma_R|$ will only serve to compensate the compression. Thus we would replace σ_u by $|\sigma_R|$ in Eqs. (6) and (7). Following a similar argument we would replace σ_f by $(\sigma_f - |\sigma_R|)$ in Eq. (5).

B. Experimental Procedure

a. Preform and Fiber Preparation

Fibers drawn from three preforms were used in this study. The preforms were made by the Molecular Stuffing process. Preform

1 was an undoped Phasil preform, #2 and #3 were step index preforms having Phasil clads and Cs_2O and Cs_2O-K_2O-Bi_2O_3 doped Phasil cores respectively.

The preforms were rinsed in methanol, air dried and drawn down to a diameter ranging from 120 μm to 180 μm on a vertical draw tower equipped with propane oxygen torches. The resultant uncoated fiber was spooled on polished aluminum drums. Precautions to protect the fiber surface were not required since the fibers were to be abraded prior to testing.

b. Abrasion technique and tensile testing

In order to detect unambiguously the strengthening effects of surface compression on the order of 70 to 240 MPa required that we have fibers exhibiting strengths of that order of magnitude and having a narrow strength distribution. Abrasion of the fibers immediately prior to testing insured that these requirements were met.

We developed a simple, rapid, reproducible method of abrading fibers. The technique is to abrade one side of a 1 to 2.5 cm length of the test fiber for 15 seconds using flaps of 220 or 400 grit silicon carbide paper. The flaps were attached to a wheel rotating in a plane perpendicular to the fiber axis at 15 rpm as shown schematically in Fig. 6. The severity of the abrasion could be controlled somewhat by the tension on the fiber during abrasion and by the stiffness of the abrasive paper. These parameters were fixed for all comparison tests.

Tensile tests were performed at a 40%/min. strain rate on 50 cm fiber lengths immediately after abrasion using an Instron

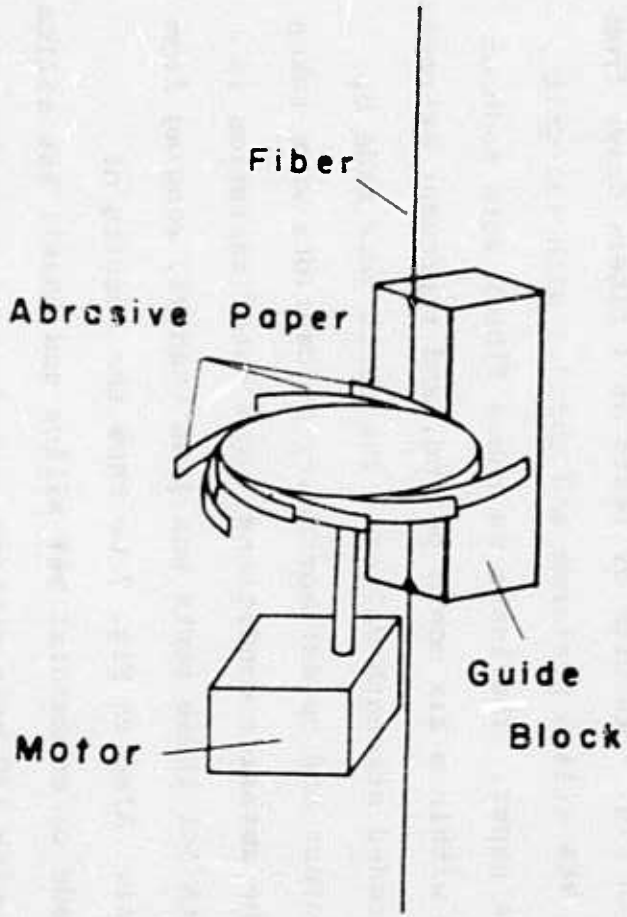

FIGURE 6 - Schematic diagram of the fiber abrasion apparatus.

model 1122 testing machine. Tests were performed in air or with the abraded portion of the fiber in liquid nitrogen. The fiber length was unimportant in these tests since the fiber always broke in the abraded section. The fiber diameter was measured at the position of the break and σ_f was determined from the load at break divided by the fiber cross sectional area.

To demonstrate the reproducibility of the abrasion and tensile tests we show in Fig. 7 results of tests on 4 fibers drawn from commercial 96% silica preforms and abraded with 400 grit silicon carbide paper. The tests on these fibers were made on different days within a six month period, and represent extremes in observed abraded strength values. The tests were made by different operators and no extraordinary precautions were taken to reproduce the abrasion conditions. The total variation in average strength for these tests was less than 7%, ranging from 18.1 to 19.4 Ksi. Also in Fig. 7 we show the results of measurements made on commercial 96% silica and Phasil 96% silica fibers abraded with 220 grit silicon carbide paper. These show no variation in average strength within experimental error and Weibull slopes varying by only 5%. This reproducibility is typical of experiments where moderate care is taken to insure that abrasion conditions for the tests are the same. For comparison we show in the same figure the failure probability for an unabraded fiber which exhibits a very broad multimode strength distribution which is unsuitable for comparitive tests.

c. Photoelastic Measurements of Residual Compression

The axial stress in glass preforms and fibers is conveniently

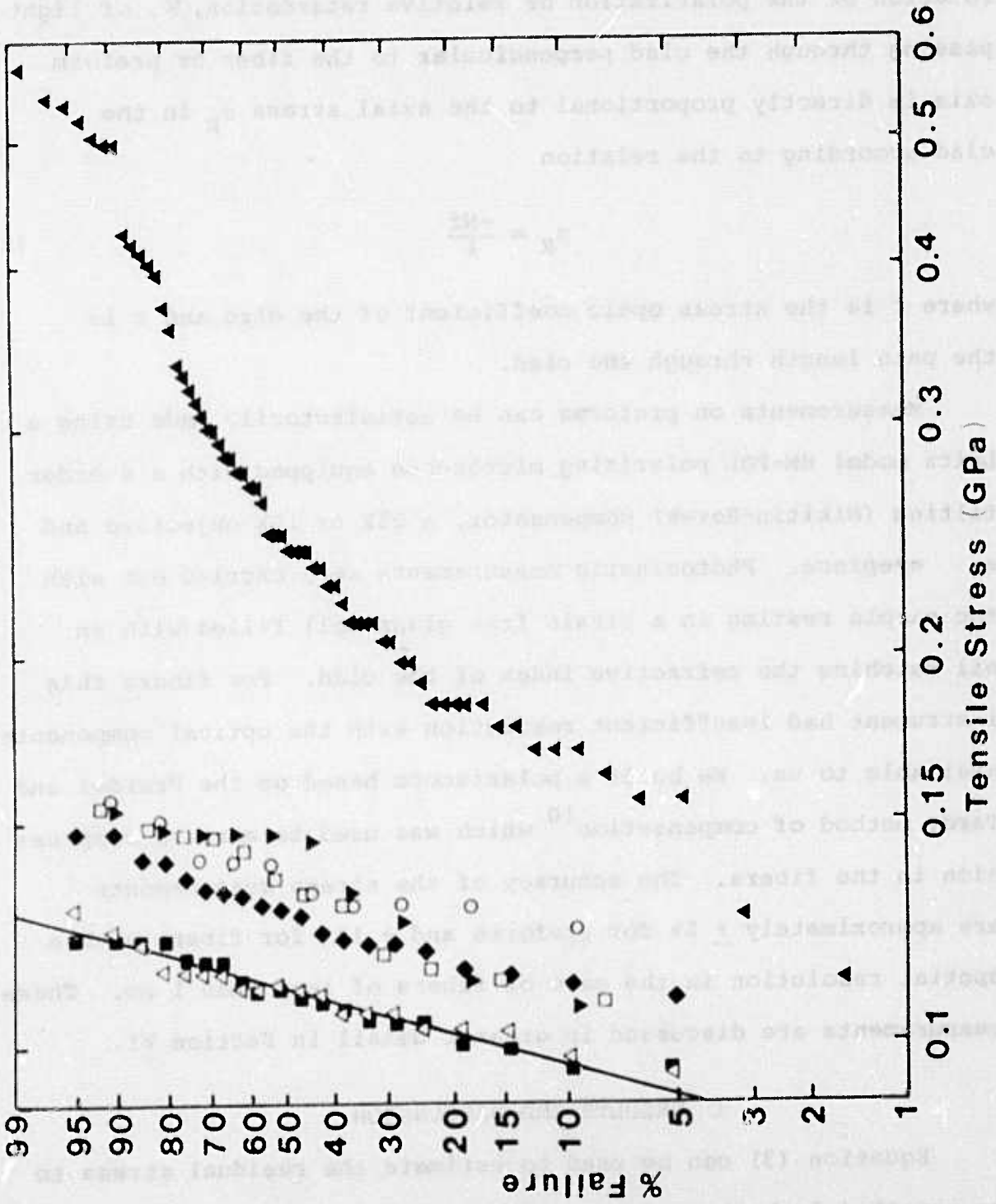

FIGURE 7 - The effect of abrasion on the tensile strength of bare fibers.

measured using standard photoelastic techniques. The degree of rotation of the polarization or relative retardation, N, of light passing through the clad perpendicular to the fiber or preform axis is directly proportional to the axial stress σ_R in the clad according to the relation

$$\sigma_R = \frac{-Nf}{\ell} \tag{8}$$

where f is the stress optic coefficient of the clad and ℓ is the path length through the clad.

Measurements on preforms can be satisfactorily made using a Leitz model HM-POL polarizing microscope equipped with a 4-order tilting (Nikitin-Berek) compensator, a 25X or 10X objective and a eyepiece. Photoelastic measurements were carried out with the sample resting in a strain free glass cell filled with an oil matching the refractive index of the clad. For fibers this instrument had insufficient resolution with the optical components available to us. We built a polariscope based on the Freidel and Tardy method of compensation[10] which was used to measure compression in the fibers. The accuracy of the stress measurements are approximately $\pm$ 5% for preforms and $\pm$ 10% for fibers with a spatial resolution in the case of fibers of less than 1 μm. These measurements are discussed in greater detail in Section VI.

C. RESULTS AND DISCUSSION

Equation (3) can be used to estimate the residual stress to be expected in both preforms and fibers. Values of the parameters used for this estimate and the results of the calculations are listed in Table I. The elastic constants were calculated from the

TABLE I

	Phasil #1	Cs_2O #2	Cs_2O-K_2O-Bi_2O_3 #3
Y	6.5×10^{10} Pa	5.04×10^{10} Pa	6.67×10^{10} Pa
K_1^*	8.75×10^{9} Pa	8×10^{9} Pa	$.87 \times 10^{9}$ Pa
α	8×10^{-7}/°C	27×10^{-7}/°C	47.7×10^{-7}/°C
α^*	----	81×10^{-7}/°C	143×10^{-7}/°C
T_2	820	820	714
ν	.19	.24	.18
b	----	81.3 μm	78.1
a	----	56.6 μm	67.95
σ_R	----	-8.85 ksi(6×10^7 Pa)	-34 ksi(2.3×10^8 Pa)

glass densities and the shear and longitudinal sound velocities measured by Brillouin scattering. The expansion coefficients were measured by a dilatometer and the T_g's were measured by a parallel plate viscometer or by a dilatometer. α^* was estimated by assuming that the value above T_g is 3 times that below T_g.[11] K_1^* was estimated as 0.25 K_1 which is approximately true for SiO_2 [12] and B_2O_3 [13] glasses. Since all of the parameters used in the calculation are not experimentally determined, the use of Eq. (3) constitutes a best estimate of the expected magnitude of the compression.

The photoelastic measurements of σ_R in the preforms and fibers are given in Table II. The measurements on the preforms were taken near the center of the clad at several positions on the preform and an average value is reported. More detailed stress profile measurements were made on the fibers. These measurements indicated that the stress in the clad was not uniform as predicted in the analysis leading to Eq. (3). This is probably due to composition inhomogeneity in the clad from incomplete removal of core dopant from the clad in the profiling and washing stages of the stuffing process. The reported stress represents an average across the clad. The stress varied by as much as 20% from the average at some points in the clad. The observed stress variations were outside the measurement error and their observation was reproducible. This is discussed in more detail in Section VI.

The strengths of the abraded fibers were measured as discussed above and the results plotted on Weibull plots as shown in Figs. 8 and 9. Figure 8 shows the results of measurements on fibers

TABLE II

	f(lb/in-fringe)	σ_R ksi
Preform #2	1070*	11.5
Fiber #2	1070	10.3
Preform #3	1037*	31.6
Fiber #3	1037	33.0

*measured in the fiber only

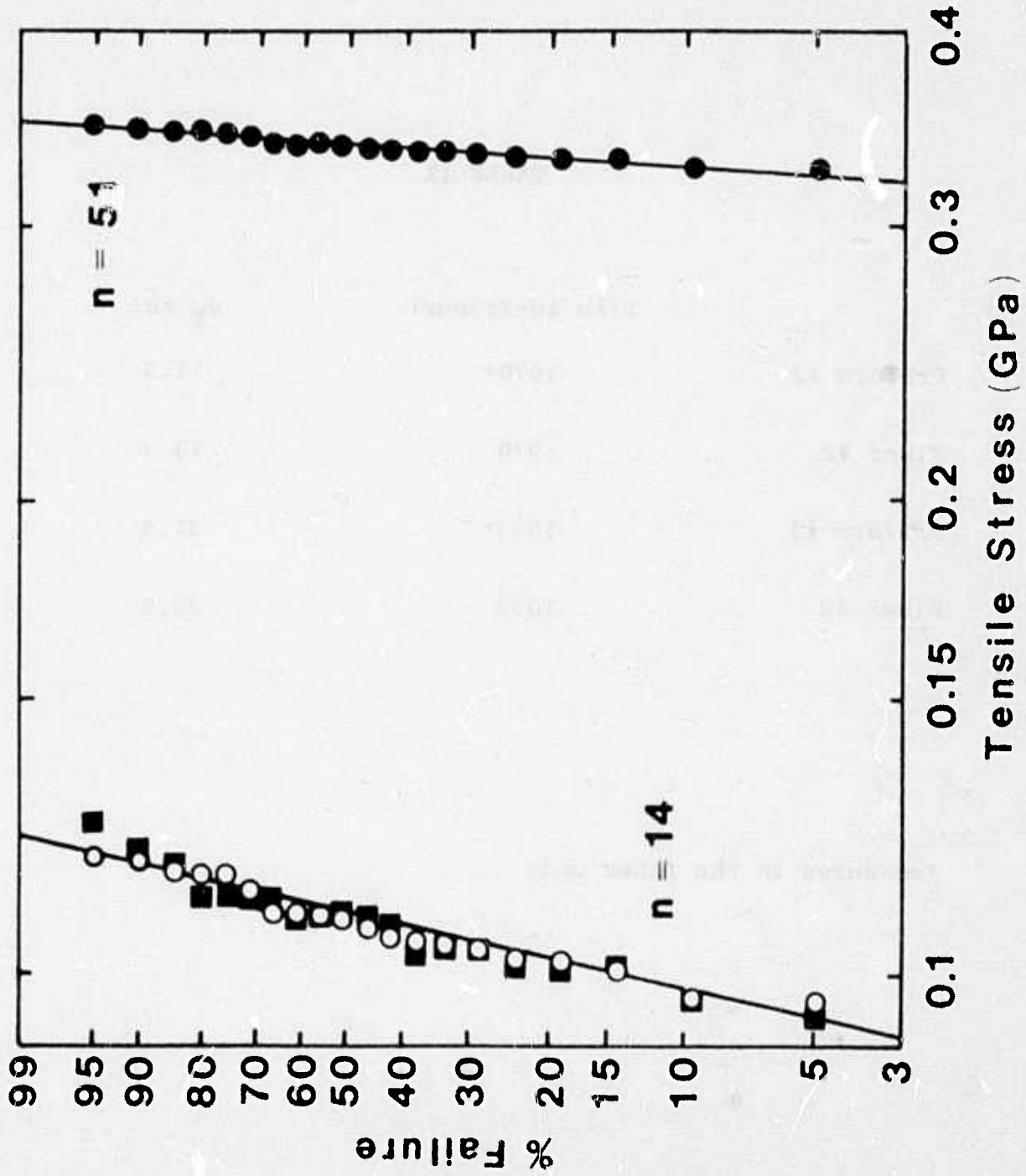

FIGURE 8 - A Weibull plot of the tensile strength of abraded Phasil and Cs-K-Bi doped fibers.

drawn from Preform #3 measured in air. The closed circles are plotted according to Eq. (7) with σ_u taken as zero. The apparent Weibull slope is 51. The ■'s represent the strength of abraded Phasil which has the approximate composition of the clad of Preform #3 but no compression. If we take the strengthening of Fiber #3 to be approximately given by the difference in the average strengths of the Phasil fiber and Fiber #3 and taking that as σ_u (σ_u = 32.9 ksi) we obtain the points plotted as open circles. The Weibull parameter is reduced to 14 which agrees with that of the abraded Phasil as one would expect if the abrasion gave comparable flaw populations to both fibers. The observed strengthening in this case is thus 32.9 ksi which is in excellent agreement both with the predictions of Eq. (3) and the photoelastic measurements.

The clad of Molecular Stuffed fibers may contain up to 0.5% by weight of the core dopant. This could lead to stress corrosion and reduced strength during a slow tensile test. By performing the tests in liquid nitrogen these effects should be eliminated. Fiber #2 was tested in liquid nitrogen and its strength compared in Fig. 9 to that of a 96% silica fiber also measured in liquid nitrogen. In this case following the same procedure as with Fiber #3, we find that the observed strengthening is 11.7 ksi which is slightly higher than determined by photoelastic measurements in the preform and fiber but differs from the value shown in Table I by 25%. The value in Table I was for the fiber at room temperature. If the value is recalculated using liquid nitrogen temperature, close agreement is obtained.

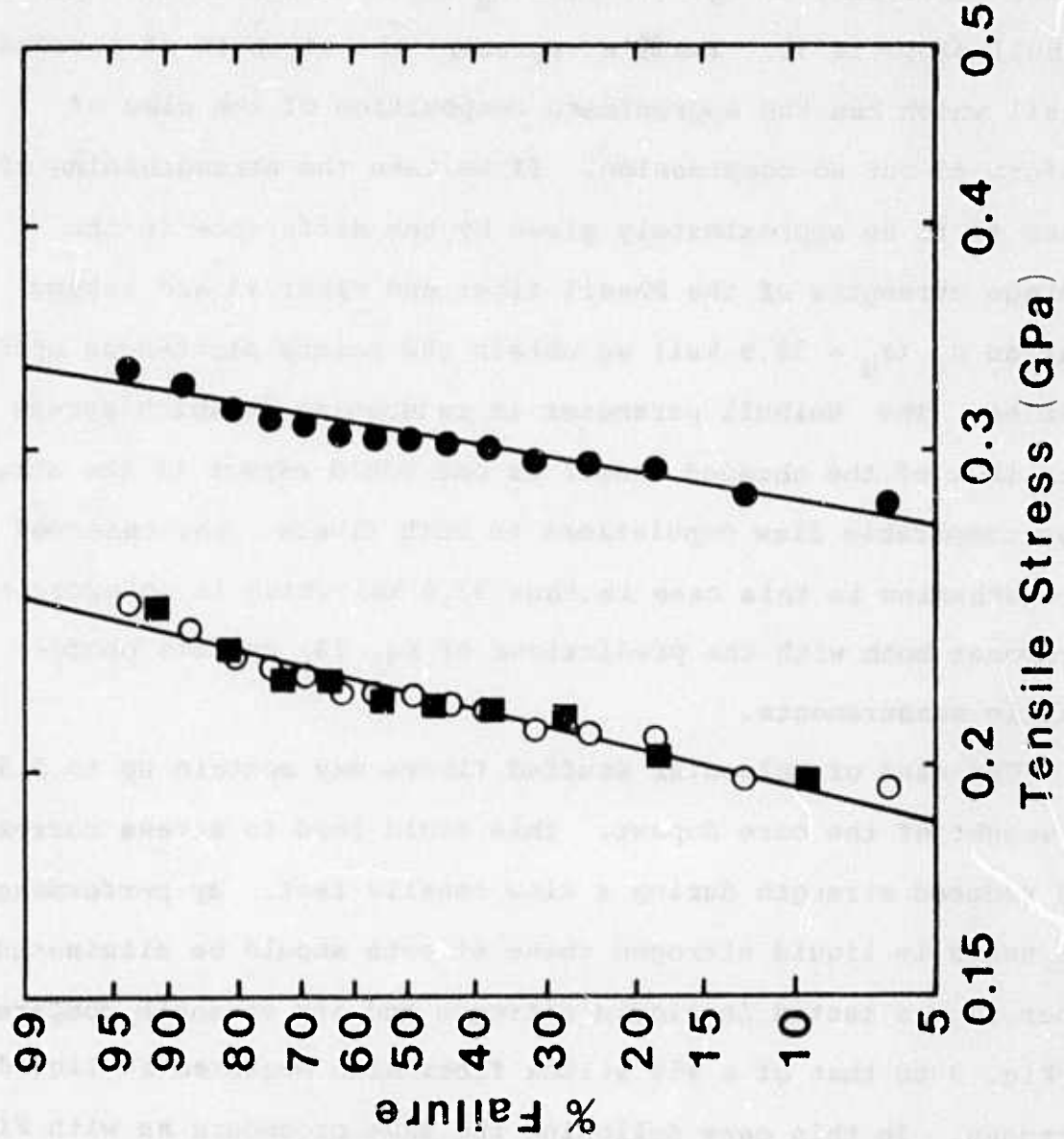

FIGURE 9 - A Weibull plot of the tensile strength of abraded Vycor and Cs doped fibers measured in liquid nitrogen.

D. CONCLUSIONS

We have shown that laminated preforms having residual surface compression as predicted by consideration of the physical parameters of the core and clad glasses can be made by the Molecular Stuffing process. The cladding stresses observed photoelastically in the preforms are transmitted to the fibers and are the same within experimental error. The observed strengthening in the fibers is consistent with the predictions of theory and with the photoelastically determined compression.

IV. STATIC FATIGUE

A. Introduction

The effects of static fatigue on the lifetime of glass optical fibers remains as a largely unknown factor in the implementation of fiber optics systems. This section attempts to demonstrate that the use of surface compression in glass fibers increases the time to failure under load in a predictable way and establishes a useful fatigue limit which guarantees no failures for expected static loads.

Improvements in preform fabrication, drawing technology and polymer coatings have resulted in the ability to draw kilometer lengths of optical fiber having tensile strengths in excess of 500 ksi.[14] Even with these high initial strengths and the abrasion protection afforded by polymer coatings our current understanding of long time static fatigue is not sufficient that we can guarantee fiber lifetimes of 20 years or more. Several possible fatigue models exist which fit the available data.[15] Unfortunately available data does not extend sufficiently in time to distinguish among these models for which long time predictions may vary by orders of magnitude.[16] At least until static fatigue is better understood it would be desireable to have a means of preventing subcritical crack growth or at least slowing it down.

It has been suggested that a fatigue limit exists for glass[17] but this is not universally accepted and remains in doubt as an answer to the problem. It has been experimentally determined that eliminating water from the glass environment will reduce or eliminate subcritical crack growth for high silica glasses.[18] Metal coatings

have been used with some success to provide a hermetic seal to the glass fiber surface and appears to eliminate static fatigue.[19] Metal coatings have fatigue and corrosion problems of their own, however, and cannot be considered a complete answer.

Surface compression, on the other hand, offers a simple means of preventing subcritical crack growth for loads less in magnitude than the surface compression. In many telecommunications applications the static loads are expected to be less than 20 ksi (corresponding to a 2.5 cm bend radius for a 125 μm diameter fiber) and we have found that compression of this magnitude can be easily obtained in optical fibers using the Molecular Stuffing process. It should be possible to use the vapor deposition technique as well to obtain surface compression of this or greater magnitude.[20]

In this paper we demonstrate the effects on fiber lifetime of surface compression by comparing the static fatigue of samples of two fibers having a 96% type silica surface, one fiber having compression and the other having no compression. For loads greater than the compression, fiber lifetime is extended in a predictable way.

B. Theory

Since the time scale of our static fatigue experiments is insufficient to aid in distinguishing among the various static fatigue models we have chosen the statistical approach of the Weibull probability distribution to represent our data. The failure probability of fibers of equal length at a given applied

stress σ is given by

$$F = 1 - A \exp(-t^b) \tag{9}$$

where A is a constant. An expression of the same form can be written which combines the effects of load and time

$$F = 1 - A' \exp\{-(\sigma - \sigma_u)^m t^b\} \tag{10}$$

where A' is a constant, σ_u is the minimum fracture stress, normally taken as zero for glass and m and b are Weibull parameters characterizing the width of the distribution in failure stress and time respectively.

If m and b are true constants or at least independent of any variable in a set of experiments one can relate data corresponding to equal failure probability by the equation

$$\sigma_1^m t_1^b = \sigma_2^m t_2^b \tag{11}$$

obtained from equation (10) where σ_1 and σ_2 are static loads and t_1 and t_2 are the corresponding failure times. This expression may be rewritten as

$$\log \frac{t_1}{t_2} = \frac{m}{b} \log \frac{\sigma_2}{\sigma_1} \quad . \tag{12}$$

If we replace m/b by n we have an expression identical to one obtained by Weiderhorn[21] by considering the relation between crack velocity, crack size, applied load and the critical stress intensity factor. n is sometimes called the static fatigue parameter. Resistance to static fatigue increases with n. If n were a constant

we could use equation (12) to make long time predictions from short time data.

The parameter n is not a true material constant, however, but appears to depend upon the environment, crack geometry as well as glass composition. Reported values for fused silica range from 15 to 35 depending on test conditions. The factors controlling n are not well determined and this fact means that long time predictions extrapolated from short time data may be in serious error. However for a small range of loads and identical test conditions one would not expect large variations in n and equation (12) can be used over a limited range in time.

If the minimum strength of a fiber is not zero as in the case of a fiber having residual surface compression of magnitude $|\sigma_R|$, then in equations (11) and (12) we must replace σ by $\sigma - |\sigma_R|$.

C. Experimental Procedure

The object of the experiment reported here was to isolate the effects of surface compression on the fatigue characteristics of glass fiber. This was done by comparing the time to failure under static load for samples of fibers with and without surface compression.

The fiber samples having compression were drawn from a step index Cs_2O doped Phasil preform prepared by the Molecular Stuffing process. The undoped Phasil clad of the fiber is a 96% silica type glass which has similar strength characteristics to commercial 96% silica glass. The nominal composition of the clad is 94% SiO_2,

greater than 5.5% B_2O_3 and less than .5% Cs_2O_2 by weight. The fiber samples not having compression were drawn from commercial 96% silica cane having nominal composition 96.5% SiO_2, 0.5% Al_2O_3, 3% B_2O_3 by weight.

Before testing, the fibers were given a uniform abrasion over a 2.5 cm length. The abrasion was performed by 400 grit silicon carbide abrasive paper as described in Section III. The abrasion served two important purposes. First, it eliminated any effects of drawing conditions or preform surface quality on the fiber strength. Second, it reduced the tensile strength of the fibers so that the measured strength was comparable in magnitude to the compressive strengthening.

Immediately after abrasion the fibers were placed under static load. The load was applied by hanging weights from a 10 cm diameter capstan which was suspended by a loop formed by the fiber. The gauge length of the fibers was unimportant since the breaks always occurred in the abraded section of the fiber.

The fibers were placed in an environmental chamber with the relative humidity and temperature set at 40% and 21°C respectively. A rod was placed through the center of the load capstans to catch the load when a fiber broke and to produce a loud noise so breakage would be immediately detected. During the day, breaks were detected and recorded manually, while at night or when the lab was unoccupied a microphone was used to detect the noise

caused by a break. The signal from the microphone was amplified and applied to a soleniod used to operate the shutter of a motor driven instant camera which photographed the broken fiber and a clock, thus giving the time of breakage for that fiber.

D. Results and Discussion

Prior to loading the samples the compressive strengthening in the CsO_2 doped fiber was determined by comparing its abraded strength with that of a similarly abraded fiber drawn from commercial 96% silica cane. The results of tensile tests made at a 40% strain rate following abrasion with 400 grit silicon carbide paper are shown in a Weibull plot in Figure 10. The observed strengthening as defined in Section III was 23.5 ksi and the abrasion yielded a Weibull slope of 8.

As described previously abraded samples of 96% silica and the Cs_2O doped fiber were loaded for static fatigue tests. The 96% silica fiber was loaded at 8 ksi and 11 ksi while the doped fiber was loaded at 30 ksi and 32 ksi. The test was conducted for 90 days and the results are shown in a Weibull plot in Figure 11.

If one considers equation (10) with σ_u given by $|\sigma_R|$ then the qualitative results shown in Figure 11 are exactly what is expected. The time to failure for a given load is shifted toward longer times by the presence of surface compression. That is the

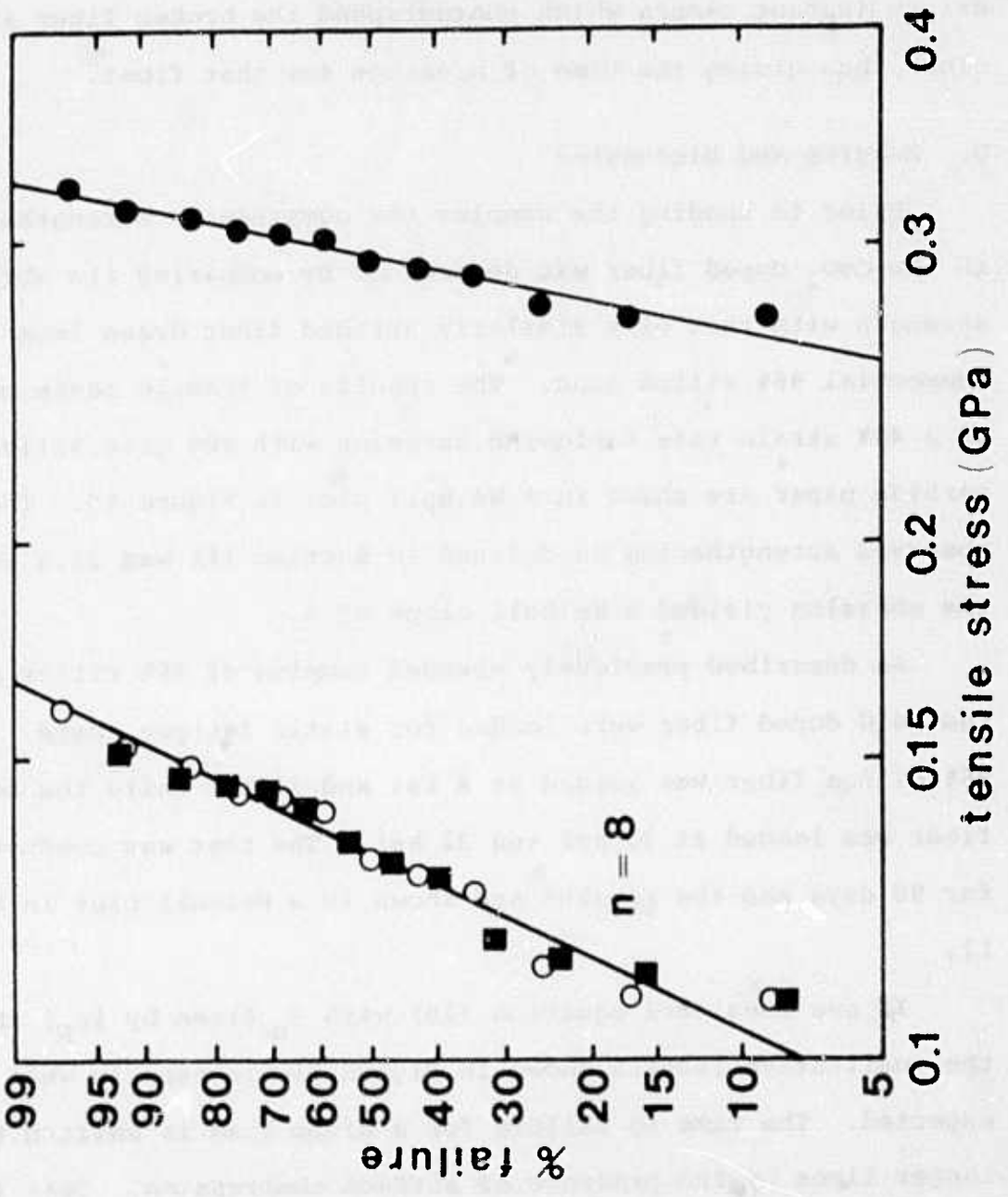

FIGURE 10 - A Weibull plot of the tensile strength of abraded Vycor and Cs doped fibers.

FIGURE 11 - A Weibull plot of the time to failure as a function of static load of abraded Vycor and Cs doped fibers.

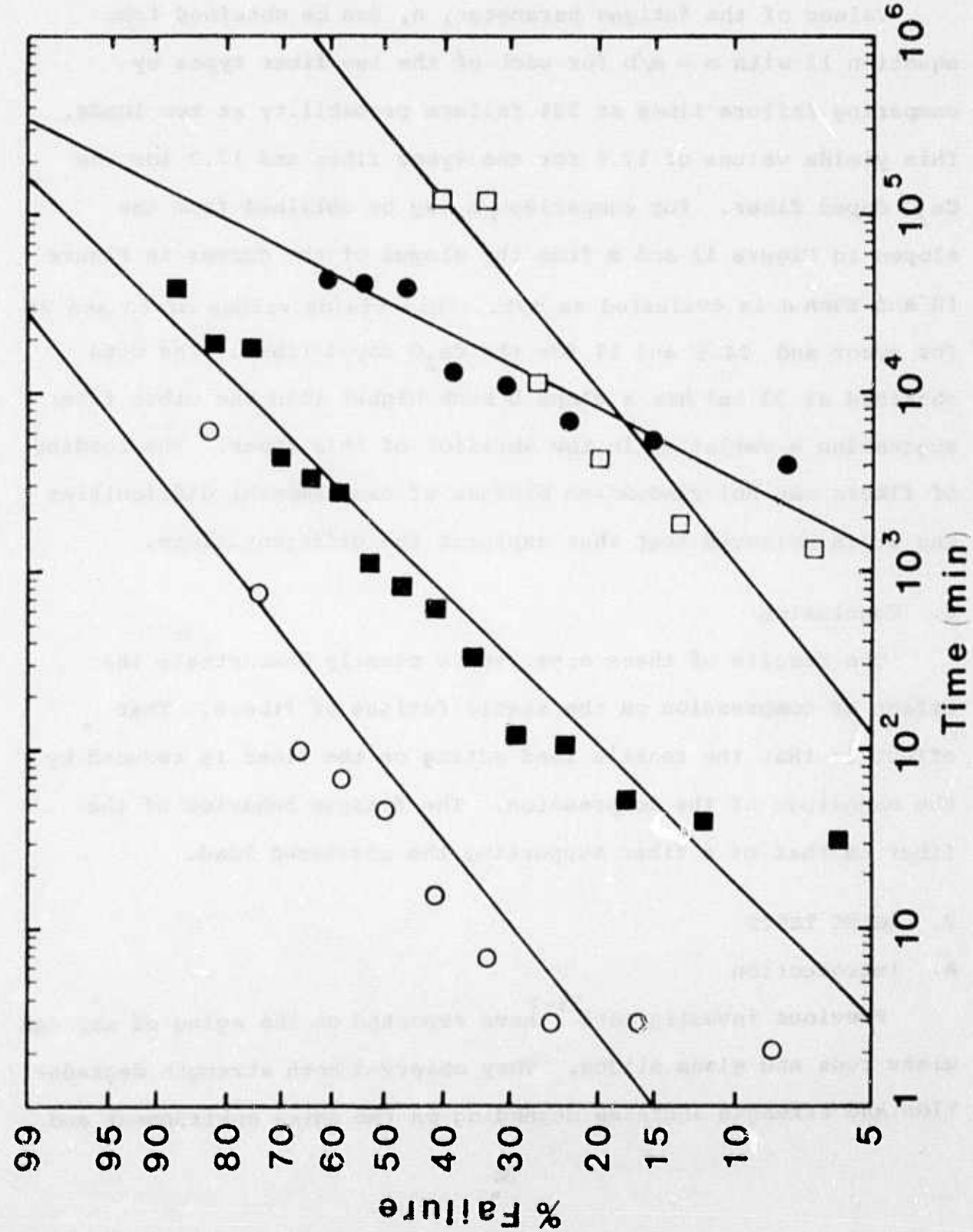

the Cs_2O doped fiber shows failure times consistent with loads of 6.5 ksi and 8.5 ksi rather than the actual loads of 30 and 32 ksi.

Values of the fatigue parameter, n, can be obtained from equation 12 with n = m/b for each of the two fiber types by comparing failure times at 50% failure probability at two loads. This yields values of 17.6 for the vycor fiber and 17.7 for the Cs_2O doped fiber. For comparison, b may be obtained from the slopes in Figure 11 and m from the slopes of the curves in Figure 10 and then n is evaluated as m/b. This yields values of 10 and 24 for vycor and 24.5 and 19 for the Cs_2O doped fiber. The data obtained at 32 ksi has a slope b much higher then the other fiber suggesting a variation in the abrasion of this fiber. The loading of fibers was not randomized because of experimental difficulties and it is believed that that explains the different slope.

E. Conclusion

The results of these experiments clearly demonstrate the effect of compression on the static fatigue of fibers. That effect is that the tensile load acting on the fiber is reduced by the magnitude of the compression. The fatigue behavior of the fiber is that of a fiber supporting the decreased load.

V. AGING TESTS

A. Introduction

Previous investigators[23-7] have reported on the aging of abraded glass rods and glass slides. They observed both strength degradation and strength increase depending on the aging environment and

on whether the aging was done before or during testing. The suggested mechanisms of aging differ depending on whether the strength increased or decreased due to aging. Those who observed decrease in the strength suggested that the strength degradation is due to one or more of the following mechanisms: 1. proton-sodium ion exchange, 2. silica-oxygen bond breakage, and 3. hydroxyl ion corrosion. Those observing strength increase suggested the following mechanisms: 1. stress release by splinters of glass wedged in the fresh cuts, 2. partial chemical healing of the cracks, and 3. chemical rounding of the crack tips.

In the present study, samples of abraded high silica glass fibers with and without surface compression wereaged in solutions of different pH under no load conditions for different lengths of time. In addition, fibers with different levels of surface compression were aged in ambient atmosphere and in controlled atmosphere under static loads less or equal to the surface compression.

B. Experimental Procedure

1. Preform and Fiber Preparation

Preform and fiber preparation is described in sections II and III. The work reported here used the Molecular Stuffing process to produce step index preforms having a Phasil clad and a core composed of cesium or Cs-K-Bi doped Phasil. The typical surface compression observed in such fibers is 12 to 33 ksi in clads 5 to 20 μm thick.

FIGURE 12 - The effect of aging for short times in different media on the strength of Suprasil (S.S.) and Vycor fibers.

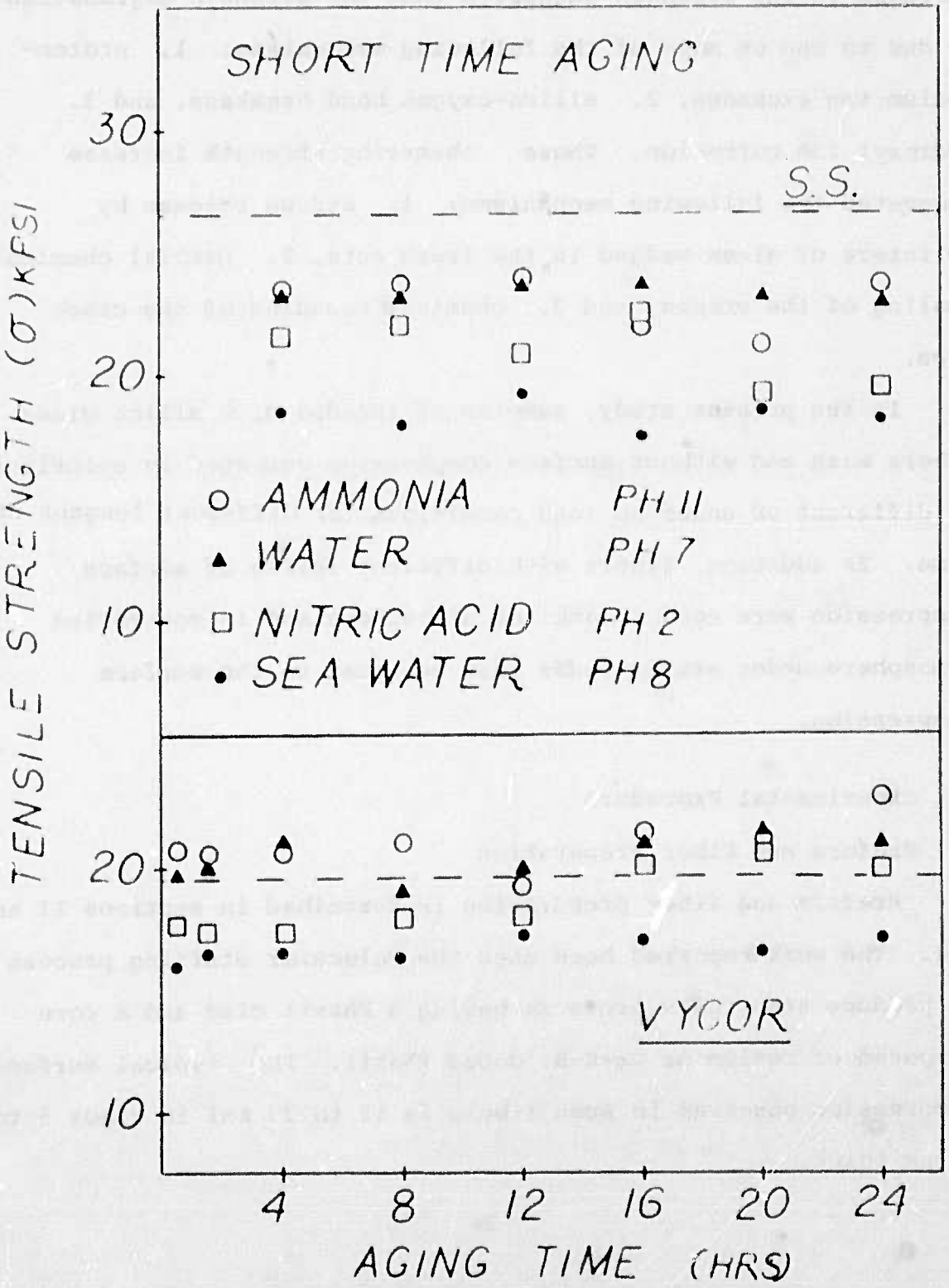

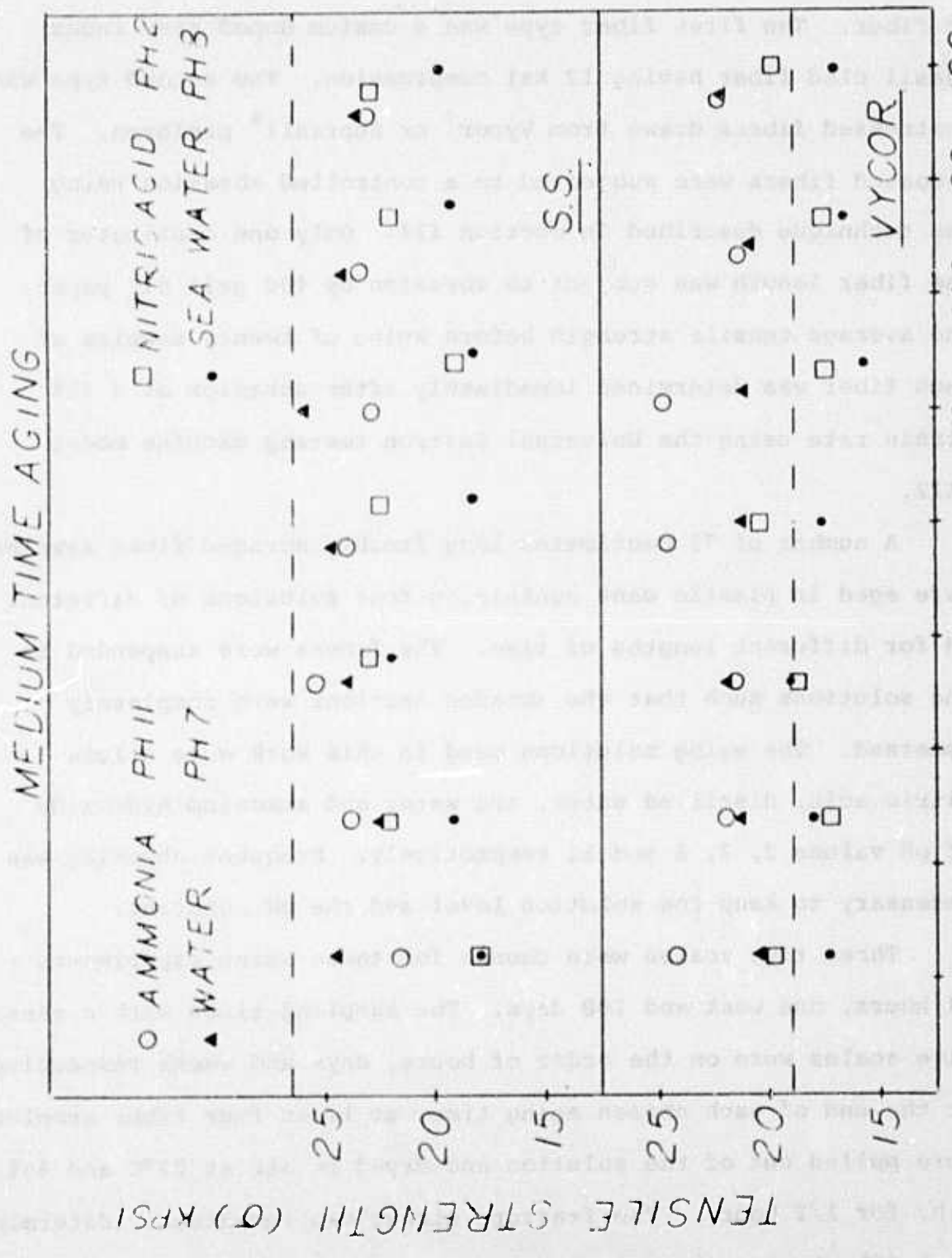

FIGURE 13 - The effect of aging for 20-180 hours in different media on the strength of Suprasil and Vycor fibers.

2. Aging Under No Load

This aging experiment was carried out on two different types of fiber. The first fiber type was a cesium doped step index Phasil clad fiber having 12 ksi compression. The second type was unstressed fibers drawn from Vycor[†] or Suprasil[‡] preforms. The uncoated fibers were subjected to a controlled abrasion using the technique described in Section III. Only one centimeter of the fiber length was subject to abrasion by 400 grit SiC paper. The average tensile strength before aging of twenty samples of each fiber was determined immediately after abrasion at a 40% strain rate using the Universal Instron testing machine model 1122.

A number of 75 centimeter long freshly abraded fiber samples were aged in plastic cans containing four solutions of different pH for different lengths of time. The fibers were suspended in the solutions such that the abraded sections were completely immersed. The aging solutions used in this work were dilute nitric acid, distilled water, sea water and ammonium hydroxide of pH values 2, 7, 8 and 11 respectively. Frequent checking was necessary to keep the solution level and the pH constant.

Three time scales were chosen for these aging experiments - 24 hours, one week and 100 days. The sampling times within these time scales were on the order of hours, days and weeks respectively. At the end of each chosen aging time, at least four fiber samples were pulled out of the solution and dryed in air at 22°C and 40% r.h. for 1/2 hours. The fracture stress was immediately determined at a 40% strain rate using the tensile testing machine. The tensile

strength after each aging time was then calculated as the average fracture stress of these fiber samples.

3. Aging Under Static Loading

Aging experiments under static tensile stress were performed on two uncoated abraded fibers: No. 1 a cesium doped step index phasil clad fiber having 24 ksi compression, and No. 2 a Cs-K-Bi doped step index phasil clad fiber having 33 ksi compression. Two sets of samples were taken from each fiber. The first set was abraded and the fracture stress immediately determined at a 40% strain rate using the tensile testing machine. The second set of samples from each fiber was similarly abraded and placed under static load by suspending weights from the fibers. The loads were in two groups of 19 and 2[illegible] ksi for fiber No. 1 and loads ranging from 10.5 to 32.5 ksi for fiber No. 2. Fiber No. 1 was aged in an environmental chamber for approximately 100 days at 40% r.h. and at 22°C. Fiber No. 2 was aged for 231 days under ambient laboratory conditions (20-80% r.h., 25 - 20°C). The aged fiber samples were then broken at a 40% strain rate on the tensile testing machine.

C. Results and Discussion

1. Short and Medium Time Aging

Vycor and Suprasil fibers were used in this experiment. The fiber strength determined at a 40% strain rate after aging was plotted against aging time as shown in Figures 12 and 13. Each point in these figures represents the average strength of at

least four fiber samples. The dashed line at 27 ksi for Suprasil and at 19 ksi for Vycor represents the average strength of the fibers measured at a 40% strain rate before aging.

The average tensile strength of the Suprasil fibers decreased after the initial aging period of 4 hours to a value of 23.6 kpsi, 23.4 kpsi, 21.5 kpsi and 18.6 kpsi after aging in ammonia solution of pH 11, water of pH 7, nitric acid solution of pH 2 and sea water of pH 8 respectively. Further aging did not seem to cause additional decrease in the tensile strength of the Suprasil fiber. The fluctuation in strength is observed within the standard deviation of the strength measurement. Figures 12 and 13 show that the degradation in the strength of Suprasil fiber as a result of aging in ammonia solution and water is not as severe as that observed when the fibers were aged in nitric acid solution or sea water.

In the case of Vycor fiber there is only slight strength change, if any, as in the case of Suprasil. Vycor fibers appear to show some strength increase in ammonia and water and very little change in nitric acid or sea water. The strength changes are only several ksi and are not significantly larger than experimental uncertainties in these measurements.

The conclusion to be reached from the short and medium time aging of these severely abraded high silica fibers is that there are only minor effects if any on the strength. These results probably cannot be extrapolated to effects on flaw free high strength fibers.

2. Long Time Aging

Uncoated abraded Vycor fibers were aged in ammonia (pH 11), water (pH 4), nitric acid pH (2) and sea water (pH 8) for periods ranged from 3 weeks to 9.5 weeks. The average tensile strength of this fiber is plotted against aging time in Figure 14. The average strength of fiber aged in ammonia increased by 37% after 21 days and by 100% after 67 days. Vycor fiber aged in water (pH 7) experienced a very gradual increase in the average strength. No significant strength change was observed as a result of aging in nitric acid or sea water.

Glass fibers with low surface compression (12 kpsi) were aged in the same solutions for 100 days. The fracture stress of 10 samples for each solution were determined at a 40% strain rate. The results are shown on Weibull plots of strength versus failure probability in Figure 15 together with the results obtained for the same fiber before aging. The increase after aging, in ammonia in the net breaking stress was 100%, however, a decrease of the strength of 10%, 31% and 43% was observed when the fibers were aged in water (pH 7), nitric acid (pH 2) and sea water (pH 8) respectively.

Figure 16 is a plot of the aging strength normalized to the original strength before aging versus aging time of Vycor and prestressed fiber (12 ksi). It is obvious that the relative strength increase is the same. We also plotted the normalized strength of prestressed fiber with relatively high surface compression (33 ksi) aged in air and in ammonia (pH 8.5) in the same figure. The increase in the strength of the high

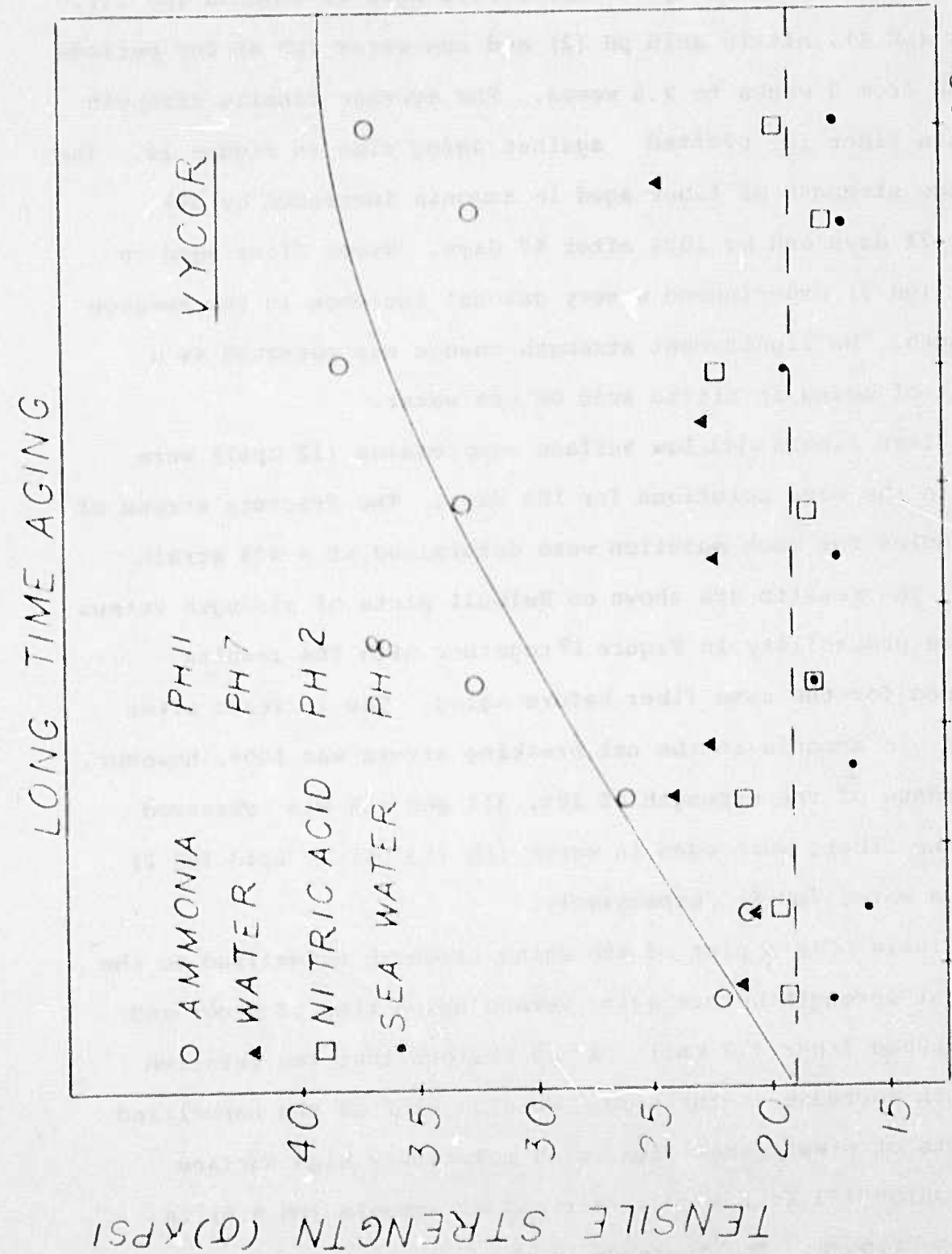

FIGURE 14 - The effect of aging for long times in different media on the strength of Vycor fibers.

FIGURE 15 - The effect of aging for 100 days on the strength of a Cs doped fiber as a function of aging media.

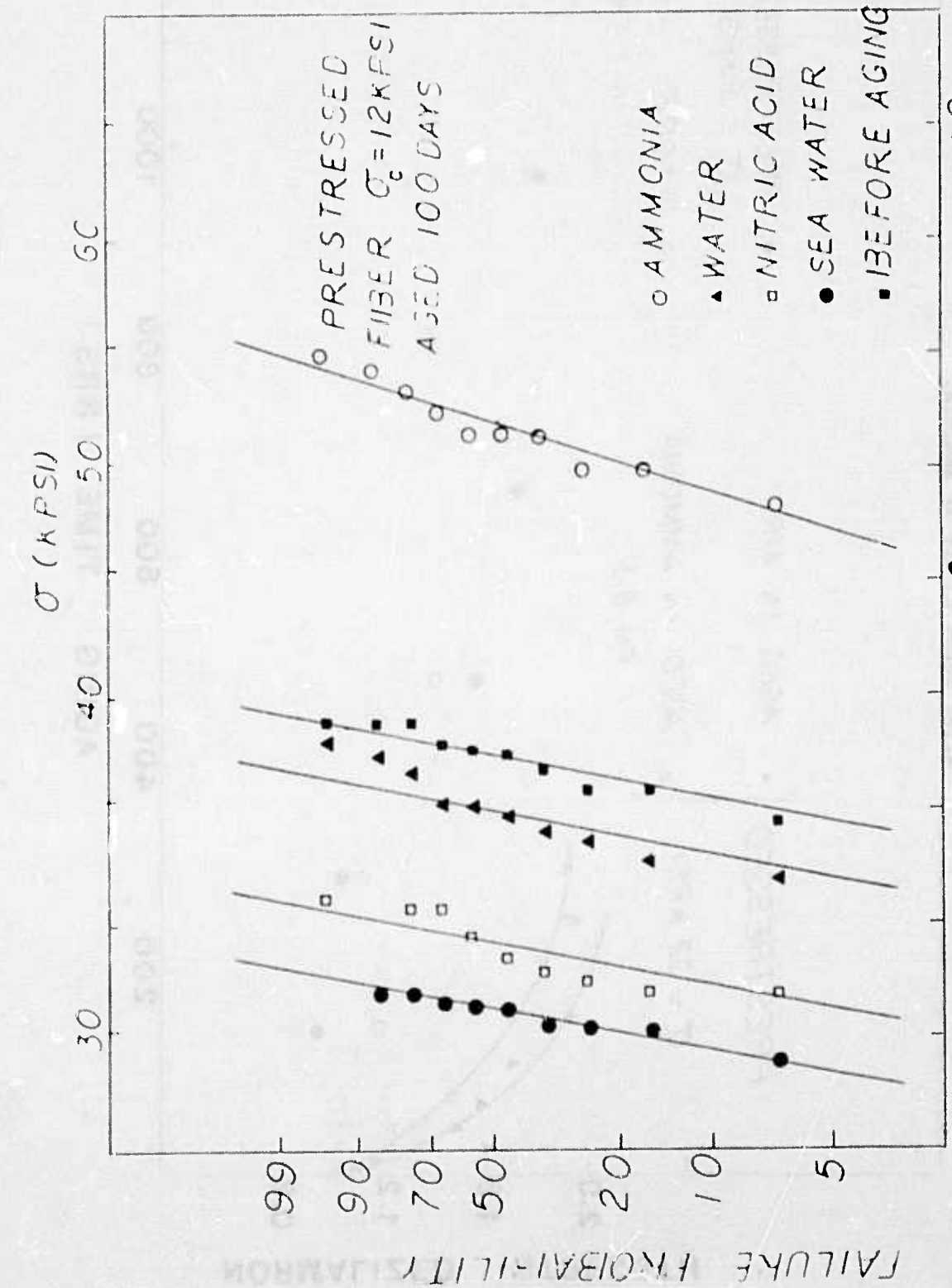

FIGURE 16 - The normalized strength increase observed in Vycor, Cs and Cs-K-Bi doped fiber after aging in air or ammonia.

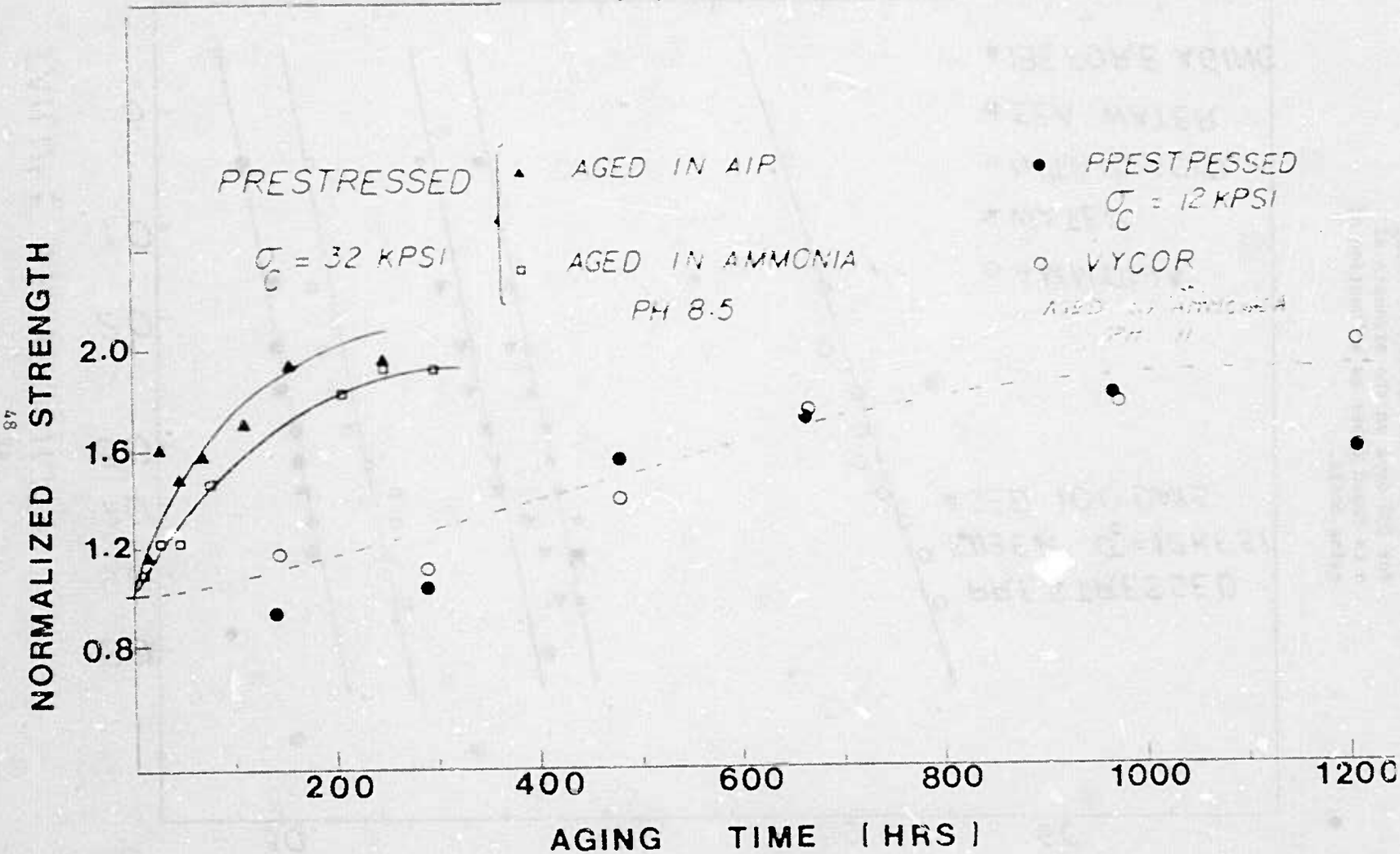

compression fiber (33 ksi) is more rapid than for the unstressed and low stress fibers but the strength increase appears to saturate at the same relative increase. In contrast to short time aging, where strength changes barely outside experimental uncertainty were observed, long time aging indicates some trends. Aging of abraded high silica fiber with small or no compression in ammonia solutions causes a strength increase which saturates at an increase of 100% after about 800 hours. In the case of fibers having high compression the strength increase was more rapid but saturated at a similar relative strength increase.

It is believed that the observed strength improvement can be explained by the chemical rounding of the tips of the abrasion induced surface flaws. The strength increase saturates because very little chemical attack is required to increase the relative magnitude of the crack radius of an initially sharp crack. The stress amplification at the crack tip varies inversely as the square root of the crack radius so strength improvement is rapid at first. As the crack tip radius becomes larger it takes increasingly more chemical attack to cause a large relative change in crack radius and strength.

The fact that the highly prestressed fiber showed more rapid strength increase than the other fibers might be due to some effect of the surface compression. It is more likely, however, that this fiber had a higher dopant concentration in the clad than the other two fibers examined. This would make it more susceptible to chemical attack and thus more rapid aging.

3. Aging Under Static Tensile Load

Aging experiments were performed on two prestressed uncoated, abraded fibers: No. 1 a cesium doped step index phasil clad fiber having 23 ksi compression and No. 2 a Cs-K-Bi doped step index phasil clad fiber having 33 ksi compression. Two sets of samples were taken from each fiber. The first sets were abraded and the fracture stress immediately determined at a 40% strain rate using a tensile testing machine. The results are shown on Weibull plots of strength versus failure probability in Figures 17 and 18. The abrasion was such that the strength of a similarly abraded and tested Phasil fiber not having surface compression was 16 to 18 ksi. This corresponds to an idealized Griffith flaw on the order of 10 μm deep.

The second set of samples from each fiber was similarly abraded and placed under static load by suspending weights from the fibers. The loads were in two groups of 19 and 23 ksi for fiber No. 1 and loads ranging from 10.5 to 32.5 ksi for fiber No. 2. Fiber No. 1 was aged in an environmental chamber for approximately 100 days at 40% r.h. and at 22°C. Fiber No. 2 was aged for 231 days under ambient laboratory conditions (20 - 80% r.h., 25°C). The aged fiber samples were then broken at a 40% strain rate on a tensile testing machine. The results were plotted on Weibull plots as shown in Figures 17 and 18.

A significant increase in the strength after aging was observed in both fibers. It did not appear that the aging depended significantly on the magnitude of the net fiber load

FIGURE 17 - The strength of a Cs-K-Bi doped fiber before and after aging under load for 231 days.

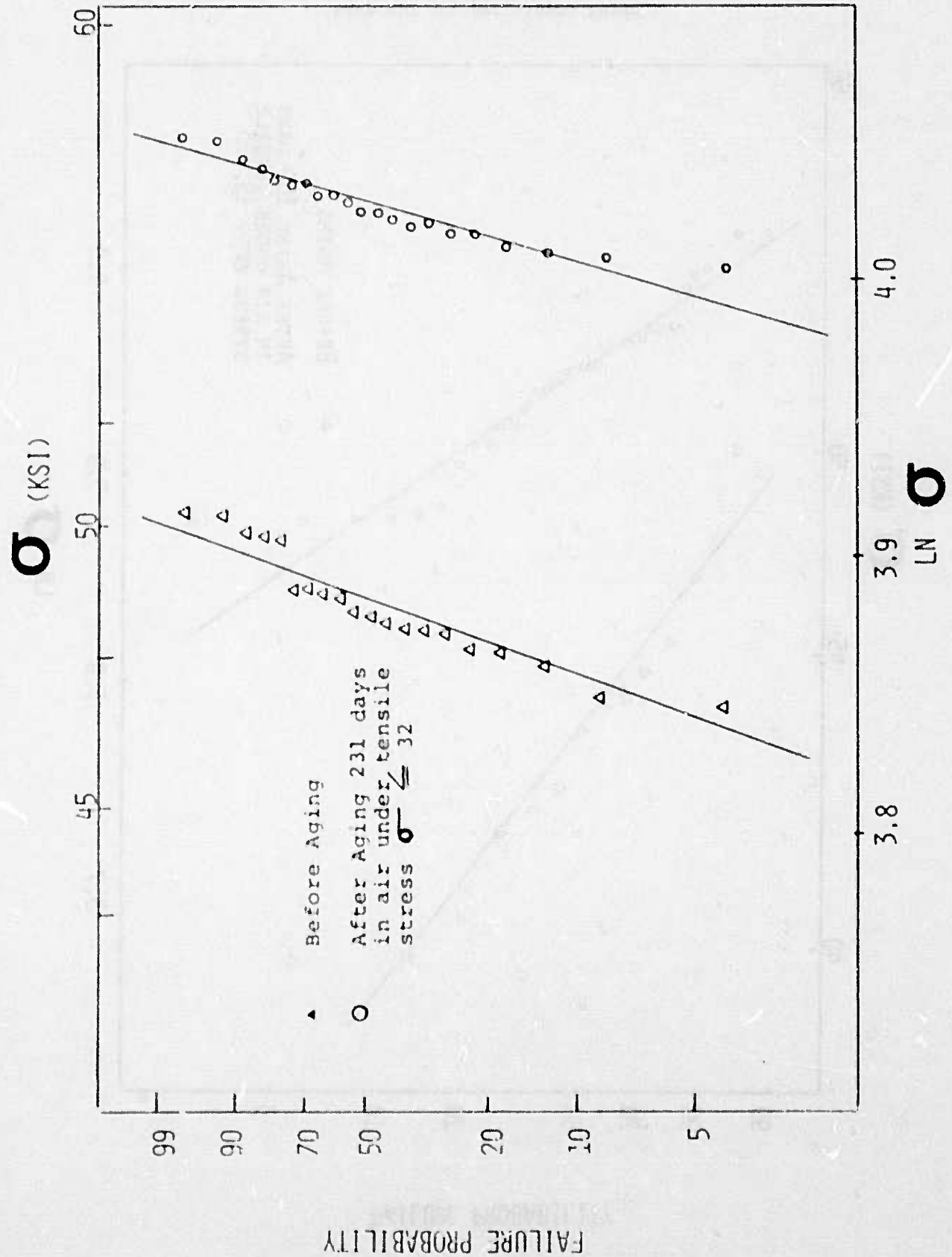

FIGURE 18 - The strength of a Cs doped fiber before and after aging under load for 100 days.

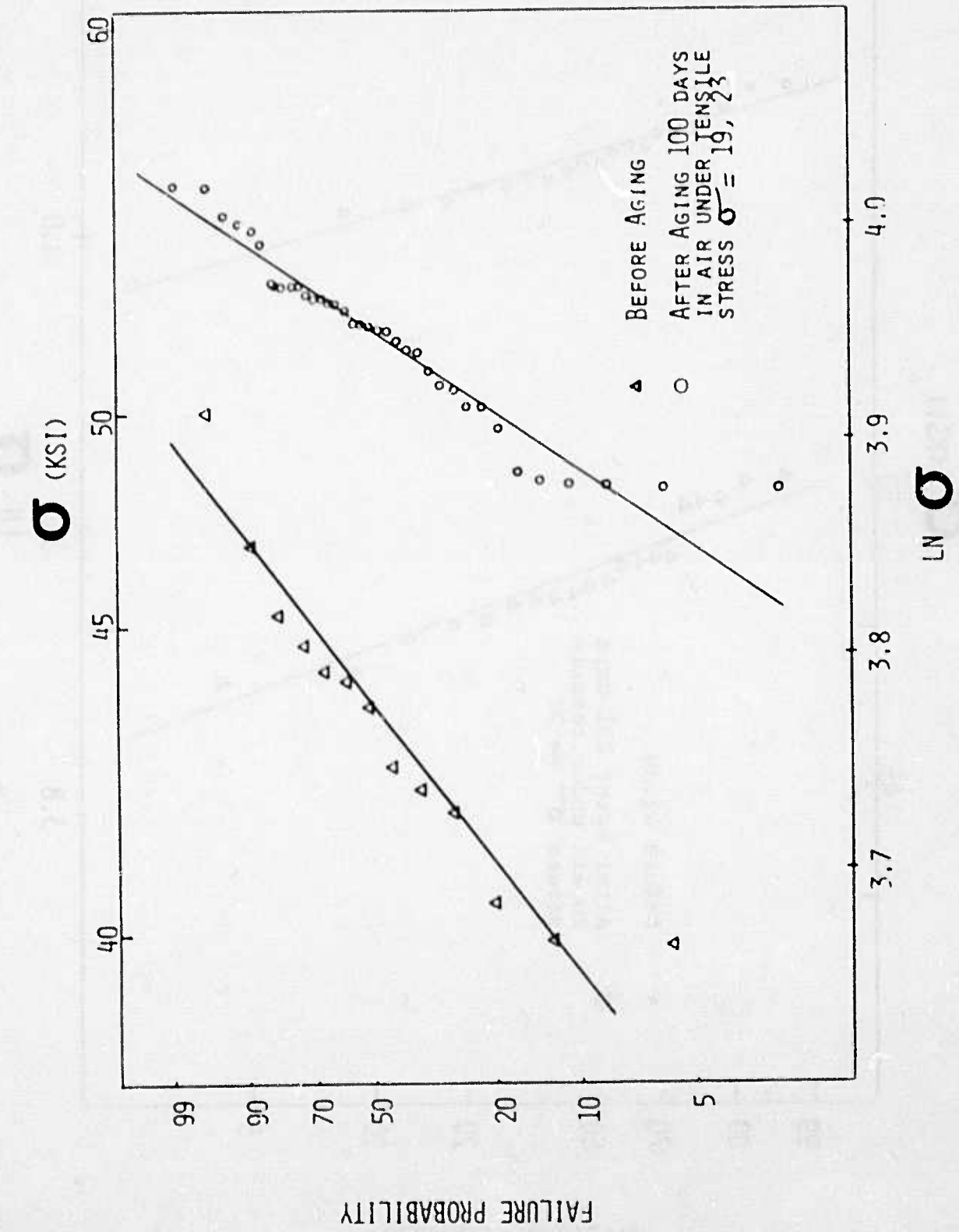

$\sigma_n = (\sigma_a - \sigma_c)$, where σ_a is the applied stress and σ_c is the magnitude of the compression, so the data for the different loads were combined for each fiber. The increase after aging in the net breaking stress measured by the tensile test was approximately 50% for both fibers. The mechanism for this strength improvement is not identified and further experimentation will be required to determine it. It is suspected, however, that rounding of crack tips due to the chemical action of water is the most likely strength improvement mechanism.

D. Conclusions

Aging experiments of a very preliminary nature were performed on abraded high silica fibers as a function of aging environment. Water and ammonia environments tended to cause strength improvement or little change depending on aging time. Nitric acid and sea water appeared to cause some strength degradation.

Surface compression does not appear to have a significant effect on aging itself. However, if a fiber is under tensile load and that load is less than the magnitude of the surface compression static fatigue does not occur and in fact the strength may improve. This may prove significant for the preservation of fiber strength for fibers stored at or deployed under conditions of moderate tensile load.

† Vycor, a product of Corning Glass Works, Corning, New York
‡ Suprasil, a product of Amersil Inc., Hillside, New Jersey

VI. The Photoelastic Measurement of Stress in Optical Fibers

A. Introduction

In previous sections we have discussed the strengthening effects observed in fibers designed to have surface compression. To verify that the strenghening was in fact due to surface compression it was necessary to measure directly the axial compression in samples of the tested fibers. The phenomenon of stress birefringence gives a convenient means of obtaining the magnitude of the stresses in glass fibers.

The birefringence produced in isotropic solids by the application of stress was discovered by Brewster.[28] From his work, the theory of photoelasticity has been developed[29] and the concept of the stress optic law has been formulated,[30,31] which in the case of a fiber is given by

$$P_z = \frac{Nf}{t} \qquad (13)$$

where P_z is the axial stress, t is the light path length in the sample and N is the relative retardation, defined as $\theta/180°$ where θ is the retardation angle. f is sometimes called the stress optic coefficient, i.e., it relates the stress to the retardation observed through a given optical path. f is wavelength dependent and is usually quoted for a wavelength of 5460 $\mathring{A}$.

We have utilized Friedel's method of compensation in developing a polariscope for measuring both the stress profile and the stress optic coefficient in optical fibers. The polariscope was found to give good reproductibility, has a spacial resolution of 0.4 μm and can be used to determine the stress optic coefficient in fibers with and without a clad. The results of the clad compression obtained

using this polariscope agree reasonably well with the observed strengthening found in the same fibers using tensile tests.

B. Theory

1. The Stress Profile

As stated previously the axial stress P_z, in the compressed clad, of the optical fiber, can be determined from Equation (13). The light path length, ℓ, can be related to the distance of the measurement point from the liquid-clad interface. From Fig. 19 it is shown that:

$$\ell = 2x \sqrt{\frac{2R}{x} - 1} \tag{14}$$

where R is the radius of the glass fiber. Thus Eq. 13 becomes

$$P_z = \frac{Nf}{2x \sqrt{\frac{2R}{x} - 1}} \tag{15}$$

The retardation angle, θ, is determined by Friedel's method of compensation. See Fig. 20.

$$\text{Let } A_1 = a \sin wt \tag{16}$$

be the amplitude of the plane-polarized beam emerging from the polarizer. At the clad of the optical fiber the polarized light can be considered as decomposed into components of amplitude A_2 and A_3 along the principal directions.

$$A_2 = A_1 \cos 45° = \frac{a}{\sqrt{2}} \sin wt \tag{17}$$

$$A_3 = A_1 \cos 45° = \frac{a}{\sqrt{2}} \sin wt \tag{18}$$

FIGURE 19

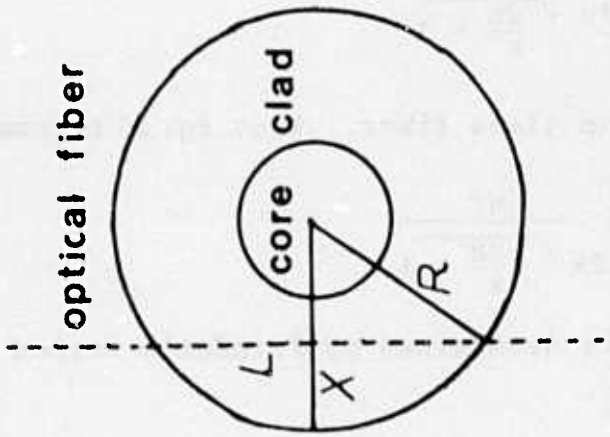

$$L/2 = \sqrt{R^2-(R-X)^2}$$

$$L/2 = \sqrt{R^2-(R^2-2RX+X^2)}$$

$$L/2 = \sqrt{2RX-X^2}$$

$$L/X = \sqrt{2R/X-1}$$

$$L = 2X\sqrt{2R/X-1}$$

FIGURE 19 - Optical path length for photoelastic stress measurement.

FIGURE 20

FRIEDEL'S METHOD OF COMPENSATION

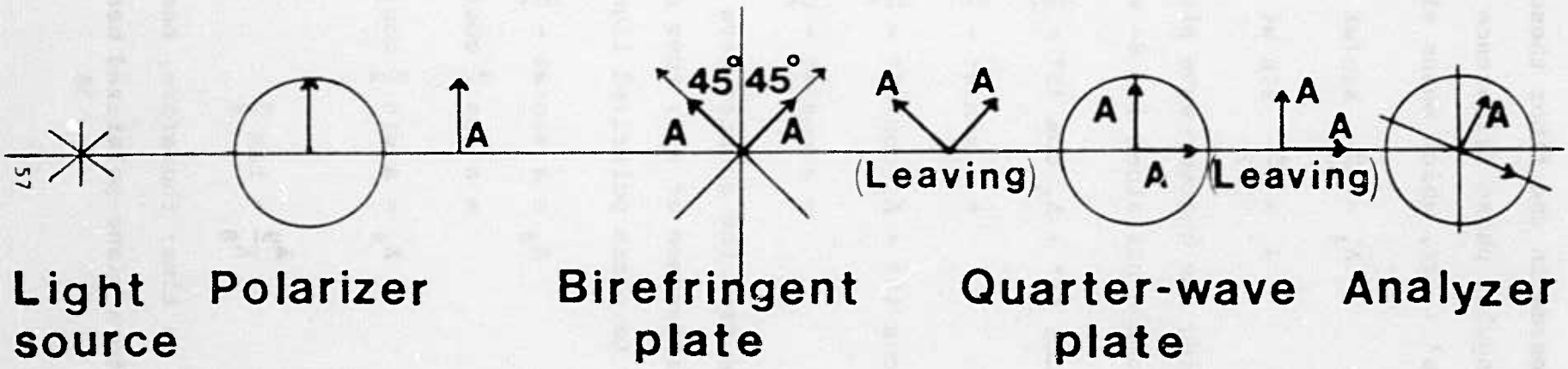

Due to stresses in the fiber these beams emerge from the fiber with an angular phase difference ($\alpha = 2k\pi + \alpha'$) where k is an integer and $\alpha' < 2\pi$, which means elliptically polarized light

$$A_4 = \frac{a}{\sqrt{2}} \sin(wt - \alpha) \tag{19}$$

$$A_5 = \frac{a}{\sqrt{2}} \sin wt \tag{20}$$

Upon entering the quarter-wave plate, these components are resolved into components along its S- and F-axes,

$$A_6 = A_4 \cos 45° + A_5 \cos 45° = \frac{a}{2} [\sin(wt - \alpha) + \sin wt]$$

$$= a \sin(wt - \frac{\alpha}{2}) \cos \frac{\alpha}{2} \tag{21}$$

$$A_7 = A_5 \cos 45° - A_4 \cos 45° = \frac{a}{2} [\sin wt - \sin(wt - \alpha]$$

$$= a \cos(wt - \frac{\alpha}{2}) \sin \frac{\alpha}{2} \tag{22}$$

The beams emerge from the quarter-wave plate with an additional angular phase difference of $\pi/2$, thus changing the elliptically polarized light to plane polarized light,

$$A_8 = a \sin(wt - \frac{\alpha}{2} - \frac{\pi}{2} \cos \frac{\alpha}{2} \tag{23}$$

$$= a \cos \frac{\alpha}{2} \cos(wt - \frac{\alpha}{2})$$

$$A_9 = a \sin \frac{\alpha}{2} \cos(wt - \frac{\alpha}{2}) \tag{24}$$

The ratio

$$\frac{A_9}{A_8} = \tan \frac{\alpha}{2} \tag{25}$$

does not depend on time; therefore, beams A_8 and A_9 when combined are equivalent to a plane-polarized beam of amplitude

$$A_{10} = (A_9^2 + A_8^2)^{1/2}$$

$$A_{10} = a \cos(wt - \frac{\alpha}{2}) \tag{26}$$

making an angle $\alpha/2$ measured clockwise from the vertical. If the optical axis of the analyzer is rotated clockwise from its initial orientation perpendicular to that of the polarizer by an angle $\theta = \frac{\alpha}{2}$, its polarizing axis becomes perpendicular to the plane-polarized beam A_{10}, and extinction is obtained. An angular phase difference at the point is

$$\alpha = 2k\pi + \alpha' \quad 2k\pi = \quad 2\theta \tag{27}$$

and the relative retardation or fringe order is

$$R = N = \frac{\alpha}{2\pi} = k + \frac{\theta}{\pi} \tag{28}$$

Thus one can find the stress at different positions, the stress profile, in the clad of the glass fiber by Eq. (13).

2. Stress Optic Coefficient

In the above section the theory explaining Friedel's method of compensation was discussed with reference to determining residual axial stress at an arbitrary point in an optical fiber if the stress optic coefficient is known. If a known axial stress is applied to the fiber instead, the same method can be used to determine the stress optic coefficient. A known stress can be applied as shown in Fig. 21 by suspending weights from the fiber.

The change in stress on the fiber is then given by

FIGURE 21

FIBER MOUNTING FOR STRESS OPTIC COEFFICIENT

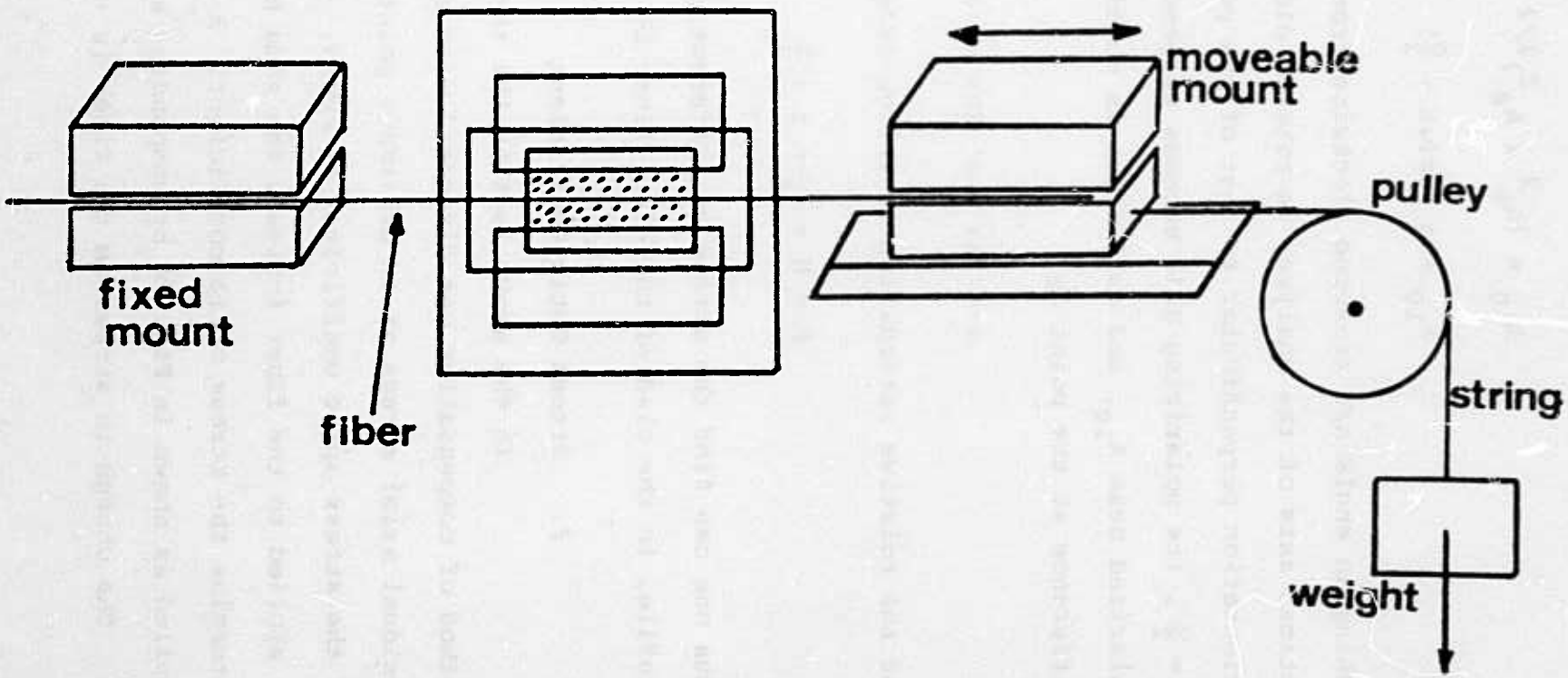

$$\Delta P_z = \frac{\Delta\omega}{\pi R^2} \tag{29}$$

where $\Delta\omega$ is the weight. Thus Eq. (15) becomes

$$\Delta\omega = \frac{\pi R^2 \, fN}{2 \times \left(\frac{2R}{x} - 1\right)^{\frac{1}{2}}} \tag{31}$$

Since $N = \theta/180$ the slope, S, of the line obtained by plotting $\Delta\omega$ versus θ for a series of weights can be used to obtain f. f is then given by

$$f = \frac{180\ell S}{\pi R^2} \tag{32}$$

This discussion assumes that when weights are suspended from the fiber the applied stress is proportional to the area of the fiber and is constant across the cross section. If, however, the Young's moduli of the core and clad E_c and E_d respectively are not equal the load will not be shared according to area. In that case the stress optic coefficient in the clad f_{clad} will be given by

$$f_{clad} = f \, \frac{E_c A_c + E_d A_d}{E_d} \, \frac{1}{A_c + A_d} \tag{33}$$

where f is the coefficient determined experimentally as described above and A_c and A_d are the core and clad areas respectively.

C. Experimental Procedure

1. Stress Profile

The stress profile in fibers was determined by the experimental set-up shown schematically in Fig. 22. A small piece of fiber (~ 15 cm) was mounted on a frame placed between a polarizer and an analyzer. The polarizer and the analyzer were rotated so

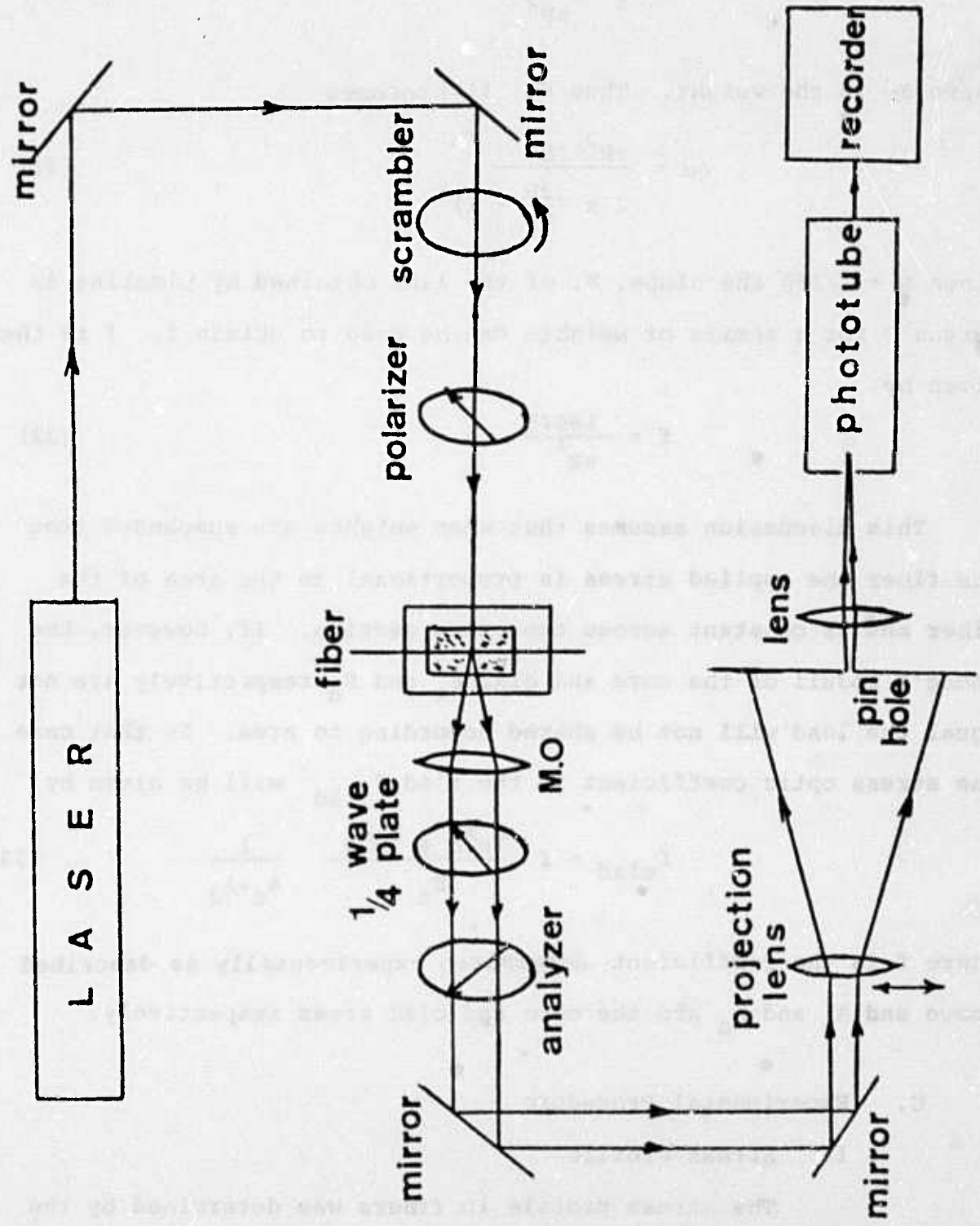

FIGURE 22 - Schematic diagram of the stress measurement apparatus.

that their axes of vibration were perpendicular to each other and at 45° with the fiber axis. A quarter-wave plate was placed between the fiber and the analyzer with one axis parallel to the axis of the polarizer. The coherent light emitted from an Argon ion laser at .5145 μm was made incoherent by passing it through a scrambler (a rotating semitransparent plastic disc). The light was incident perpendicular to the fiber axis. In order to avoid light bending due to the curvature of the fiber surface, the fiber was immersed in a liquid with refractive index 1.458, which closely matched the refractive index of the phasil clad. The liquid and fiber were held in a cell constructed of microscope slides. A 20X microscope objective and a projection lens were used to expand and image the fiber cross section on the plane of a .7 mm diameter pinhole. A ~ 150 μm diameter fiber was expanded into a ~15 cm diameter image.

Accurate focusing of the fiber image on the pinhole plane was found to be difficult due to interference effects. Low light intensity also makes focusing difficult. Initial attempts using a xenon lamp and a 50 mw He-Ne laser were unsuccessful or marginal. Ar. argon ion laser was found to be most convenient for our purposes. High power is available for focusing. However, the power should be reduced during measurements to ~ 80 mw or less to avoid heating of the index matching liquid. It was determined that focus was achieved when the clad liquid interface was observed to disappear.

Different locations in the fiber could be examined by scanning the image of the fiber across the pinhole by translating the projection lens using a micrometer translation screw. The linearity of the imaging system (20X microscope objective plus the projection lens) was verified by replacing the fiber holder with a calibrated

microscope scale. The magnification of the imaging system and calibration of the micrometer translation screw were also determined by a similar procedure.

To obtain the retardation due to stress at a point within the fiber that point is imaged on the pinhole. The analyzer is then rotated through an angle θ determined by extinction of light passing through the pinhole. The light intensity is detected by a photomultiplier and monitored on a chart recorder. The retardation profile is found by determining the extinction angle as a function of position in the fiber.

2. Stress Optic Coefficient.

The apparatus for measuring the stress optic coefficient in fibers is identical to that for measuring stress profiles with the exception of the fiber mount. The mounting arrangement for these measurements is shown schematically in Figure 21. The two fiber ends are clamped in the fixed and moveable mounts. Force is transmitted to the fiber by suspending weights from the string. In this way a known stress can be applied to the fiber and the resultant retardation can be determined as described above. Care must be taken that the addition of weights does not displace the fiber and thus the fiber image at the pinhole. The fiber was held in guide grooves to prevent this. However, since the magnification of the optical system was very large(~ 1000), the position of the core clad interface was determined after each weight was added and the retardation angle determined at three points in the fiber near the center of the clad. The position of the core clad interface is easily determined because the retardation reaches a maximum at

that point and decreases rapidly as the observation path begins to include the core. Positions with respect to the core clad interface are reproducibly determined using the calibrated micrometer translater.

After retardation is found as a function of the applied weight the stress optic coefficient f is found through eq. 32. If the Young's moduli of the core and clad are different they must be determined experimentally and the modified eq. 33 must be used to determine f_{clad}.

To determine the Young's moduli we first determined the longitudinal and transverse sound velocities V_L and V_t respectively for the glasses using Brillouin spectroscopy and then used these to calculate the moduli. The Young's modulus is given by

$$E = \rho V_t^2 \quad \frac{3V_L^2 - 4V_t^2}{V_L^2 - V_t^2} \tag{34}$$

where ρ is the glass density.

D. Results and Discussion

1. Stress Optic Coefficient

The stress optic coefficient was measured in the clads of four fibers using the method described above. Before doing this the stress optic coefficient was measured in a Suprasil fiber in order to verify the accuracy of the technique. In this case the observed point was taken to be the center of the fiber. There the light retardation is a maximum and the light path is equal to the fiber diameter and varies only slowly with position.

The result of this experiment is shown in Fig. 23 where the weight applied to the fiber was plotted as a function of the light retardation in the fiber. From the best linear fit of the applied

FIGURE 23 - Retardation versus load for a suprasil fiber.

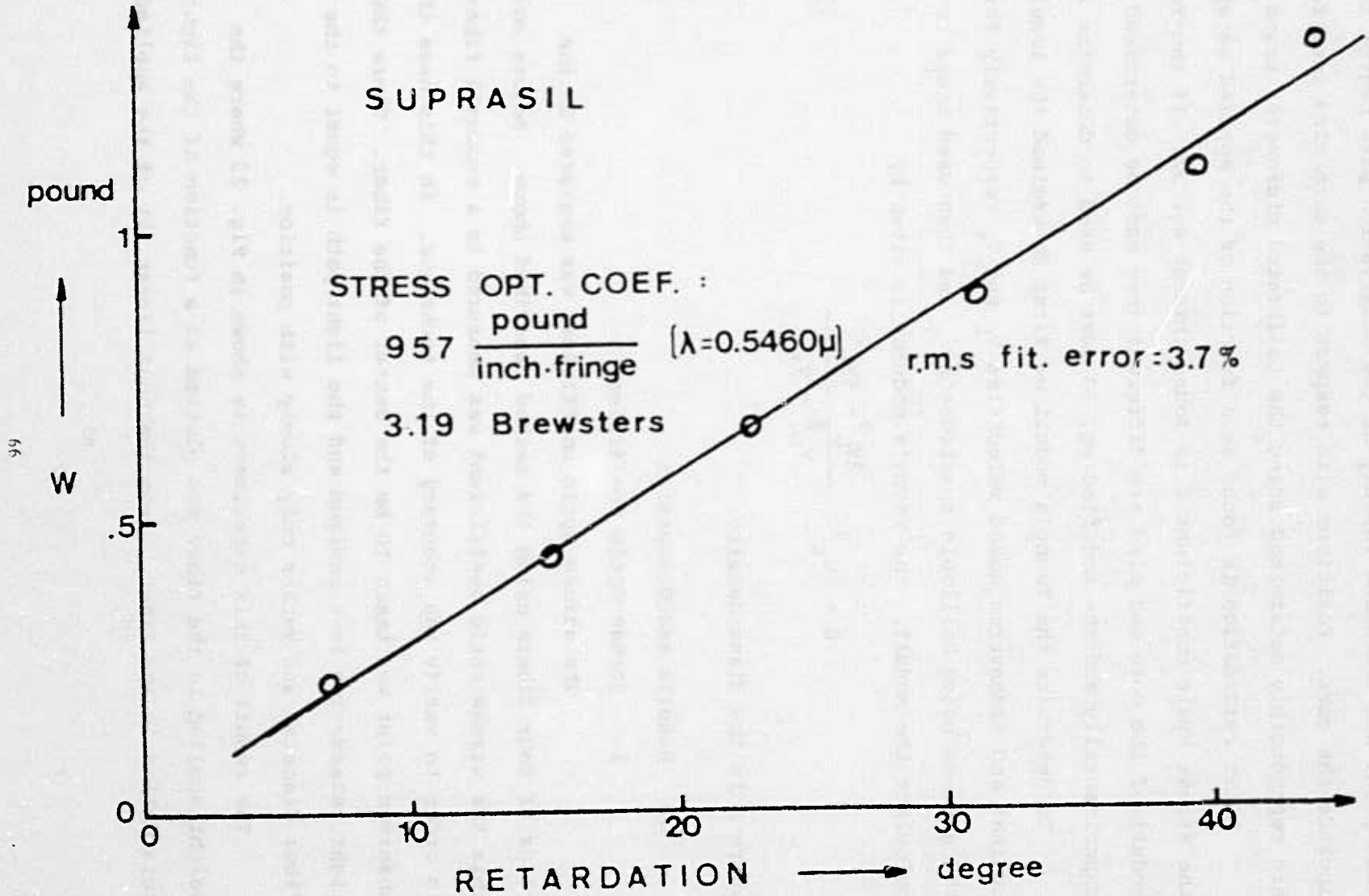

weight vs. retardation the slope, S, was obtained. Then from Eq. (32). with $\ell = 2R$ we can obtain the stress optic coeffcient, f. Three experiments were done using different sections of a Suprasil fiber. The results obtained are summarized in Table III. An average value for the stress optic coefficient, f, of 904 lb/in fringe was found for a wavelength of 5145 A.

In order to normalize these values to $\lambda = 5460$ A, the wavelength at which f is usually quoted, one simply multiplies f determined at 5145A by 5460A/5145A. A related parameter β which is also called, more correctly, the stress optic coefficient and is wavelength independent can be obtained using the relation[30]

$$\beta = \frac{0.56\lambda}{f} \tag{35}$$

where λ is the wavelength in angstroms at which f was measured. β is in units of Brewsters and f is in lb/in fringe.

This gives

$$f = 959 \ \frac{\text{pound}}{\text{inch-fringe}} \quad (\lambda = 5460 \text{ A}) \ ;$$

or 3.19 Brewsters for Suprisil which agrees with published values. Next unclad Phasil was measured using 4 different sections of a Phasil fiber and the results are summarized in Table III. The average stress optic coefficient obtained from these experiments was found to be:

$$f = (913 \pm 4\%) \ \frac{\text{pound}}{\text{inch-fringe}} \ (\lambda = 5145 \text{ A})$$

$$= (969 \pm 4\%) \ \frac{\text{pound}}{\text{inch-fringe}} \ (\lambda = 5460 \text{ A}).$$

or,

(3.16 $\pm$ 4% Brewsters

TABLE III

SUMMARY OF RESULTS FOR STRESS OPTIC COEFFICIENT

Fiber	Stress optic coefficient, f.			Core Dopant
	Brewsters	Pound / inch-fringe λ = 5460 A	Average f brewsters	
Suprasil (without clad)	3.19±4%	957	3.19±4%	
	3.18±4%	961		
	3.19±3%	957		
Phasil (without clad)	3.27±7%	935	3.16±4%	
	3.23±7%	947		
	3.03±9%	1009		
	3.10±5%	986		
Fibers with clad (clad:phasil, core:doped)	3.16±7%	968		Cs_2O
	2.80±5%	1093		Cs_2O
	2.69±7%	1136		Cs_2O
	2.78±7%	1100		Cs_2O-K_2O-Bi_2O_3

slightly larger than the coefficient found for a Suprasil fiber.

The experimental procedure outlined in Section C was then utilized to obtain the stress optic coefficient of the clad of 4 of the 8 fibers whose stress profiles were studied. These coefficients were expected to be similar to the coefficient of the Phasil fiber since the clad of these fibers was Phasil. The reproducibility of the experimental results was checked and found to be within 7%, becoming worse as the clad thickness becomes smaller. In these fibers the stress optic coefficient is given by Eq. (33) and it requires the knowledge of the Young's modulus for the core and the clad. The Young's modulus, E, can be calculated from Eq. (34) in terms of the glass density, the shear (V_t) and the longitudinal (V_L) sound velocities measured by Brillouin scattering. It was found that:

$$E_{ph} = (6.5 \pm .1) \times 10^{10} \text{ N/m}^2,$$

$$E_{c_s} = (6.6 \pm .1) \times 10^{10} \text{ N/m}^2,$$

$$E_{c_s} + B_i + K = (6.7 + .2) \times 10^{10} \text{ N/m}^2$$

where E_{ph}, E_{c_s} and $E_{c_s} + B_i + K$ is the Young's modulus in Phasil preforms, in preforms doped with Cs_2O and in preforms doped with $Cs_2O - K_2O - B_{i_2} O_3$ respectively. The results for the stress optic coefficient in the clad of the 4 fibers are summarized in Table III.

2. Stress Profile

The experimental procedure outlined in Section C was used to determine the stress profile in 8 step index fibers

all made using the Molecular Stuffing process. The clad of the fibers was Phasil (96% silica type glass) under compression and the core was doped with Cs_2O or Cs_2O-K_2O-Bi_2O_3. The value for the stress optic coefficients determined experimentally and given above were used to calculate the clad compression.

A typical retardation profile for a C_s-K-B_i doped fiber is shown in Fig. 24. The inflection in curvature observed near the liquid clad interface is due to instrumental resolution (diffraction effects and the finite size of the sampling pinhole) estimated to be approximately 0.4 μm. The position of the interface is required in calculating the path length in the fiber and thus the stress. We obtain that position by extrapolating the curve of retardation versus position as indicated by the dashed curve.

The stress profile calculated from the retardation for this fiber is shown in Fig. 25. The low stress values near the liquid clad interface are probably the result of the large uncertainty in the light path length for these points i.e. the path in the clad changes rapidly near the interface due to the fiber curvature. The discontinuities observed in the stress profile near the core clad interface are outside experimental error and may be due to inhomogeneities in the clad glass.

In determining the average clad stress, the data points close to the liquid-clad interface were ignored due to the large uncertainty in the path length at those points.

The reproducibility of the experimental results was checked by repeating the stress profile measurements on samples of three fibers. From those experiments similar profile shapes were

FIGURE 24

MOLECULARLY DOPED FIBER

CORE : $Cs_2O + Bi_2O_3 + K_2O$

RETARDATION PROFILE

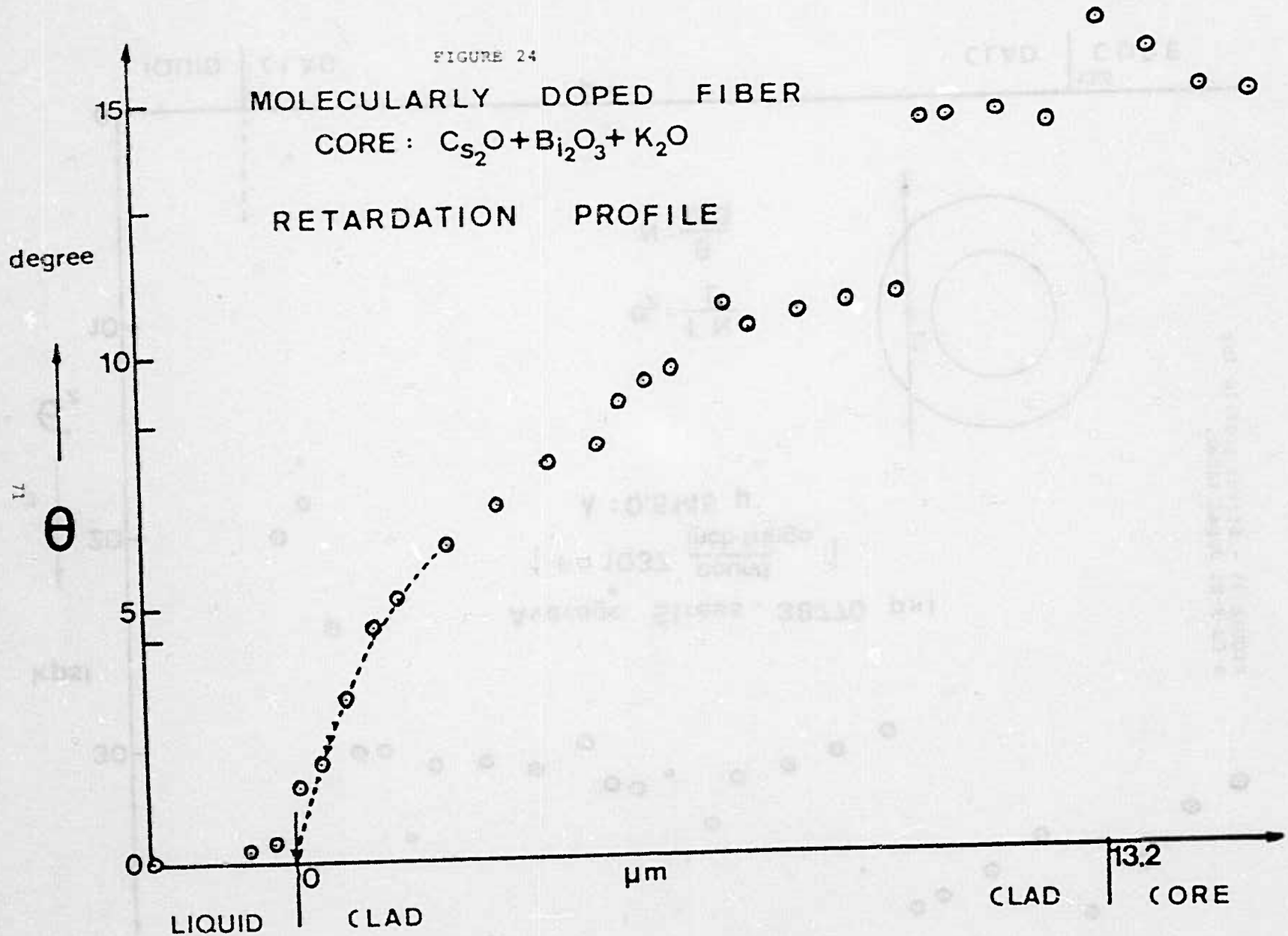

FIGURE 25 - Stress profile for a Cs-K-Bi doped fiber.

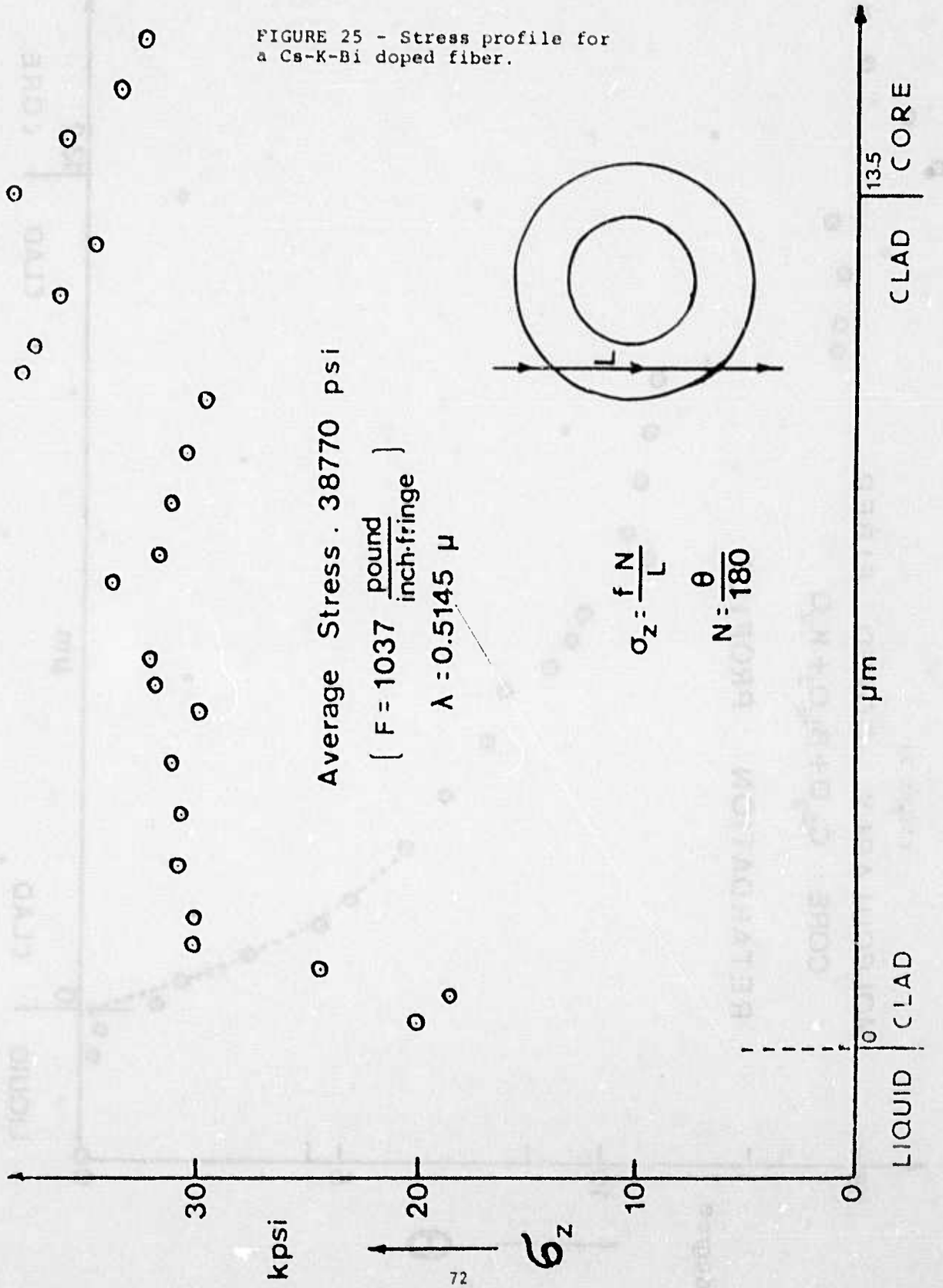

obtained and the average clad compression was reproducible to within 7%. The stress within the fiber clad was found to fluctuate as much as ± 12% in some fibers, as indicated in the third column of Table IV.

The clad stress measured on fibers was compared to the stress measured on the preforms using an optical microscope. Such a comparison indicates how stresses on performs transfer to fibers. Measurements on preforms were made using a Leitz model HM-POL polarizing microscope equipped with a 4-order tilting (Nikitin-Berek) compensator, a 2.5x or 10x objective and a 10x eye piece. The stress obtained at the middle of the clad for 7 performs is listed in Table IV second column, and is compared to the average stress in the clad found on the fibers drawn from these preforms given in the third column.

In addition the photoelastic measurements are compared to the strengthening observed in tensile tests listed in column 4 of Table IV and as described earlier in Section III. It can be seen that there is good agreement among the three measurement techniques giving us reasonable confidence that the strengthening effects we observe in compressively clad fibers is due to the compression.

E. Conclusions

We have developed a method suitable for the accurate measurement of stress optic coefficients and stress profiles in optical fibers. Small compositional differences in 96% silica type glasses appear to strongly affect the magnitude of the coefficient. In our fibers compositional differences are due in part to small amounts up to 0.5%, of dopants from the core which may have

TABLE IV

SUMMARY OF RESULTS FOR CLAD COMPRESSION

Stress optical coefficient $\left[\frac{\text{pound}}{\text{inch-fringe}}\right]$ (λ = 5460 Å)	PREFORM Stress kpsi	FIBER Average Stress kpsi	Strength results kpsi
968 ± 7%		19 ± 15%	24 ± 7%
1093 ± 5%	14 ± 5%	10 ± 12%	11 ± 4%
1136 ± 7%	12	10 ± 12%	10 ± 5%
1100 ± 7%	26	21 ± 12%	22 ± 5%
	33	33 ± 10%	32 ± 6%
	34	31 ± 8%	36 ± 5%
	31	26 ± 9%	24 ± 5%
	25	20 ± 13%	22 ± 4%

not been completely removed from the clad during processing.

The clad stresses we have measured in fibers agree well with those found in the preforms. In addition the compression observed photoelastically manifests itself in improved strength characteristics for the fibers.

VII. MOLECULAR STUFFING EXPERIMENTS

In this section we discuss the details of the experimental procedures involved in Molecular Stuffing to obtain strengthened fibers. Stuffing, unstuffing and washing solutions and the schedules for their use are presented. Drying, oxidation and collapsing schedules are also presented. The process details are included for the most successful of the dopant systems examined. Finally the experimental results of surface compression are shown for these dopant systems.

A. Selection of Dopant Materials

There are a number of criteria that dopants must satisfy to be useful for compressive strengthening of optical fibers using Molecular Stuffing. The most important of these are listed below and are discussed in detail in this section.

i. The oxide of the dopant must be miscible with silica and the other dopants.

ii. The dopant compound must undergo thermal decomposition to the oxide form below or near 620°C.

iii. The dopant compound and its oxide should have high distillation temperatures.

iv. The dopant oxide should lower the glass transition temperature of the silica matrix.

v. The dopant oxide should raise the expansion coefficient of the silica matrix.

vi. Dopants are required which raise the refractive index; others are required which have little effect on index.

vii. The dopant should have high solubility in water below 100°C. Solvents must be available for which the dopant solubility is about 10% and 1% by weight.

viii. The dopant must be available in high purity form (less than 20 ppb of most transition metals).

1. Phase Separation and Crystallization

To form a homogeneous glass having low light scattering phase separation and crystallization must be prevented. The tendency for phase separation becomes greater as the field strength of the cation, defined as Z/r, becomes larger (where Z and r are the ionic charge and radius respectively). In a binary silicate melt, each silicon ion coordinates with four oxygen ions tetrahedrally and the other cations bond to the non-bridging oxygen ions of the network. If Z/r of the cation is low, its coordination is weak and a single phase dominated by the silicon-oxygen network will result. On the other hand, if Z/r of a cation is high it can lead to a large bond strength, meaning that it can coordinate with non-bridging oxygens quite easily. These groups form a separate phase coexisting but not mixing with a high silica phase (i.e., liquid-liquid immiscibility). The effectiveness of alkali oxides in reducing phase separation is in the order:[32]

$$Cs > Rb > K > Na > Li \quad .$$

A similar order of reduced tendency to phase separation exists in binary alkaline-earth oxides:[33]

$$MgO > CaO > SrO$$

Alkaline-earth oxides break up the silica network and each cation produces two non-bridging oxygen ions.

Oxides such as Al_2O_3, BeO, TiO_2 and ZrO_2 are usually classified as intermediates because they can join the continuous network. For instance Al^{+3} ions can substitute for Si^{4+} ions forming an AlO_4 tetrahedra with negative charge in the network. Lead oxide can be introduced in the silica network in large amounts (e.g., 80% mole). Bi is expected to act as Pb in the network since it has a similar electronic shell configuration to Pb.[34]

Crystallization usually commences from a separated phase which is potentially more susceptible to nucleation and growth of crystals than the parent glass. Like phase separation, crystallization becomes more likely as the field strength of the cation becomes larger. The rate of growth is controlled both by heat flow and a diffusion process at the melt-crystal interface. Diffusion involved in crystallization is viscosity dependent, and at lower viscosity crystallization becomes more enhanced because molecules can move and rearrange themself to the more stable crystalline form. The velocity V of crystallization of a melt at temperature T is given by the following expression:[32]

$$V = \frac{L(T_m - T)}{3\pi a^2 \eta T_m} \tag{36}$$

Here L is the heat diffusion at the melting temperature T_m, η is the viscosity of the melt, and a is a distance on the order of a lattice spacing. Equation (36) indicates that glasses containing oxides which reduce the network viscosity are vulnerable to crystallization (e.g., those with Li_2O and Na_2O).

2. Dopant Decomposition

The dopant compound must undergo thermal decomposition to the oxide form below 620°C. At about 680°C the porous glass begins to sinter, therefore, if the decomposition temperature is around 680°C or above the gases produced by decomposition can not be removed. Accumulation of gases will give rise to a large pressure, which is capable of breaking the preform. Most of the nitrates are not thermally stable at high temperatures and will decompose below 620°C under reduced pressure and thus are good dopant candidates.

Cation polarizing power, defined as Z/r^2 is important in determining the thermal decomposition temperature. The higher Z/r^2 is, the more distorted is the NO_3 ion and the lower is the thermal decomposition temperature. Table V presents decomposition temperatures of some alkali and alkaline-earth metal nitrates.[35]

3. Distillation

A major problem arising in conjunction with thermal decomposition is dopant distillation which destroys the concentration profile by transporting dopants from the interior to the surface of the preform upon heating. For instance, the nitrates of all the alkali metals tend to distill at reduced pressure (vacuum is required during heating to remove water). This is enhanced by their ability to sublime. In most cases, distillation starts before the nitrate is fully decomposed. Nitrates of all the alkali metals are more volatile than their corresponding oxides. The distillation temperature of alkali

METAL NITRATE	Z/r^2	DECOMPOSITION TEMP. OF NITRATE (^oC)
$LiNO_3$	2.2	474
$NaNO_3$	1.0	529
KNO_3	0.57	533
$RbNO_3$	0.46	549
$CsNO_3$	0.36	584
$Be(NO_3)_2$	17.0	125
$Mg(NO_3)_2$	3.3	450
$Ca(NO_3)_2$	1.8	575
$Sr(NO_3)_2$	1.2	635
$Ba(NO_3)_2$	1.0	675

Table V

metal nitrates are given in Table VI.[36]

The extent of distillation can be reduced by depressing the decomposition temperature making it near or below the distillation temperature. This is accomplished by employing a thermally unstable salt, called the secondary salt, which has a catalytic effect on decomposition of the other nitrate compounds. The secondary salts must not interfere with optical or mechanical properties and must undergo decomposition below 300°C. An excellent example of a secondary salt is bismuth nitrate which thermally decomposes as low as 140°C. Strontium nitrate also appears to be useful in this role. The effect of bismuth nitrate in lowering the decomposition temperature of $CsNO_3$ is illustrated in Fig. 26. The pressure peak due to decomposition of $CsNO_3$ is shifted to lower temperatures by almost 100°C by the presence of bismuth nitrate. The pressure peak is observed by monitoring the pressure as a preform is rate heated while under vacuum.

4. Glass Transition Temperature

Dopants for strengthening must lower the glass transition temperature (T_g) of the matrix. T_g is dependent on the viscous behavior of the glass at high temperature. For glasses the activation energy for viscous flow is highest for vitreous silica (e.g. 170 kcal/mol at 1200-1400°C.). Any dopant oxides added to the silica network will tend to break up the network thus making viscous flow easier. For example, T_g falls rapidly as the sodium content of a glass is increased.

Both the alkaline earth and the alkali oxide, are effective in lowering T_g. Binary alkaline earth silicates have activation

SALT	MELTING POINT (^{o}C)	DISTILLATION FIRST OBSERVED (^{o}C)	STEADY DISTILLATION (^{o}C)
$NaNO_3$	310	350	450
KNO_3	335	350	450
$RbNO_3$	315	390	450
$CsNO_3$	415	450	500

Pressure = 50 millitorr

Table VI

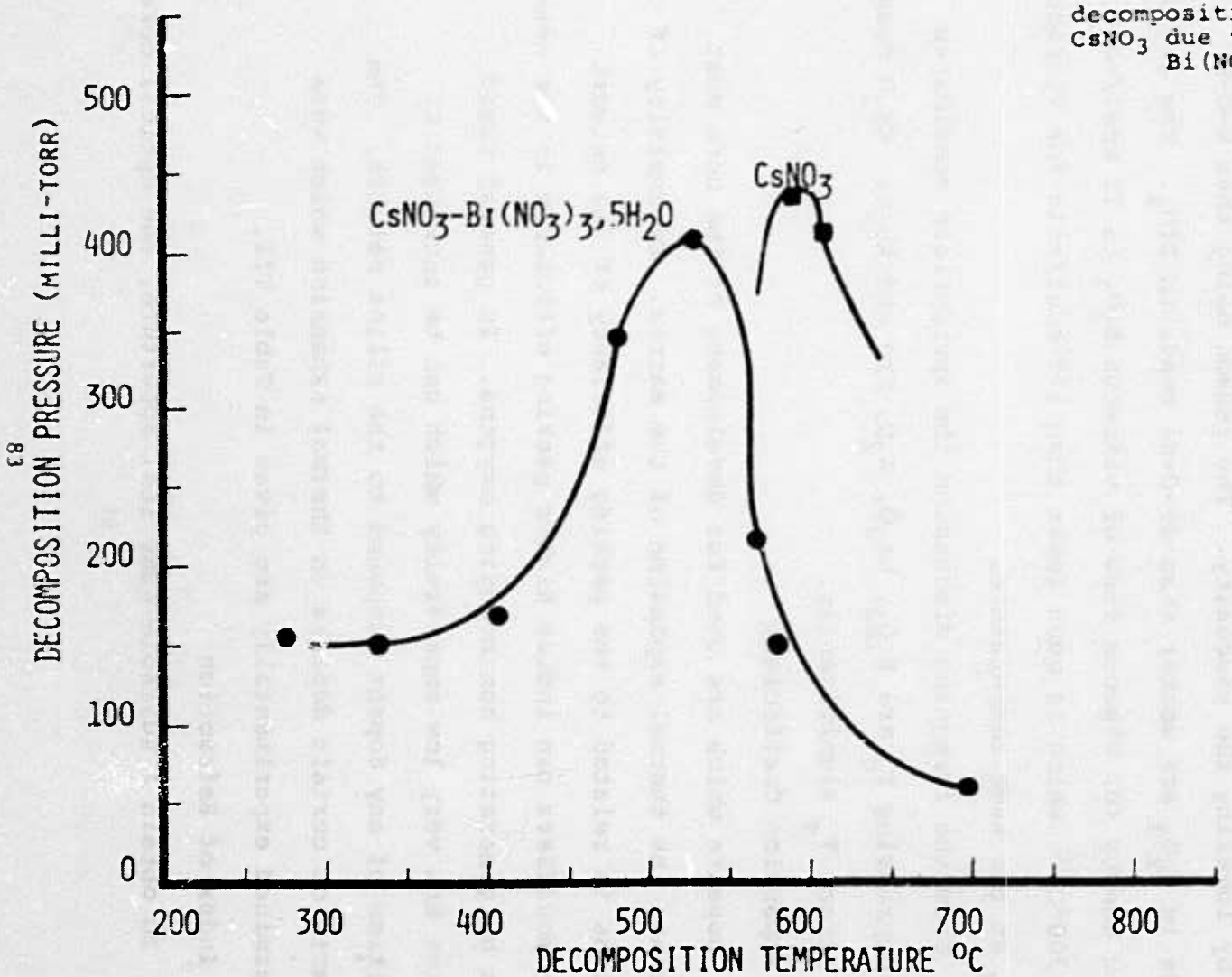

FIGURE 26 - The depression of the decomposition temperature of $CsNO_3$ due to the presence of $Bi(NO_3)_3$, $5H_2O$.

energies for viscous flow of 40 to 50 kcal/mole at high temperature for glasses having 25 to 50% modifier oxide content. Binary alkali oxide silicates have even lower activation energies of about 20 kcal/mole for a 50% alkali oxide silicate.[37]

Another important compound which can reduce T_g effectively is B_2O_3, not by breaking the network since B_2O_3 is a glass former but by lowering the viscosity. The reason being that B-O-B bonds in B_2O_3 are weaker than Si-O-Si bonds in SiO_2. The activation energy for viscous flow of vitreous B_2O_3 is 12 kcal/mole at 1300°C,[36] which is much lower than 170 kcal/mole for vitreous SiO_2 at the same temperature.

From the foregoing discussion the appropriate candidates for depressing T_g are B_2O_3, Na_2O, K_2O, SrO and Rb_2O. Cs_2O does not affect T_g significantly.

5. Expansion Coefficient

Dopants which are used for development of the core must increase the thermal expansion of the matrix. Expansivity of a glass is related to the packing efficiency of its network. Some modifiers can induce higher packing efficiency in the network by generating non bridging oxygens. In general fused silica has very low expansivity which can be increased by addition of any dopant compound to the silica network. The effects of certain dopants on thermal expansion which were determined experimentally are given in Table VII.

6. Index of Refraction

To obtain a suitable numerical apperture, the optical core

should have a relatively high refractive index. The refractive index in a material depends on its polarizability which is related primarily to the arrangement of the electrons. A higher refractive index will be associated with a greater electron density and thus with higher mass density or greater atomic number. However, low optical attenuation requires that dopant oxides, when introduced in the matrix, not provide any color centers in the finished glass. This requirement eliminates all the ions whose absorption bands are in the wavelength range of .2μ to 2μ. These are ions of:

(i) the first, second and third transition series elements,

(ii) the rare-earth group, and

(iii) closed ion shells.

The highest values of refractive index are given by Pb^{2+}, Bi^{3+}, Te^{+} and Cs^{+}.

On the other hand dopants which are to be used for the development of the inner clad in multiclad preforms must have a low refractive index compared to those used for the optical core, in order to enhance the index difference between optical core and clad regions and therefore the obtainable NA. Alkali ions such as Na^{+}, K^{+} and Rb^{+} are considered to be suitable candidates.

7. Solubility

The dopant compound must have a high to moderate solubility in water at about 100°C. The physical properties of the glass, such as refractive index, expansion coefficient and T_g are

dependent on the amount of dopant oxides which are deposited in the matrix. Therefore for maximum NA, and residual surface stress a high concentration of dopants in both optical and mechanical cores is required.

In addition to the requirement of high solubility needed to obtain high dopant levels in the porous glass it is necessary that the solubility be controllable. When the desired concentration profile is obtained in the porous preform the dopant must be precipitated rapidly. The solubility of many nitrates in water is controlled adequately by the temperature of the water. In general, however, it is necessary to use temperature and solvent mixtures to control solubility.

Unstuffing and washing procedures require solvents for which the dopant or in most cases dopants have particular solubility levels. In the unstuffing and washing stages, solubilities of about 10% for unstuffing and 1% or lower for washing are required. In most cases it is possible to find solvent mixtures which will provide the desired solubilities for several dopants simultaneously. A great deal of experimentation is required, however, to determine the proper solvents. The presence of one solute may affect the solubility of another, so information of solubilities found in the literature are only of marginal value. The design of proper solvents is a task of major importance in successful profiling by Molecular Stuffing.

8. Dopant Purity

Since there is no purification possible after the dopant is deposited in the porous glass, the dopant and its solvents must be available in very high purity (20 ppb or less of most transition metals). The development of fiber optics has led to the commercial availability of many high purity dopants while high purity solvents have been available for some time.

Many of the alkali and alkaline earth nitrates which are used in Molecular Stuffing are readily purified by a combination of filtration and ion exchange techniques. One important dopant which is not available in pure form is bismuth nitrate. The chemistry of bismuth is not sufficiently different from the transition metals to permit purification in the same manner as the alkali and alkaline earths. We have not found a solution to this problem.

In conclusion, according to the above criteria, the following dopants are selected from a larger group of modifiers, BO_3H_3, $Bi(NO_3)_3\text{-}5H_2O$, $NaNO_3$, KNO_3, $RbNO_3$, $Sr(NO_3)_2$ and $CsNO_3$. The oxides of the above compounds retain the following final properties in the glass network.

B_2O_3 Network former. Will join network structure of silica glasses, reduces viscosity without producing adverse changes in thermal expansion, chemical durability and refractive index. It lowers the glass transition temperature significantly.

Na_2O Network modifier. Markedly lowers T_g, raises thermal expansion and ionic conductivity, reduces durability, small effect on refractive index.

K_2O Network modifier. Similar to Na_2O but larger K^+ ion, improves the refractive index.

Rb_2O Network modifier, similar to K_2O but larger Rb^+ ion.

Cs_2O Network modifier, significant effect on refractive index, increases thermal expansion, leaves T_g unchanged.

SrO Has small effect on refractive index, appears to prevent distillation as does bismuth oxide.

Bi_2O_3 Network former can link SiO_4 tetrahedra. Markedly increases refractive index and thermal expansion, small effect on T_g.

The effects on α, T_g and n of several of these dopants when incorporated in Phasil have been determined experimentally. If the effects of the dopants are linear and additive functions of their concentration (a reasonable assumption for α, T_g and n) the effects can be expressed as a coefficient. The coefficients for these parameters as well as α, T_g and n for pure Phasil are given in Table VII.

TABLE VII

T_g = 820°C

$\alpha = 8 \times 10^{-7}$ 1/°C

n = 1.458

Oxide	Increase in α/ mole of oxide (1/°C) x 10^7	Decrease in T_g/ mole of oxide °C	Increase in n/ mole of oxide
K_2O	6.7	28.3	.0041
Rb_2O	7.3	18.8	.0053
Cs_2O	8.3	4.8	.0079
Bi_2O_3	7.7	19.45	.018

B. Profiling Procedures and Results

Two profile types were examined in this study. The first was a step index profile and the second a profile having two clads. The procedures for producing these profiles are similar, however, the multiclad preforms require more complicated solvents and have a more restricted list of available dopants. In this section we will describe the procedures, stuffing, unstuffing and washing solutions, and the experimentally determined compressive stresses obtained.

1. Stuffing Solutions and Stuffing Procedure

The concentration and temperature of the solutions used for molecular stuffing are selected from the experimentally determined solubility diagrams of concentration vs. temperature for each combination of dopants. As an example the diagram of the system $CsNO_3$-H_2O is given in Fig. 27 (solid line). According to the figure, the working range ΔT, at a given concentration is bounded at the low end by T_s (saturation temperature), and the high end by T_b (boiling temperature). This range, ΔT, becomes zero at about 112°C with a saturation concentration of 132 gm/100 cc of soln.

For proper control of fabrication conditions it is desirable to have as large a working range as possible. A suitable secondary salt can depress T_s, raise T_b and provide higher doping levels if it is mutually soluble with the first salt. The dashed line in Fig. 27 demonstrates the increase in working range which results from the addition of bismuth nitrate to the saturated solution of cesium nitrate. Table VIII shows the concentrations of $CsNO_3$ and $Bi(NO_3)_3$, $5H_2O$ for these solutions.

FIGURE 27 - The working range as a function of concentration for $CsNO_3$ and $CsNO_3$-$Bi(NO_3)_3$ solutions

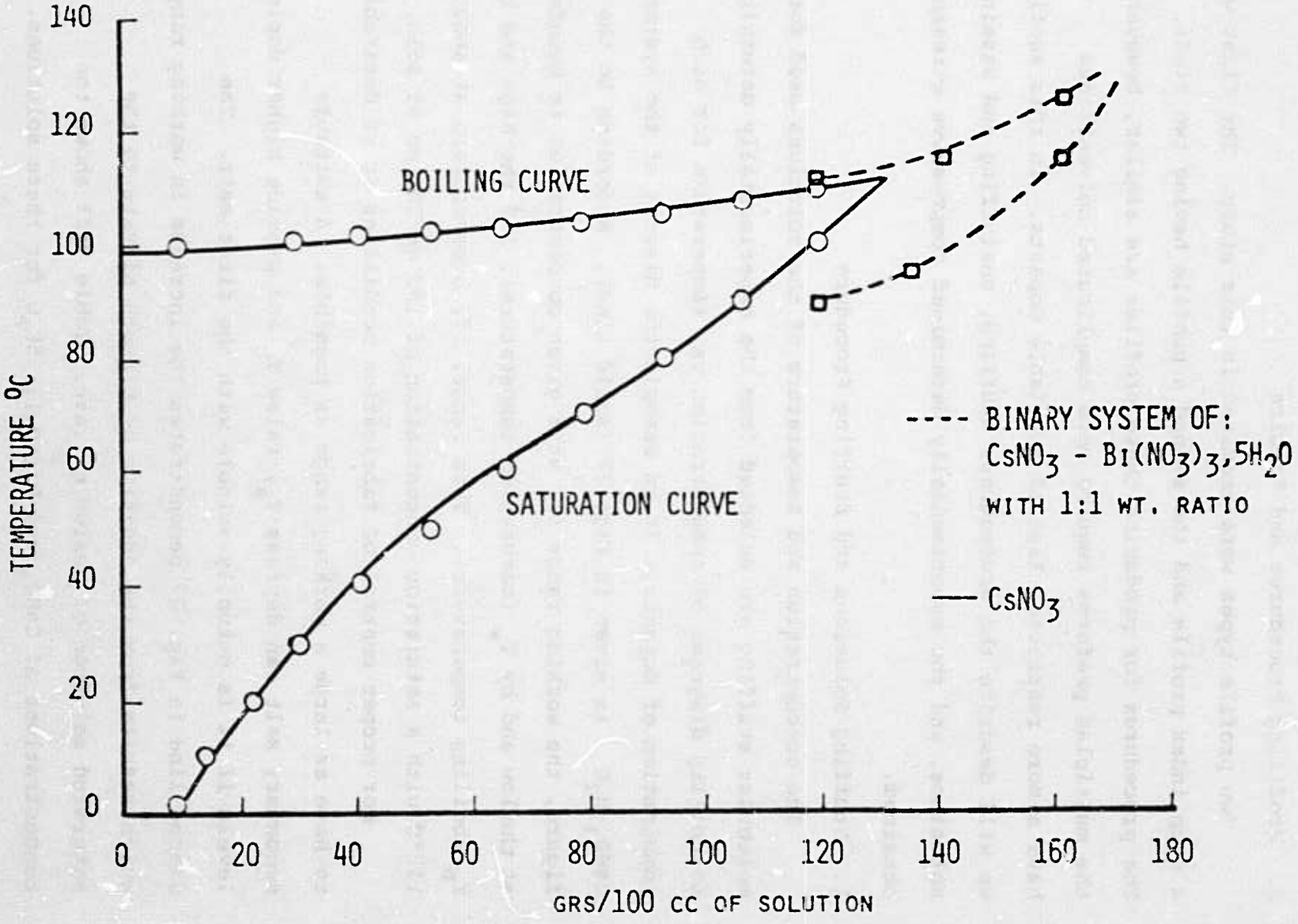

CONCENTRATION OF NITRATES IN THE BINARY SYSTEM OF: $CsNO_3$ - $Bi(NO_3)_3.5H_2O$ CONCENTRATION IN gr/100cc of soln.			SATURATION CONCENTRATION OF $CsNO_3$ CONCENTRATION IN gr/100cc of soln.	
$CsNO_3$	$Bi(NO_3)_3.5H_2O$	$\Delta T(^{\circ}C)$	$Cs\ NO_3$	$\Delta T(^{\circ}C)$
120	100	22	120	10
136	136	20	136	0
162	162	10	ABOVE BOILING POINT	

INCREASE IN THE WORKING RANGE DUE TO ADDITION OF BISMUTH NITRATE.

Table VIII

CONCENTRATION OF NITRATES IN THE BINARY SYSTEM OF: KNO_3 - $Bi(NO_3)_3.5H_2O$ CONCENTRATION IN wt%		$T_s(^{\circ}C)$	$T_b(^{\circ}C)$	ΔC
KNO_3	$Bi(NO_3)_3.5H_2O$			
30.4	65.2	85	112	30.6
40.4	47.4	88	109	21.5
60.8	14.2	98	104	5.0

INCREASE IN THE CONCENTRATION OF KNO_3 DUE TO ADDITION OF $Bi(NO_3)_3.5H_2O$

Table IX

Note the increased solubility for $CsNO_3$. Likewise, bismuth nitrate can be added in large amounts to the aqueous solution of all the alkali metal nitrates with similar effects. Table IX shows the increased solubility of KNO_3 with the addition of $Bi(NO_3)_3$, $5H_2O$.

In Table X we have listed a number of the stuffing solutions used in the final stages of this contract. The stuffing solutions were prepared and maintained in a closed system to minimize evaporation losses causing variations in concentration while stuffing at high temperatures. The solutions were heated during stuffing using a Corning hot-plate with stirring action (model PC-351), coupled to a temperature controller (Love Controls model-49), giving accurate and dependable control of the stuffing temperature. The stuffing apparatus is illustrated in Fig. 28.

As a diffusion controlled process, the stuffing rate and loading, depends on temperature, concentration and pore-geometry. The time taken to saturate the pores with the stuffing solution can be determined by monitoring the weight-gain of the preform with time. When the weight reaches a constant value, the stuffing process is complete. However, if the preforms are pre-dried in a furnace above 150°C, prior to stuffing one can visually determine the end of the stuffing period. As the stuffing progresses, the solution boundary fronts move toward the axis of the preform until they merge indicating all the pores are completely filled with the solution. Accordingly the length of stuffing times were determined to be from 2 hours for low

STUFFING SOLUTIONS COMPOSITION

DOPANTS-CONCENTRATION IN gr/100cc of soln.

SOLUTION GROUP no.	H_3BO_3	$CsNO_3$	$RbNO_3$	KNO_3	$Bi(NO_3)_3.5H_2O$	STUFFING TEMPERATURE (°C)
I.1	-	120	-	-	100	105
I.2	-	81.5	-	73	88	115
I.3	30	120	-	-	-	100
II.1	-	-	188	-	-	120
II.2	-	-	140	140	-	112
II.3	-	-	-	104	24	104
III.1	-	153	-	-	129	104
III.2	-	162	-	-	162	125

MOLTEN SALT, CONCENTRATION IN wt%

SOLUTION GROUP no.	$CsNO_3$	$RbNO_3$	KNO_3	$NaNO_3$	EUTECTIC TEMPERATURE (°C)
I.4	54.51	-	45.49	-	220
I.5	47.12	-	26.95	25.93	140
I.6	44.15	22.27	33.58	-	230

Table X

STUFFING APPARATUS

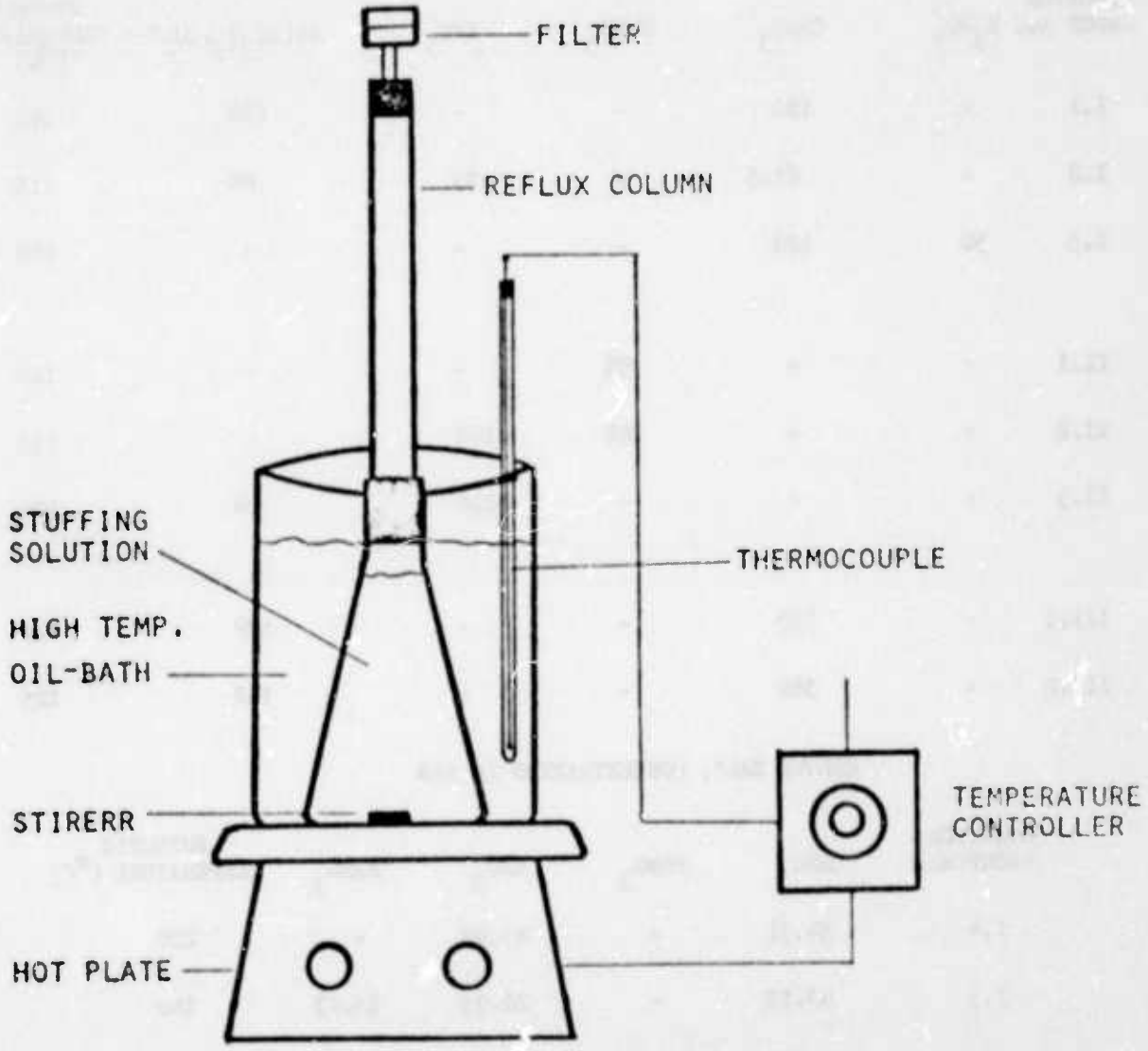

Figure 28

SOLVENT NO.	COMPOSITION IN VOL% H_2O	CH_3OH*	C_2H_5OH**	HNO_3*
U.1	82	13	-	5
U.2	80	20	-	-
U.3	78	21	-	1
U.4	96	-	-	4
U.5	83	6	-	11
W.1	16	82.3	-	1.7
W.2	5	95	-	-
W.3	10	90	-	-
W.4	6	-	94	-
W.5	5	-	94	1
W.6	-	98	-	2
W.7	4	95	-	1

TABLE XI

COMPOSITION OF THE COMPOUNDED UNSTUFFING AND WASHING SOLVENTS WHICH ARE ABBREVIATED IN THE PROCESSING TABLES.

* A.C.S. REAGENT GRADE (FISHER)

** DENATURED (FISHER)

ROD no	STUFFING (day)	UNSTUFFING TEMPERATURE 4°C SOLUTION	UNSTUFFING TEMPERATURE 4°C TIME(hr)	WASHING 1 SOLUTION	WASHING 1 TIME(hr) 0°C	WASHING 1 TIME(hr) 25°C	WASHING 1 TIME(hr) 0°C	WASHING 2 TEMPERATURE 4°C SOLUTION	WASHING 2 TEMPERATURE 4°C TIME(hr)
I.1.1	1	U.1	8	W.1	39	-	-	Methanol	48
I.1.2									
I.1.3									
I.1.4	2	U.1	5	W.1	48	-	-	Methanol	24
I.1.5									
I.1.6	4	U.1	6	W.1	26	-	-	-	-
I.1.7	3	U.1	6	W.1	20	-	-	Methanol	24
I.1.8	2	U.5	5	W.1	92	-	-	-	-
I.2.1	2	U.1	4	Methanol	48	-	-	-	-
I.2.2	3	U.5	2	Methanol	24	-	-	-	-
I.2.3	2	U.5	1	Methanol	26	-	-	-	-
I.3.1	1	U.2	4	Methanol	48	-	-	-	-
I.3.2	1	U.2	6	Methanol	48	-	-	-	-
I.4.1	4	Water	3	W.3	29	-	-	Methanol	19

Table XII

ROD no.	STUFFING (day)	UNSTUFFING TEMPERATURE 4°C SOLUTION	TIME(hr)	WASHING 1 SOLUTION	TIME (hr) 0°C	25°C	0°C	WASHING 2 TEMPERATURE 4°C SOLUTION	TIME(hr)
II.1.1	2	Water	1	Methanol	20	4	1	Propanol	48
II.1.2	1	Water	3	Methanol	5	2	1	Propanol	24
II.1.3									
II.1.4	3	Water	4.5	Methanol	5	3	15	Propanol	24
II.1.5	4	Water	4	W.2	1	2	1	Propanol	48
II.1.6									
II.1.7									
II.1.8									
II.2.1	1	U.2	4.5	Methanol	17	6	2	Propanol	16
II.2.2									
II.3.1	1	U.3	1	W.2	2	19	6	-	-
II.3.2	1	U.3	1.5	W.2	2	19	6	-	-
II.3.3	1	U.3	2	W.2	2	19	6	-	-

Table XII

ROD no.	STUFFING TIME (day)	HIGH TEMP.[1] UNSTUFFING TIME (min)	LOW TEMP.[2] UNSTUFFING TIME (min)
III.1.1	3	10	90
III.1.2	1	10	90
III.1.3	3	25	90
III.1.4	5	65	60
III.1.5	6	40	90
III.1.6	3	60	90
III.1.7	2	80	205
III.1.8	3	70	70
III.1.9	2	100	80
III.1.10	1	90	120
III.2.1	10	10	120
III.2.2	4	45	205
III.2.3	2	70	100
III.2.4	4	45	150

(1) Unstuffing solution is 70% (wt%) of KNO_3 at 100°C.

(2) All the preforms were quenched in propanol prior to the low temperature unstuffing. Unstuffing solvent was solution U.1 whose composition can be found in table A-1.

Table XII (cont'd.)

	WASHING 1	TIME(hrs)			WASHING 2	TIME(hrs)		
ROD no.	SOLVENT	0°C	25°C	0°C	SOLVENT	0°C	25°C	0°C
III.1.1	W.1	16	-	-	Methanol	24	2	1
III.1.2	W.1	16	-	-	W.4	24	2	1
III.1.3	W.1	14	-	-	Ethanol	24	5	1
III.1.4	W.1	15	1	1	W.5	24	1	2
III.1.5	Methanol	16	2	2	W.5	24	1	2
III.1.6	W.1	16	-	-	Ethanol	24	5	2
III.1.7	W.1	16	-	-	Methanol	24	1	2
III.1.8	W.1	16	1	1	Ethanol	24	1	2
III.1.9	Methanol	24	2	1	W.7	7	2	2
III.1.10								
III.2.1								
III.2.2								
III.2.3								
III.2.4								

As the final step, all the specimens were washed in cold propanol for 6-24 hrs. All the preforms from III.1.9 to III.2.4 were soaked in 2N HNO_3 at 65°C for 4-5 min, prior to the unstuffing at high temperature.

Table XII

concentrations to 24 hours for higher concentrations.

2. Unstuffing and Washing

Unstuffing and washing solutions were determined experimentally by measuring the solubilities of particular dopant combinations in mixtures of alcohols , water and nitric acid. We list below in Table XI several of the important solutions for the dopant combinations represented in the stuffing solutions given in Table X.

Stuffing, unstuffing and washing schedules are given for a few representative samples in Table XII. The Roman numeral and Arabic numeral of the rod number identifies the stuffing solution used. Roman numerals I and II are for step profile preforms, and numeral III is for multiclad preforms.

3. Drying and Collapsing

The preforms are dried, the nitrates decomposed and the preforms collapsed using rate heating in vacuum and under a partial pressure of oxygen. The following schedule is typical although minor variations have been used with success with certain dopant combinations.

a. Drying under vacuum at 4°C for 24 hours

b. Rate heating under vacuum at 15°C/hr from 25°C to 625°C

c. Holding under vacuum at 625°C for 28 hours

d. Rate heating at 50°C hour from 625°C to 850°C under 1/5 atmosphere of O_2.

4. Clad Compression Obtained in Molecular Stuffed Preforms

In this section we present experimental results of the clad compression obtained in preforms for several dopant systems. The

compression was measured photoelastically as described in Section VI. An assumed value for the stress optic coefficient of 850 lb/in-fringe was used in calculating the stress. This corresponds to the value reported in the literature for commercial 96% type silica.[31]

We have found that the 96% silica clads we produce have stress optic coefficients as much as 25% higher than those of the commercial type. Thus, the magnitude of the compression we report is probably low. Measurements of stress optic coefficients were made only on pure phasil and the clads of Cs_2O and Cs_2O-K_2O-Bi_2O_3 doped preforms. In the case of Cs_2O-K_2O-Bi_2O_3 the measured stress optic coefficient is more than 25% higher than the assumed value.

Since the stress optic coefficient was measured for only one of the preform types we discussed here, we have not recalculated the stresses. If the stress optic coefficient becomes available, the data can be corrected by simply multiplying the stress by the ratio of the correct and assumed coefficients.

We show the experimentally observed compression for the following dopant systems:

Dopant	Figure
$RbNO_3$	29
$CsNO_3$ - H_3BO_3	30
KNO_3 - $Bi(NO_3)_3,5H_2O$	31
$CsNO_3$ - $Bi(NO_3)_3 5H_2O$	32
$CsNO_3$ - $Bi(NO_3)_3,5H_2O$ - KNO_3	33
" " Multiclad	34
$Sr(NO_3)_2$ - KNO_3	35

FIGURE 29 - Compression as a function of clad thickness to radius ratio for $RbNO_3$.

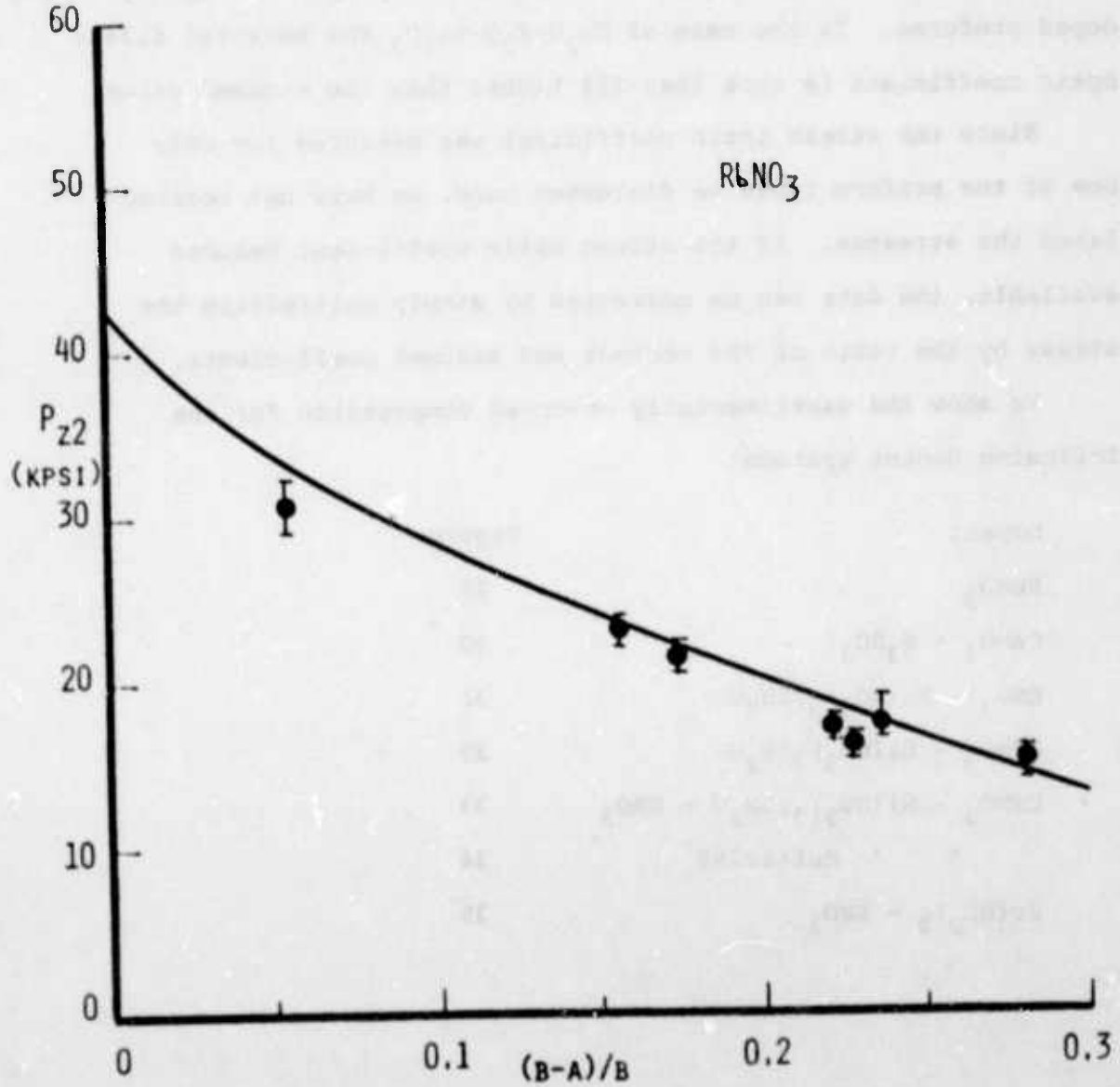

FIGURE 30 - $CsNO_3$ - H_3BO_3

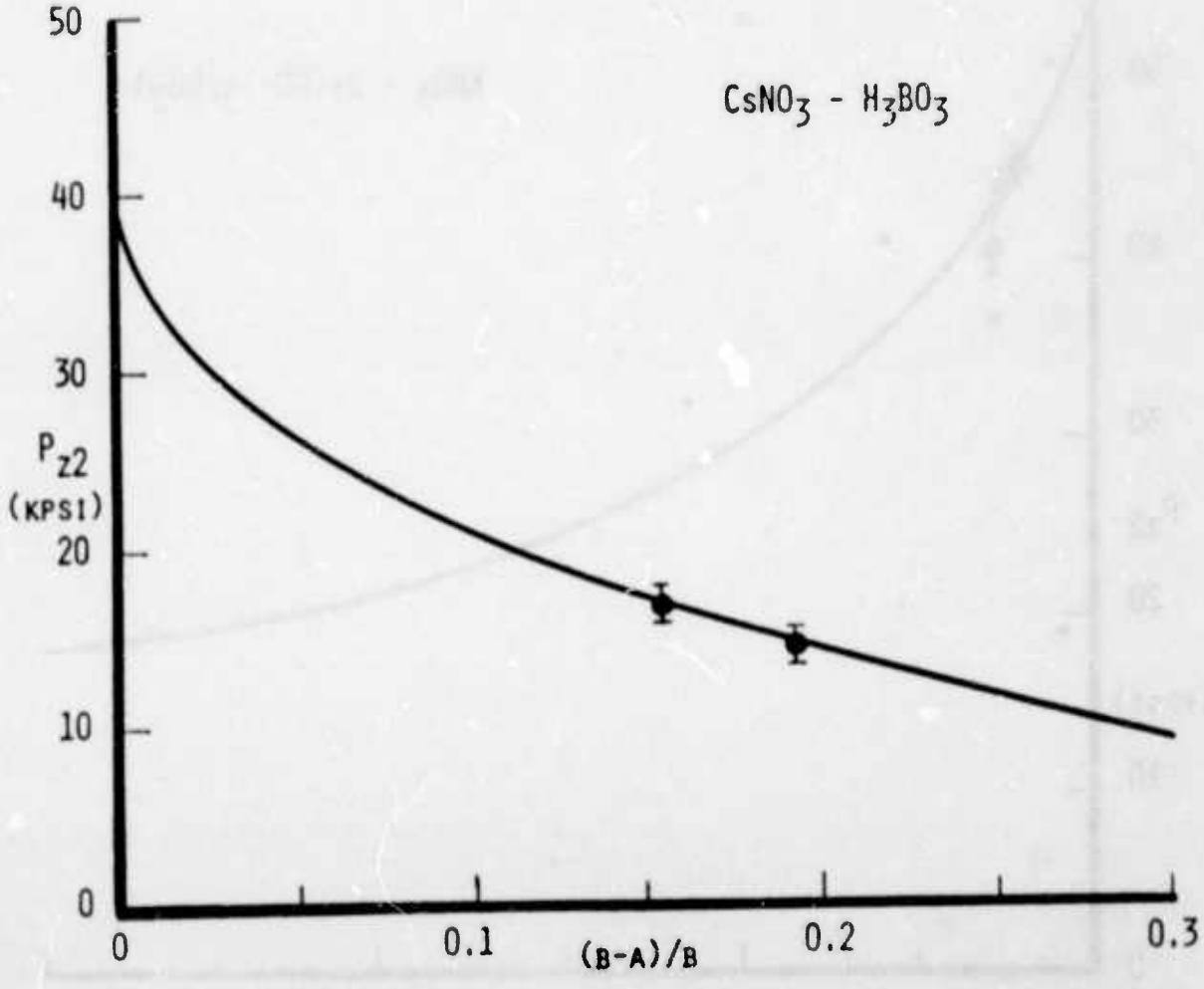

FIGURE 31 - KNO_3 - $Bi(NO_3)_3$, $5H_2O$.

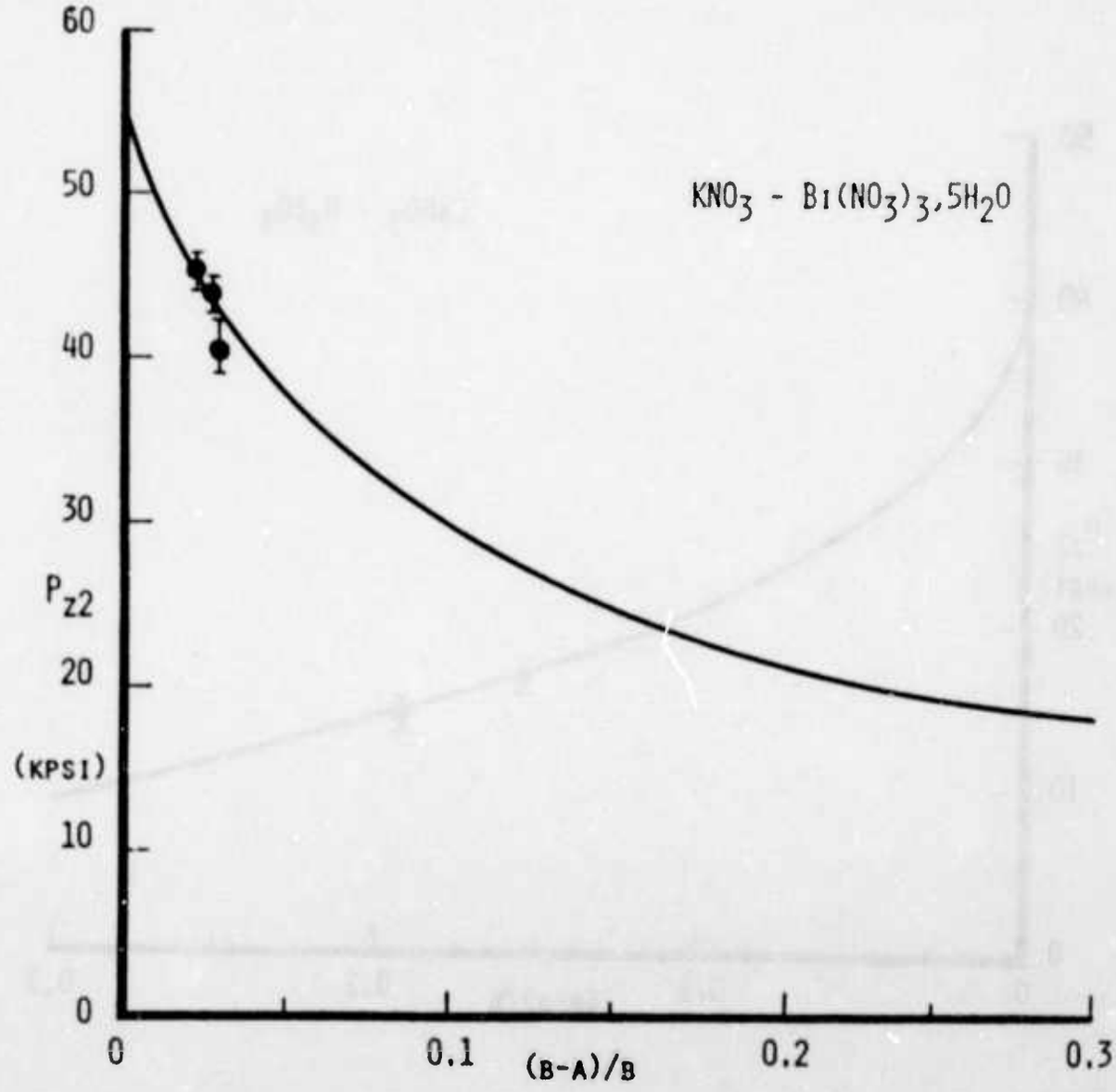

FIGURE 32 - $CsNO_3$ - $Bi(NO_3)_3 5H_2O$

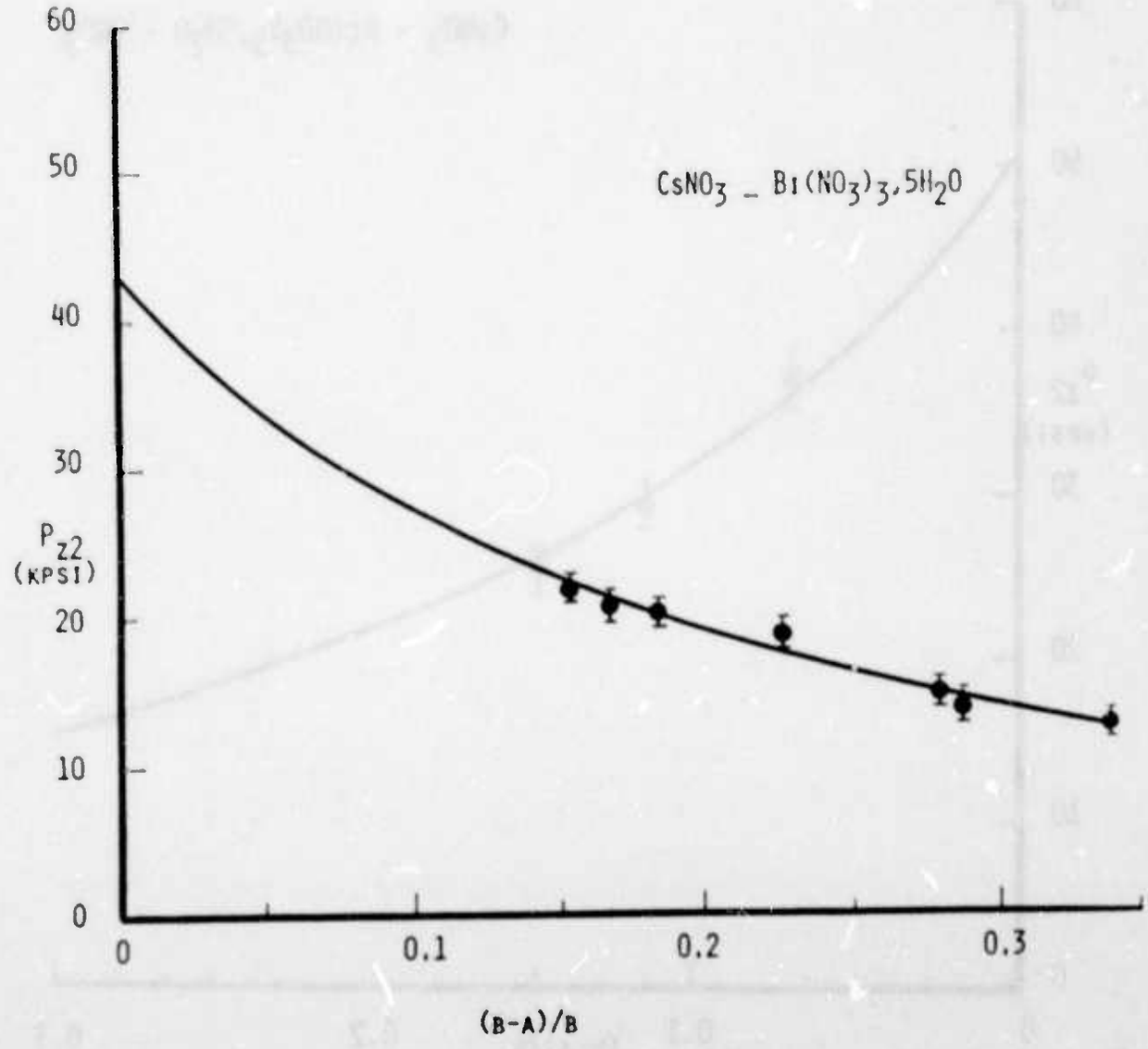

FIGURE 33 -

$CsNO_3$ - $Bi(NO_3)_3 5H_2O$ - KNO_3

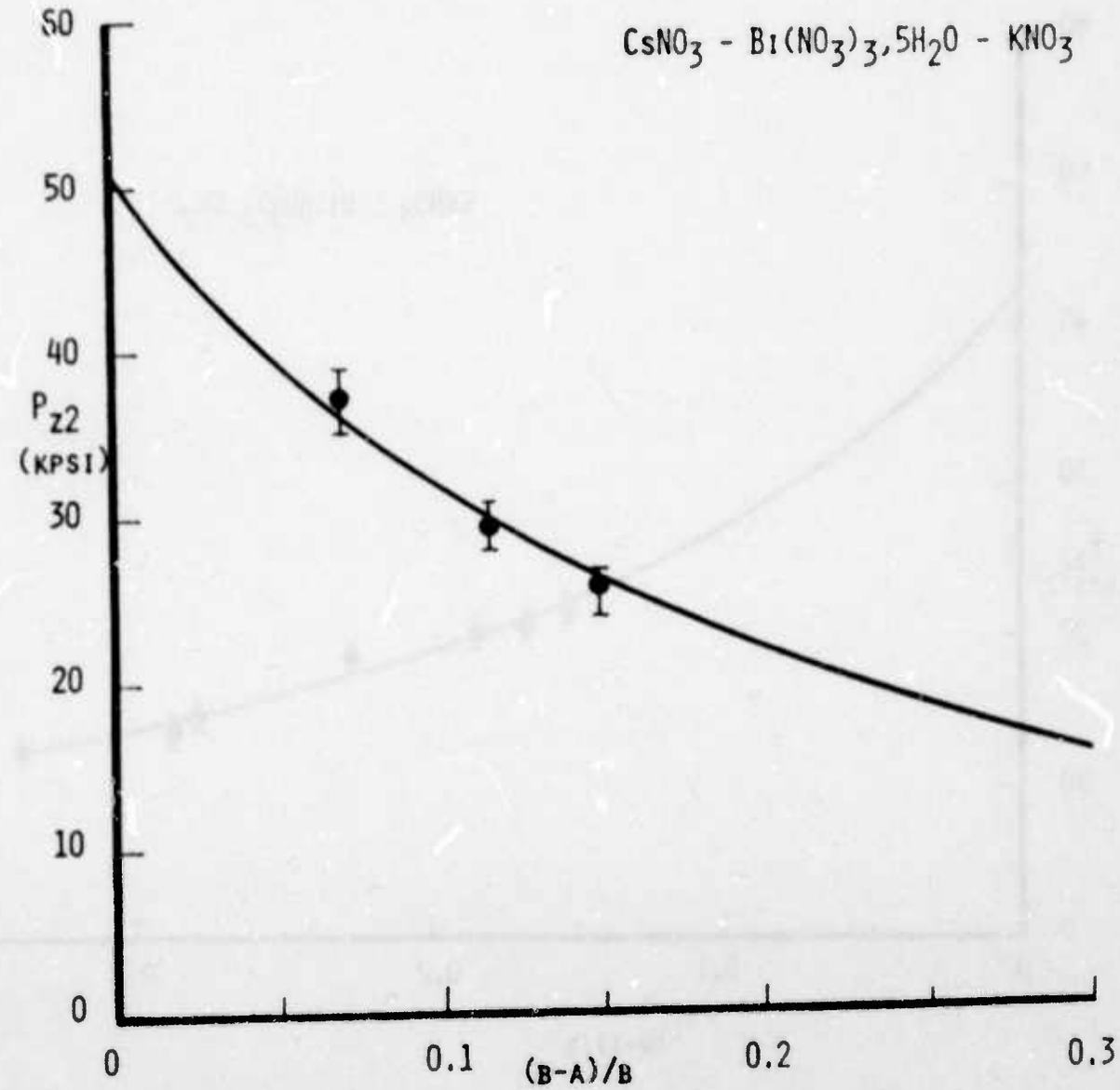

FIGURE 34 -

$CsNO_3$ - $Bi(NO_3)_3 5H_2O$-KNO_3

Multiclad preforms

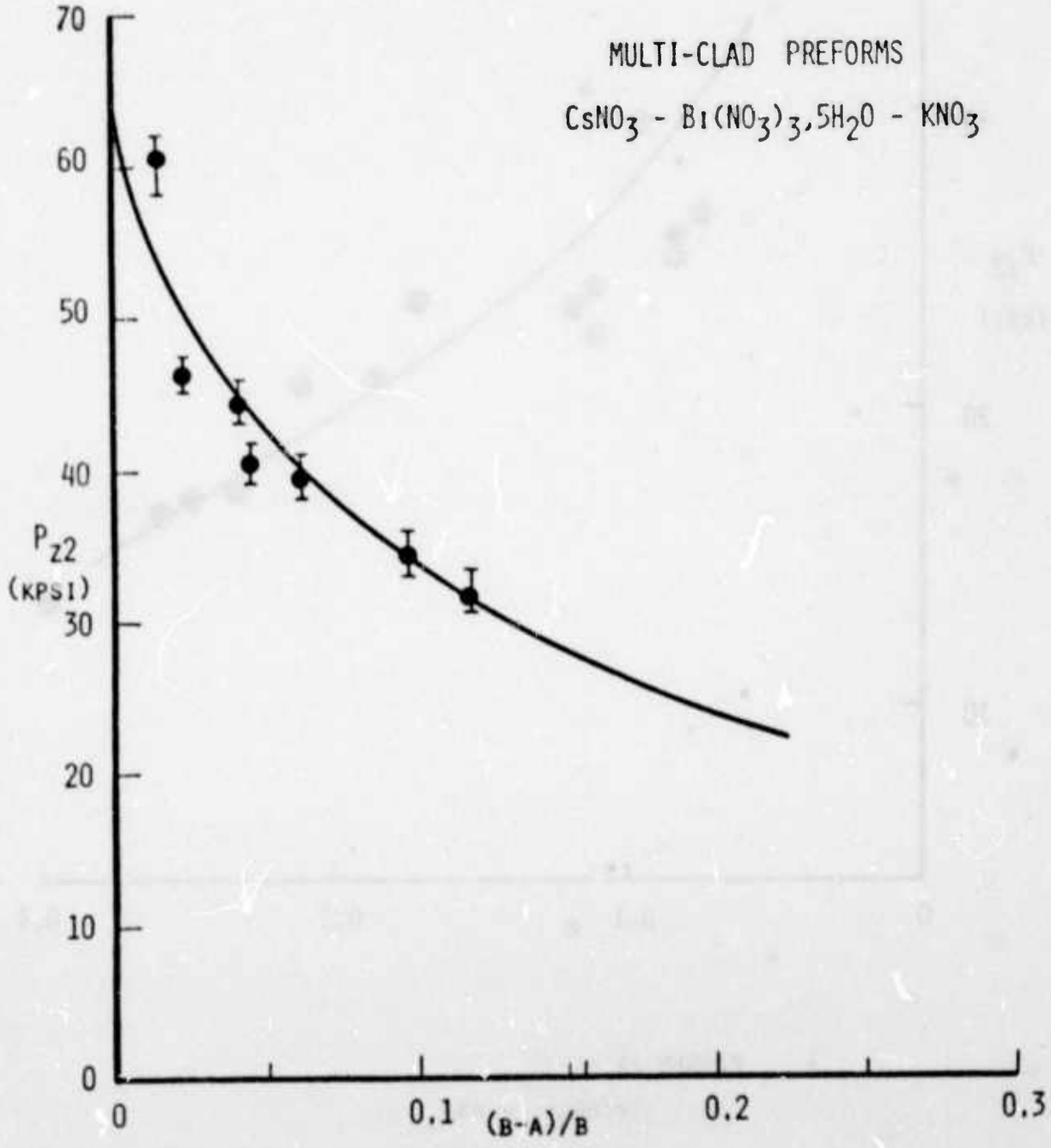

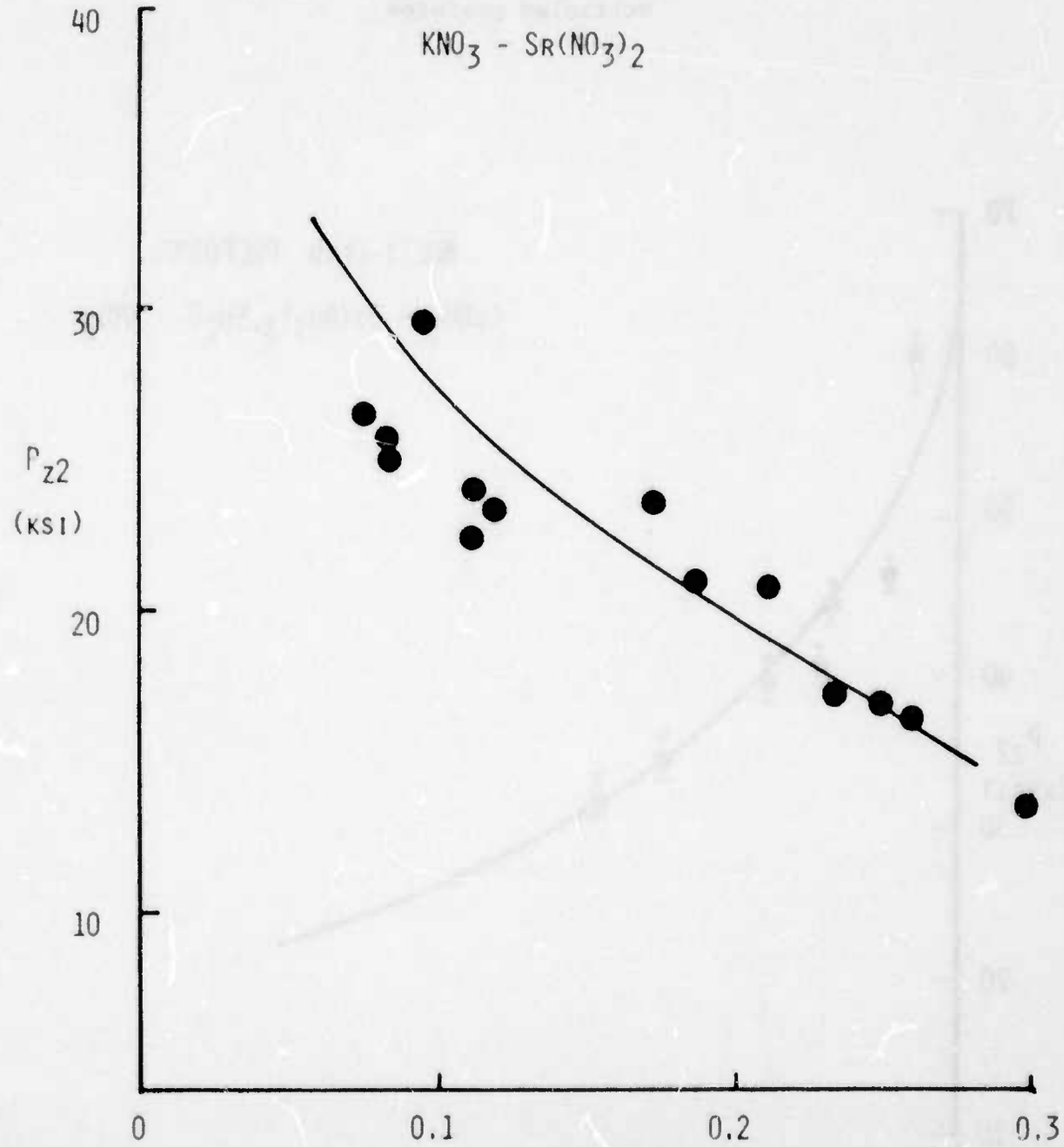

FIGURE 35 -

$Sr(NO_3)_2$ - KNO_3

The solid lines represent best fits to the experimental points for Eq. (3). Since the stress optic coefficient was measured for the $CsNO_3$ - $Bi(NO_3)_3$, $5H_2O$ - KNO_3 dopant system the maximum observed stress was approximately 75 ksi rather than 60 ksi as shown on the graph. The other values plotted probably have similar corrections.

C. Conclusions

In this section we have given details for the Molecular Stuffing of a number of dopants which were found to be useful in compressive strengthening. The greatest degree of control and experience were obtained using the dopant combination Cs-K-Bi. With this combination compression in preforms on the order of 75ksi was obtained.

Obtaining high compression (> 40ksi) was found to be difficult whereas obtaining compression ranging from 20ksi to 35ksi was found to be relatively easy. Compression of this magnitude is sufficient to prevent static fatigue indefinitely for optical fibers used in the majority of ordinary telecommunication applications. We consider this fact to be a major contribution of this research.

* The composition and profiling study represented in this chapter is derived primarily from the Doctoral research of Hamid Hojaji. Much of the data and text were excerpted from his dissertation entitled "Analysis of the Molecular Stuffing Strengthening Process for Glass Fiber Optical Waveguides", Copyright by Hamid Hojaji, May 1979.

REFERENCES

1. D.G. Holloway, The Physical Properties of Glass, Wykeham Publications Ltd., London, (1973) 190.

2. D.A. Krohn and A.R. Cooper, J. Am. Ceram. Soc., 52, 661 (1969).

3. M.G. Drexhage and P.K. Gupta, J. Am. Ceram. Soc., to be published.

4. J.H. Simmons, R.K. Mohr, D.C. Tran, P.B. Macedo and T.A. Litovitz, J. Appl. Opt., to be published.

5. W. Weibull, Ingenioersvetenskapsakad, Hand 1. (1939) #151, 45.

6. S.B. Batdorf and H.L. Heinisch, Jr., J. Am. Ceram. Soc., 6, 355 (1978).

7. A.A. Griffith, Phil. Trans. R. Soc. A221, 163 (1920).

8. S.M. Weiderhorn, J. Am. Ceram. Soc., 52, 99 (1969).

9. W. Weibull, J. Appl. Mech. 293, (Sept. 1951).

10. Tardy, H.L., Rev. Opt. 8, 59 (1929).

11. E.B. Shand, Glass Engineering Handbook, 2nd ed., McGraw Hill Book Co., New York, (1958) 33.

12. J.A. Bucaro and H. Dardy, J. Non-Crys. Solids 20, 149 (1976).

13. P.K. Gupta and C.T. Moynihan, J. Chem. Phys., 65, 4136 (1976).

14. C.R. Kurkjian, paper TUC1, "Optical Fiber Communication," Technical Digest, Optical Society of America, March 6-8, 1979 Washington, D.C.

15. O.L. Anderson, "The Griffith Critereon for Glass Fracture," in Fracture, B.L. Averbach, D.K. Felbeck, G.T. Hahn and D.A. Thomas, eds., John Wiley and Sons, Inc. New York (1959).

16. B.K. Tariyal and Dr. Kalish, "Kinetics of Strength Degradation in Polymer-Coated Optical Fibers," presented at the 80th Annual Meeting of the Am. Ceram. Soc., Detroit, Michigan, (1978).

17. R.H. Doremus, Glass Science, John Wiley and Sons, New York, (1973) p. 302.

18. S.M. Weiderhorn, H. Johnson, A.M. Diness and A.H. Heuer, J. Am. Ceram. Soc., 57, 336 (1974).

19. D.A. Pinnow, G.D. Robertson, G.R. Blair and J.A. Wysocki, paper TUC5 (same as Ref. 14.)

20. M.S. Maklad and C.K. Kao, paper TUC3 (same as Ref. 14).

21. S.M. Weiderhorn, "Subcritical Crack Growth in Ceramics," In Fracture Mechanics of Ceramics, Vol. 2, R.C. Bradt, D.P.H. Hasselman and F.F. Lange Ed. Plenum Pub'ishing Co., New York, p. 613.

22. J.R. Hutchins, III and R.V. Harrington, "Glass" Encyclopedia of Chemical Technology, 2cn Ed., 10, John Wiley and Sons, Inc., New York (1966) p. 533.

23. R.E. Mould, J. Amer. Ceram. Soc., 43, 160, (1960).

24. A.J. Holland and W.E.S. Turner, J. Soc. Glass Tech., 21, 383 (1937).

25. T.C. Baker and F.W. Preston, J. Appl. Phys., 17, 179 (1946).

26.. A.G. Metcalfe, M.E. Gulden and G.K. Schmitz, Glass Tech., 12, 15 (1971).

27. W.C. Levengood, J. Appl. Phys. 29, 820 (1958).

28. Sir David Brewster, Phil. Trans. (105), 60 (1815); Phil. Trans. (106), 156 (1816); Trans. Roy. Soc. Edinburgh 8, 369 (1818).

29. E.G. Coker and L.N.G. Filon, Treatise on Photoelasticity (Cambridge University Press, London, 1931).

30. A.J. Durelli and W.F. Riley, Introduction to Photomechanics, Prentice Hall, Englewood Cliffs, NJ (1965).

31. D.A. Krohn, J. Amer. Ceram. Soc., 53, 505 (1970).

32. L. Shartsis, H.F. Shermer and A.G. Bestul, J. Am. Ceram. Soc. 41, (6), 507 (1958).

33. R.H. Doremus, Glass Science, John Wiley and Sons, New York (1973).

34. G.O. Jones Glass, 2nd ed., Chapman and Hall Ltd., Guteshead, G. Britain, (1971) 42.

35. C.C. Addison and N. Logan, "Anhydrous Metal Nitrates," in Advance in Inorganic and Radio-Chemistry, 6, Plenum Press, New York, (1964) pp. 115-124.

36. B.L. Mozzi and B.E. Warren, J. Appl. Cryst., 3, 251 (1970).

37. M. Goldstein and M. Nakonecznyj, Phys. Chem. Glasses, 6, 126 (1965).

MISSION
of
Rome Air Development Center

RADC plans and executes research, development, test and selected acquisition programs in support of Command, Control Communications and Intelligence (C^3I) activities. Technical and engineering support within areas of technical competence is provided to ESD Program Offices (POs) and other ESD elements. The principal technical mission areas are communications, electromagnetic guidance and control, surveillance of ground and aerospace objects, intelligence data collection and handling, information system technology, ionospheric propagation, solid state sciences, microwave physics and electronic reliability, maintainability and compatibility.

Printed by
United States Air Force
Hanscom AFB, Mass. 01731